The role of metabolism in cardiomyocyte maturation, disease and regeneration

Jason Wayne Miklas

A dissertation

submitted in partial fulfillment of the

requirements for the degree of

Doctor of Philosophy

University of Washington

2018

Reading Committee:

Hannele Ruohola-Baker, Chair

Michael Regnier

Peter Rabinovitch

Program Authorized to Offer Degree:

Department of Bioengineering

Jason Wayne Miklas

University of Washington

Abstract

The role of metabolism in cardiomyocyte maturation, disease and regeneration

Jason Wayne Miklas

Chair of the Supervisory Committee:
Hannele Ruohola-Baker, Ph.D., Professor
Department of Biochemistry

Cardiovascular disease, broadly encompassing both genetic and environmental cardiac pathology, remains the leading cause of death. As such, there is a great need to better model cardiac diseases in an attempt to find novel therapeutics as well as discover novel ways to regenerate the damaged heart. One such disease that is the leading fatty acid oxidation disorder with no known cure is mitochondrial tri-functional protein (MTP) deficiency. With the advent of human pluripotent stem cell derived cardiomyocytes (hPSC-CMs), it is now possible to study human cardiac diseases *in vitro*. However, stem cell derived cardiomyocytes are more representative of fetal cardiomyocytes instead of a more mature adult like cardiomyocyte.

Consequently, in order to utilize this cell type to model disease, strategies to mature hPSC-CMs must first be discovered.

In order to mature hPSC-CMs we developed a microRNA maturation cocktail, termed MiMaC, that rapidly shifts the fetal like transcriptome in hPSC-CMs to a more adult like transcriptome to mature the cell. MiMaC consists of four microRNAs, the overexpression of Let7 and miR-452, and the knockout of miRs-122 and -200a. MiMaC treated hPSC-CMs displayed larger cell size, greater twitch force, greater metabolic activity and the ability to utilize long chain fatty acids for ATP production as compared to control hPSC-CMs. To better understand the way in which MiMaC brought about maturation in the hPSC-CMs we examined the predicted targets of the MiMaC microRNAs. We found that both of the knockout microRNAs had homeodomain-only protein (HOPX) as a common predicted target. To study the role of HOPX in hiPSC-CM maturation, we generated a doxycycline inducible HOPX overexpression hiPSC line that overexpressed HOPX in hiPSC-CMs. We found that HOPX overexpression led to a robust increase in cell size and the repression of cell cycle via the repression of nuclear kinetochore genes. Furthermore, we identified that HOPX overexpression led to the repression of serum response factor gene loci. These data suggest that MiMaC, in part, acts to mature hiPSC-CMs via the stimulation of CM growth and cell cycle repression.

Utilizing MiMaC we were now able to study human cardiac diseases *in vitro*. MTP deficiency, due to mutations in hydratase subunit A (HADHA), results in sudden infant death syndrome (SIDS) and cardiomyopathies. MTP deficiency results in impaired fatty acid β-oxidation, however, immature hPSC-CMs can not use fatty acids. This is why it was essential to develop a tool like MiMaC to mature hPSC-CMs so they could utilize fatty acids and make it possible to study this disease. Since MTP deficiency results in sudden death, it is difficult to study MTP deficiency using *in vivo* model organisms. Consequently, we generated the first human *in vitro* model of MTP deficiency utilizing HADHA deficient hiPSC-CMs. Mutations in

exon 1 of HADHA were generated using CRISPR/cas9. We found HADHA mutant (Mut) CMs challenged with fatty acids displayed sarcomere dissolution, abnormal calcium handling, elongated repolarization, erratic beating, an inability to utilize fatty acids as compared to wild type (WT) CMs and swollen and poorly functioning mitochondria. We discovered that many of the cardiac pathologies were a result of the mitochondrial dysfunction. We continued to probe the mitochondrial disfunction in HADHA Mut CMs and discovered there was abnormal cardiolipin remodeling occurring. Consequently, we elucidated the potential underlying etiology of MTP deficiency to defective cardiolipin remodeling that may be a direct or indirect cause of the mutation in HADHA.

The other aspect of cardiac disease is due to non-genetic cardiac insults such as myocardial infarctions (MI). After a MI, the heart loses a large amount of muscle tissue and is replaced by non-contractile scar tissue. As a result, patients have reduced contractility resulting in reduced blood ejection and eventual heart failure. One way to remuscularize the heart is to promote cell proliferation of existing cardiomyocytes. However, adult mammalian cardiomyocytes are unable to re-enter the cell cycle yet, neonatal mice can regenerate their heart and some fish like the zebrafish, are able to regenerate their heart at both the neonatal and adult state after injury. Consequently, these two model organisms provide a means to study the molecular mechanisms governing cardiomyocyte proliferation.

We discovered one of the earliest signaling pathways that are engaged during zebrafish heart regeneration was Wnt/β-catenin signaling. Utilizing a cell ablation model of cardiomyocyte injury, we elucidated that Wnt/β-catenin signaling was active as downstream targets showed high protein abundance 3-12 days post injury (dpi). Furthermore, we showed that Wnt/β-catenin signaling directly regulated the expression of Myc, electron transport chain protein complex I and cell proliferation during heart regeneration. Since many Myc targets are oxidative phosphorylation genes and mitochondrial biogenesis genes we examined how the metabolic

state of the heart changes during regeneration. We identified that 7 dpi there was a dramatic increase of many metabolic pathways including oxidative phosphorylation, citric acid cycle, glycolysis and fatty acid metabolism. This led to the discovery of a unique metabolite profile found in the adult uninjured heart, high glutamine levels which depleted during the first week of regeneration while an essential amino acid, leucine, became enriched during the first week of regeneration. We showed that this dynamic amino acid profile was stimulating the mammalian target of rapamycin complex 1 (mTORC1) and that mTORC1 signaling was necessary for heart regeneration. This led to the realization that the primed state for a pro-regenerative cardiomyocyte was one with an abundance of glutamine. Finally, we showed that a primed pro-regenerative cardiomyocyte with high glutamine was conserved in the young mammalian heart. These data together provide novel insight into how a unique metabolic state primes a cardiomyocyte to enter the cell cycle which, could potentially be leveraged to develop novel therapeutics.

TABLE OF CONTENTS

iv

LIST OF FIGURES

LIST OF TABLES

ACKNOWLEDGEMENTS

The past five years have been a wonderful time and I am very thankful to everyone who has shared this time with me. I would like to thank my committee members for all of their time and input over the past years. Your guidance has been wonderful and your support for me as I continue on in science is very appreciated. I would also like to thank all the members of the Ruohola-Baker lab, past and present, that I have had the pleasure to get to know and work with during my PhD. It has been a real pleasure to always be surrounded by such lively and upbeat people that make the day to day work fly by. To all the collaborators that have helped with my PhD projects, thank you very much. Many of my projects would not have been possible without your amazing scientific acumen, knowledge and expertise.

To the friends that I have made in the Bioengineering department and at South Lake Union, you are the best. From snack breaks during the day, weekend brunch and dim sum, exploring Seattle, conferences and our amazing vacations have made these past five years very fun. I will miss all of you and look forward to yearly reunions!

To my family, especially my parents Greg and Linda Miklas and brothers Andrew and David Miklas, your continued support and love mean a great deal to me. I am very lucky to have family that never waiver and are always there to listen. To Michael, I am so very glad that we met. I look forward to many more years to come.

Finally, to my Professor, Hannele Ruohola-Baker. I am very grateful you accepted me as a graduate student and that I had the chance to work with you and learn from you over these past years. You have given me a very special gift that only family and close friends share and that is your time. You have truly been an exceptional mentor and friend, always willing to spend time to listen, teach and enrich my life. I can not think of a better way to have spent the past five years

than learning and exploring science in your laboratory. These memories and lessons will truly last

a lifetime; *minä istun iloissani ja annan surun huilata*.

Chapter 1. INTRODUCTION

1.1 CARDIOVASCULAR DISEASE

Cardiovascular disease is the leading cause of death globally and is estimated to remain the leading cause of death until at least 2030 [1]. The burden of cardiovascular disease on the health care system is reaching epidemic proportions. With the yearly estimated costs of heart failure reaching $34.4 billion in health care services in the United States alone [2], an increasing need for novel therapeutics is necessary. Yet, with high costs and attrition rates of novel drugs, the total number of new drugs making it to market has decidedly declined over the past decade. The cost of bringing a new drug to the clinic has been estimated at $1.2 billion, up from a 2003 average of $802 million [3], and pharmaceutical companies face their largest losses when drugs fail in the late stage of trials, such as Phase III and the post-marketing stage [4].

Cardiovascular disease can be subdivided into two categories: environmental insults and genetic cardiomyopathies. One point in common between many cardiovascular diseases is that the mitochondria acts as a central and pivotal organelle that when mismanaged leads to a diseased state. Consequently, studying the mitochondria in cardiomyocytes during development/maturation, disease and regeneration can help us better understand how to control this energy system in cardiomyocytes to help dictate cell state and prevent disease and reverse injury.

1.2 CARDIOMYOCYTE MATURATION

The ability to generate cardiomyocytes from hESCs [5] and hiPSCs [6] provides an unprecedented opportunity to generate hPSC-CMs. Using a human based source of cardiac cells to generate *in*

vitro models of human cardiac tissues, platforms can now be created for the testing of novel cardiac therapeutics. However, while these advances in stem cell biology enable us to reliably obtain human cardiomyocytes from stem cells [5, 6], there are still serious limitation to the use of hPSC-CMs for pre-clinical screening of novel therapeutics.

hPSC-CMs are typically characterized as fetal-like cells and are not representative of the adult cardiomyocyte phenotype. Specifically, hESC-CMs display an immature sarcomere structure characterized by the absence of H zones, I bands and M lines (embryoid bodies (EBs) day 40 [7]), high proliferation rates (~17%, EBs day 37 [8], ~10%, EBs day 21-35 [7]), spontaneous beating due to high pacemaker currents [9], immature sarcoplasmic reticulum [10] and a round/oval shape [11]. In order for hPSC-CMs to be used as a reliable cell source for pre-clinical testing, means to mature hPSC-CMs need to be developed.

In order to improve the maturity of hPSC-CMs many different aspects of cardiac biology have been mimicked *in vitro*, such as: hormone treatment [12], microRNAs [13], culture time [14], mechanical stimulation [15, 16], electrical stimulation [17], shear forces [18, 19], cell composition [20] and decellularized cardiac extracellular matrix [21, 22]. However, these techniques do not achieve an adult like cardiac phenotype. For instance, mechanical stimulation seems to provide the necessary cues to instigate cardiomyocyte hypertrophy which results in cell enlargement through myofibrillogenesis [15]. Yet, the calcium handling and electrophysiology of cardiomyocytes during mechanical cyclic stretch has not been shown to mature. Moreover, in some instances, cyclic stretching resulted in abnormally long action potential durations (up to 1200ms) with resting membrane potentials of hPSC-CMs at -49.1mV [16], less negative than the comparable 7-8 week old EBs which had -60.7mV resting potential. Contrasted to this, electrical

stimulation has been shown to improve cardiomyocyte resting membrane potential and develop a functioning sarcoplasmic reticulum but, is not able to stimulate myofibrillogenesis [17].

1.3   FATTY ACID OXIDATION

Fatty acid oxidation is a process in which fats are broken down to supply the citric acid cycle with Acetyl-CoA to generate ATP. Fatty acids (FAs) are categorized into four categories: short chain (SC), medium chain (MC), long chain (LC) and very long chain (VLC) fatty acids. SCFAs, carbon length 1-5, along with MCFAs, carbon length 6-12, do not require active transport mechanisms to enter the mitochondria via the carnitine shuttle. These FAs supposedly get functionalized in the mitochondrial matrix by different acyl-CoA synthetases [23]. VLCFAs, carbon length 22 and greater, are too long to be oxidized in the mitochondria and are instead oxidized in peroxisomes. LCFAs, carbon length 13-21, require active transport into the mitochondria. FAs are typically produced by lipolysis, transported through the blood bound to albumin to the cell [24]. LCFAs are taken up by the cell via the CD36 membrane bound transporter. Once in the cell, fatty acid binding proteins will bind and stabilize the free fatty acids and be transported into the mitochondria via one of the long chain fatty acid CoA ligase (ACSL) proteins. This will convert the free fatty acid into a fatty acid acyl-CoA ester as a result "activating" the fatty acid for fatty acid β-oxidation [25].

Fatty acid acyl-CoAs that are in the outer membrane of the mitochondria will be transported into the mitochondrial matrix via the mitochondrial carnitine palmitoyl transferase system [25]. Carnitine palmitoyl transferase I (CPT I), located on the outer mitochondrial membrane, will take a long-chain acyl-CoA and carnitine and create a long-chain acyl-carnitine. This long-chain acyl-carnitine is readily transported across the inner mitochondrial membrane by carnitine:acylcarnitine translocase (CACT). Finally, once inside the mitochondrial matrix, CPT II

takes the long-chain acyl-carnitine and frees the carnitine to reform the long-chain acyl-CoA. The carnitine is now free to be recycled and the long-chain acyl-CoA is now ready to undergo fatty acid β-oxidation.

Fatty acid β-oxidation is a four-step process in which a two-carbon acetyl-CoA is removed from a FA-acyl-CoA to be used for ATP production in the TCA cycle. The first step of β-oxidation is controlled by a family of enzymes that each bind to a specific chain length of FA. The acyl-CoA dehydrogenase family of FAD-requiring oxidoreductases consist of very long-chain, long-chain, medium-chain and short-chain acyl-CoA dehydrogenase (VLCAD, LCAD, MCAD and SCAD). VLCAD is a membrane bound enzyme while MCAD and SCAD are found in the mitochondrial matrix [26, 27]. Steps two through four take the FA through a hydratase, dehydrogenase and finally a β-ketothiolase step to cleave a two carbon group with an acetyl-CoA and the subsequent fatty acid with its acyl group. For LCFAs, a protein called mitochondrial tri-functional protein controls steps two through four while a series of other proteins are responsible for MCFAs and SCFAs.

MTP is a hetero-octamer composed of four alpha and four beta subunits: HADHA and HADHB [28]. HADHA contains β-oxidation steps two, hydratase, and three, dehydrogenase, while HADHB contains the finally fourth step, β-ketothiolase [29, 30]. The MTP complex needs to be assembled in order for membrane translocation and catalytic stability of the individual enzymes [31, 32]. For MCFA and SCFA, step two is controls by short-chain enoyl-CoA hydratase (ECHS1). For step three, there is a medium- and short-chain L-3-hydroxyacyl-CoA dehydrogenase (HADH) [33, 34] while for step for there is MCKAT [29, 35, 36].

1.4   FATTY ACID OXIDATION DISORDERS

Fatty acid oxidation disorders consist of about 20 defects in genes associated with fatty acid transport and mitochondrial fatty acid β-oxidation (Table 1-1). These inherited disorders are autosomal recessive disorders with an incidence rate ranging from 1:8000 to 1:100,000 [37]. Fatty acid oxidation disorders have a broad spectrum of clinical presentation with either neonatal onset with hyperammonemia, transient hypoglycemia, metabolic acidosis, cardiomyopathy and sudden death [38]. Late onset is typically characterized with neuropathy, myopathy and retinopathy [37]. Fortunately, there are now newborn screening methods using mass spectrometry to assess the composition of blood spots. However, one of the most severe fatty acid oxidation disorders is mitochondrial tri-functional protein deficiency. This disorder results in impaired long-chain fatty acid oxidation and has not cure.

Table 1-1: Fatty acid oxidation disorders

Type of disorder	Gene	Location of protein
Disorders of plasma membrane function	SLC22A5	Plasma membrane
	CD36	Plasma membrane
Disorders of fatty acid transport across the mitochondrial membranes	CPT I	Outer mitochondrial membrane
	CACT	Inner mitochondrial membrane
	CPT II	Inner mitochondrial membrane
Disorders of long-chain fatty acid β-oxidation	VLCAD	Matrix
	MTP	Matrix
	LCHAD	Matrix
Disorders of medium-chain fatty acid β-oxidation	MCAD	Matrix
	HADH (MSCHAD and SCHAD)	Matrix
	MCKAT	Matrix
Disorders of short-chain fatty acid β-oxidation	SCAD	Matrix

1.5 MITOCHONDRIAL TRI-FUNCTIONAL PROTEIN DEFICIENCY AND LCHAD DEFICIENCY

Mitochondrial trifunctional protein (MTP) deficiency is a disease that manifests in the cardiac system after birth since the main dietary source, breast milk, is high in fats and precipitates the disease pathology. MTP deficiency is caused by mutations in either hydroxyacyl-CoA dehydrogenase/3-ketoacyl-CoA thiolase/enoyl-CoA hydratase subunit A (HADHA) or subunit B (HADHB). The result is a severe limitation in long chain fatty acid oxidation (FAO) and is considered one of the more severe FAO disorders without pharmacological treatment [28]. Mitochondrial fatty acid oxidation (FAO) disorders are recessively inherited, and defects in FAO are estimated to affect ~1 in 10,000 [39]. The estimated prevalence of MTP defects in association with fetal MTP defects in the US is 1 in 38,000 pregnancies [40].

Mutations that occur in either HADHA or HADHB can result in MTP deficiency with a reduction in enzymatic activity across all three enzymes [41]. MTP deficiency is characterized biochemically when all three enzymes are deficient resulting in no immunoreactive protein detection. This occurs when there are mutations in both HADHA [40, 42, 43] and HADHB [31, 44]. A second cause of MTP deficiency is a result of mutations primarily in the second enzyme pocket of HADHA, long-chain 3-hydroxyacyl-CoA dehydrogenase (LCHAD). When LCHAD is the primary region where mutations occur, typically the enzyme activity of the thiolase in HADHB is unaffected. When assaying these enzymes biochemically, there is a normal amount of immunoreactive protein. This form of MTP deficiency is typically referred to as LCHAD deficiency [45]. A common mutation has been identified in LCHAD deficient patients where at least one of the alleles harbors a G1528C mutation substituting glutamate at the amino acid position 474 by glutamine (E474Q) [46-48].

The clinical manifestation of MTP deficiency can be presented with great variability but there are three general phenotypic groups that have emerged. 1) a lethal form with predominating cardiomyopathy, 2) beginning during infancy there are mostly hepatic complications and 3) a milder and later-onset presentation of neuro-myopathic complications [49]. In almost all cases reported with complete MTP deficiency, the infants have died during the first week of life despite immediate therapeutic interventions. The lethal phenotype of these infants is characterized by severe dilated cardiomyopathy, lactic acidosis and a Reye-syndrome like presentation with hypoketotic hypoglycemia and hepatic encephalopathy. In the infants with a less severe phenotype, category 2 hepatic phenotype, typically suffer from episodes of hypoketotic hypoglycemia and lethargy that is typically triggered by minor infections or fasting [50]. However, only half of the patients diagnosed with MTP deficiency show the fatal form of the disease and instead manifest less severe phenotypes later in childhood and even in adolescence or adulthood [43, 49].

The clinical manifestation of LCHAD deficiency is more uniform as compared to MTP deficient patients. Patients with LCHAD deficiency typically present with the common mutation, G1528C, with at least one allele carrying this point mutation. This results in an intact mutant protein that has significantly reduced LCHAD activity with the other enzyme activities found in HADHA (LHYD) and HADHB (LKAT) remaining at 60% or greater of their normal capacity [50]. The clinical manifestation is LCHAD deficient patients is moderate or severe multiorgan involvement either neonatally or during the first two years of life. The liver is one of the most affected organs displaying hypoketotic hypoglycaemia. Following this are cardiomyopathy, severe liver disease with cholestasis and hypotonia [51]. Peripheral neuropathy is common as a long-term complication in LCHADH deficient patients. LCHAD deficiency has an associated

high morbidity and mortality, however, the disorder can also be managed resulting in long-term survival of patients diagnosed and treated from an early age [51, 52].

1.6   CURRENT TREATMENTS FOR MTP AND LCHAD DEFICIENCY

The main therapy for patients that are suffering from MTP or LCHAD deficiency are dietary changes. Since patients can not process long-chain fatty acids, the majority of treatments revolve around minimizing the consumption of long-chain fatty acids [53]. This results in a low-fat diet where 10% of caloric intake is long-chain fatty acid, 11% as medium chain, 12% as protein and 66% as carbohydrates [54]. It is also important that the children do not fast as the body will begin to metabolise fats during this period. A few centers that treat patients for this disease have implemented strict guidelines to avoid fasting by including a gastrostomy tube with continuous overnight feeding [55].

1.7   FATTY ACID LIPID TOXIC INTERMEDIATES

It is unclear how MTP deficiency results in sudden death and cardiomyopathy. A mouse model of MTP deficiency has been generated by Ibdah *et al.* [56]. HADHA$^{+/-}$ and HADHA$^{-/-}$ mice were generated. It was found that the heterozygous mice had minimal complications other than slight growth retardations, however, the HADHA KO mice displayed intrauterine fetal growth retardation, hypoglycemia and early neonatal death. When examining amounts of fatty acids in the mice, the HADHA KO mice displayed elevated C8-C14 urine dicarboxylic acids and C14-C18 serum acyl carnitines and fatty acids [56]. Furthermore, serum free carnitine levels were significantly reduced in the HADHA KO mice as compared to WT. These data suggest that the neonatal heart may be highly susceptible to the toxic effect of long chain free fatty acids and acylcarnitines.

The same buildup of fatty acids seen in the HADHA KO mouse have also been identified in human patient fibroblasts [57]. MTP deficient patients displayed abnormally low 3-hydroxybutyrate levels and increased urinary excretion of a range of dicarboxylic acids. When MTP deficient patient fibroblasts were cultured, they showed lowered rates of palmitate oxidation along with depressed functionality of long-chain enoyl-CoA hydratase, long-chain 3-hydroxyacyl-CoA dehydrogenase and long-chain 3-oxoacyl-CoA thiolase [57]. In both LCHAD or MTP deficient patient fibroblasts there was an increase of hydroxylated fatty acids. Specifically, 3-OH-hexadecanoic and 3-OH tetradecanoic FAs were increased in both LCHAD and MTP deficiency fibroblasts [58].

Acylcarnitines cause issues. Palmitoylcarnitine has been shown to have detergent properties on isolated canine myocytic sarcolemmal membranes and can potentiate free radical-induced lipid membrane peroxidative injury in ischemia [59].

Lack or impairment of mitochondrial trifunctional protein leads to impaired FA β-oxidation. It is possible that lack of MTP could lead to SIDS due to respiratory from a poorly functioning diaphragm or cardiac abnormalities. In MTP null mouse pups, it was found that the all pups that died after birth had both acute degenerative changes in the cardiac and diaphragmatic myocytes. Pups that were symptomatic after birth were found to have moderate to severe cardiomyocyte degeneration and necrosis but no acute degenerative changes in the diaphragm. The authors concluded that the underlying etiology for sudden death was the cardiac and diaphragmatic lesions. Furthermore, the cardiac lesions may have caused cardiac arrhythmias [56]. Other studies also point towards the potential for arrhythmogenicity intermediary metabolites of fatty acids, such as long-chain acylcarnitines, that could be causing arrhythmias

[60]. It is clear that defects in fatty acid oxidation have a role in SID, however, the exact mechanism of action is not understood.

One of the hallmark symptoms of MTP deficiency is sudden infant death syndrome (SIDS). In general, fatty oxidation disorders present with cardiomyopathy, progressive skeletal myopathy and hepatic failure, however, sudden death and arrhythmia are highly associated as well [60]. In 107 patients diagnosed with fatty acid oxidation disorders, 24 cases had the main symptom of arrhythmia. Out of these 24 cases there were 15 ventricular tachycardias, 4 atrial tachycardias, 4 sinus node dysfunctions with episodes of atrial tachycardia, 6 atrioventricular blocks, and 4 left bundle-branch blocks in newborn infants. It was found that conduction disorders and atrial tachycardias were in patients that had long-chain fatty acid transport across the inner mitochondrial membrane disorders and in patients with MTP deficiency [60]. While it is clear that MTP deficiency can result in cardiac arrhythmias, most likely resulting in SIDS, it is unclear how the cardiomyocyte enters an arrhythmic state due to fatty acid intermediate and/or long-chain acylcarnitine build up.

1.8 HADHA'S POTENTIAL ROLE AS AN ACYL-TRANSFERASE

It has been previously shown that the HADHA protein has a similar enzymatic function to monolysocardiolipin acyltransferase (MLCL AT) [61]. MLCL AT transfers mainly unsaturated fatty acyl chains to lyso-CL. It therefore seems plausible that HADHA has a direct role in remodeling cardiolipin to produce mature tetra[18:2] CL species in cardiomyocytes. Once tetra[18:2] CL species begin to deplete, the CM can fall into a pathological state of mitochondrial disarray. These data suggest that a mutation in the HADHA enzyme results in increased levels of MLCL and production of abnormal cardiolipin species. Lack of correct cardiolipin species can be causal for mitochondrial defects and pathology seen in HADHA CMs.

1.9 CARDIOLIPIN'S ROLE IN HEALTH AND DISEASE

Cardiolipin (CL) is a critical component of the mitochondrial inner membrane. It is an atypical phospholipid composed of four (instead of two) acyl chains that are connected with a glycerol moiety. This atypical structure of cardiolipin results in a conical shape that is thought to be critical for inner mitochondrial membrane structure and function [62]. In particular, cardiolipin has been shown to function in organizing the electron transport chain (ETC) higher order structure, important for ETC activity, and acts as a proton trap on the outer leaflet of the inner mitochondrial membrane [63-65].

CL is the major phospholipid of the mitochondrial inner membrane and is synthesized in the mitochondria. CL is dynamically remodeled during postnatal development and disease [66, 67] with the most abundant species of CL in the adult human heart being tetralinoleoyl-CL (tetra18:2) [68] . Hence, the reduction of the mature form of CL results in mitochondrial abnormalities such as proton gradient loss, ETC depression resulting in depressed ATP production and abnormal mitochondrial architecture [64]. Specifically, in cardiac diseases such as diabetes, ischemia/reperfusion and heart failure, or in more specific Tafazzin mutant in Barth syndrome, tetra18:2 CL levels decrease [69-72].

Cardiolipin synthesis occurs in the inner membrane of the mitochondria unlike many mitochondrial membrane lipids that are synthesized in the endoplasmic reticulum [73]. There are a series of enzymatic steps that convert phosphatidic acid (PA) to CDP-diacylglycerol (CDP-DAG) [74]. CDP-DAG gets converted into a phosphatidylglycerolphosphate (PGP) via PGP synthase [75]. PGP is then dephosphorylated to phosphatidylglycerol (PG) via PGP phosphatase [76] and finally CL synthase adds a second phosphatidyl group to PG to make CL [77].

Once CL has been synthesized, it undergoes a remodeling process that is tissue specific. CL remodeling is the process in which different acyl chains are added or removed to CL. As previously mentioned, the majority of CL in the heart is remodeled so that it contains four linoleoyl-acyl groups. Currently, it is thought that CL can be remodeled through two mechanisms. The first way is through a two-step mechanisms where CL is deacylated to monolyso-CL (MLCL) by phospholipases (iPLA$_2\beta$, iPLA$_2\gamma$, cPLA$_2$ and sPLA$_2$) [78] and then re-acylated to remodeled CL by tafazzin [79]. In the one-step mechanism, CL is remodeled directly by transacylation. This can occur via MLCL acyltransferase 1, which is most likely HADHA, acyl-CoA:lysocardiolipin acyltransferase-1 (ALCAT1) and tafazzin (TAZ) [64, 80, 81]. It is clear that mutations or the absence of TAZ results in altered CL species. However, the loss of MLCL-AT1/HADHA or ALCAT1 do not consistently have altered CL acyl chain compositions. Currently, it is thought that MLCL-AT1/HADHA or ALCAT1 do not significantly contribute to normal CL acyl chain remodeling but rather have a smaller supporting role in comparison to TAZ [82].

Pathological remodeling of CL has been implicated in the mitochondrial dysfunction observed in diabetes, heart failure, neurodegeneration, and aging [64, 83]. Interestingly, previous studies using HeLa cells have suggested HADHA exhibits acyl-CoA transferase activity upon monolysocardiolipin (MLCL) for its remodeling into cardiolipin [61]. As such, these data suggest that defects in HADHA directly cause impaired cardiolipin remodeling resulting in the inability to produce and possibly maintain the acyl chain composition of mature cardiolipin [84]. However, the exact contribution of this acyltransferase to physiological CL remodeling has been unclear [61].

Cardiolipin is highly susceptible to reactive oxygen species, resulting in oxidative damage [85]. When this occurs, there is a reduction in the enzymatic activities of complexes I, III and IV

[86, 87]. It has also been shown that the stability of the electron transport chain super-complex is affected by CL oxidation and that similar issues of CL alternations and ETC attenuation has been reported in Barth syndrome patients [88, 89]. It is thought that CL is the phospholipid that is required to stabilize the ETC proteins since exogenously added CL-liposomes almost completely prevented the loss of complex I, III and IV activities when CL was oxidized. Moreover, other phospholipids such as phosphatidycholine (PC) and phosphatidylethanolamine (PE) and oxidized CL were unable to rescue the complexes I, III and IV function [90]. These data suggest that CL is highly susceptible to oxidation and that oxidized CL results in reduced ETC efficiency.

1.10 MODELING METABOLIC CARDIOMYOPATHIES USING HIPSC-CMS

There are a number of metabolic based cardiomyopathies that result in disrupted metabolism [91]. With the advent of iPSC technology, we can now study human patient specific diseases to 1) better understand the disease using a human model and 2) perform drug screens to elucidate novel therapies. Two examples of iPSC-CM cardiac metabolic disease modeling have been recently published examining Barth syndrome and diabetic cardiomyopathy.

Barth syndrome, an x-linked cardiac and skeletal myopathy, is the result of a mutation in the gene tafazzin [79]. Tafazzin is the gene responsible for producing the enzyme acyltransferase. When acyltransferase has reduced function, the normal acylation of cardiolipin, the major phospholipid of the mitochondrial inner membrane [92], is decreased and leads to mature cardiolipin depletion [93]. Using a combination of patient derived cardiomyocytes and Cas9-mediated genome editing, it was shown that a mutation in tafazzin was sufficient to cause the patient disease phenotype. Furthermore, it was shown that the contractile deficit found in the Barth syndrome hiPSC-CMs was not a result of global cellular energy depletion but rather tafazzin deficiency resulted in impaired sarcomere assembly and contractile stress generation. However,

tafazzin deficiency did lead to increased reactive oxygen species (ROS) production while the suppression of ROS led to the normalization of metabolic, sarcomerogenesis and contractile phenotypes in Barth syndrome hiPSC-CMs [93].

Diabetic cardiomyopathy (DCM), a complication of type 2 diabetes mellitus (T2DM), has been shown to result in dilated cardiomyopathy and heart failure [94]. T2DM induces a pathological metabolic state in cardiomyocytes that is different from non-diabetic complicated heart failure. As previously discussed, heart failure results in a reversion of cardiomyocytes from fatty acid β-oxidation to a fetal like profile that has increased reliance on glucose oxidation. However, since there is insulin resistance in T2DM myocardium, T2DM instead promotes fatty acid β-oxidation in cardiomyocytes with pathological consequences. The three main perturbations are: 1) decreased ATP per O_2 produced during fatty acid β-oxidation, 2) accumulation of toxic lipid metabolites and 3) mitochondrial dysfunction and ROS production that elevate proteases which results in cleaved myofilament proteins. Drawnel *et al*. generated two hiPSC lines from patients of different clinical histories to best test the likelihood that genetic/epigenetic predisposition would affect phenotype. A fast progression (FP) patient that showed cardiovascular disease within 5 years of initial diabetes diagnosis and a slow progression (SP) with no cardiovascular disease despite 15 years of T2DM were generated [95].

The authors showed that their *in vitro* diagnosis model of DCM was able to distinguish differences in disease severity between the FP and SP hiPSC-CMs. Using this platform, a small molecule screen was performed to find novel therapeutics that may rescue the DCM phenotype. Many traditional pathways common to treating diabetic cardiac dysfunction such as molecules that prevent calcium entry, reduce calcium in the sarcoplasmic reticulum or inhibit calcium-regulated proteins were found. A novel pathway of DCM rescue that came from this screen was the category

of small molecules related to protein synthesis inhibition. It is known that DCM cardiomyocytes experience lipotoxicity and lipid peroxidation which suggests the activation of proteolytic enzymes, promotion of ER stress and leakage of calcium from the sarcoplasmic reticulum [96]. Since the promotion of ER stress leads to an increase in the unfolded protein response to increase cellular resilience, the authors postulated that using inhibitors of protein synthesis prevents accumulation of nascent unfolded proteins and reduces load on the ER. As a result, protein synthesis inhibition would protect the cell from further loss of sarcomeric integrity [95].

1.11 MYOCARDIAL INFARCTION

Myocardial infarction (MI) as a result of cardiovascular disease continues to be a top cause of mortality in the United States [97]. While current MI treatments alleviate the immediate and acute symptoms of MI, they fail to address the later-stage cardiomyocyte remodeling, fibrosis, and scarring that leads to deterioration of cardiac function. Consequently, patients experience chronic heart failure and recurring MI episodes that require frequent hospitalizations, placing a heavy burden on the healthcare system [97]. Moreover, patient quality of life is severely compromised due to the physical, emotional, and psychological stress that these effects impose. However, current medications merely address the symptoms (high blood pressure, high cholesterol) rather than the adverse remodeling that occurs post-MI [97].

For nearly a century, cardiovascular disease (CVD) has remained the top cause of mortality in the United States and worldwide, almost reaching 800,000 deaths in 2009 [97]. CVD is correlated with risk factors such as obesity, smoking, and diabetes, and is especially prevalent in developed countries. Nearly 15.4 million Americans have coronary heart disease (CHD) [97], which left unaddressed may result in myocardial infarction (MI) due to occlusion of the coronary arteries that supply blood to the heart. In MI, oxygen deprivation results in necrosis and scarring

of the left ventricle, resulting in long-term, adverse consequences for the patient: physical limitations due to reduced cardiac functionality and emotional and psychological stress for fear of another MI episode. Moreover, patients often have recurring MI episodes and therefore require frequent hospitalizations, checkups, and surgical intervention, placing a significant burden on the healthcare system ($195.2 billion/year) [97]. These consequences are greatly underscored and exacerbated by the limited regenerative capacity of the heart.

1.12   THERAPIES TO REGENERATE THE HEART

Due to the inability of the heart to regenerate there has been considerable interest in developing strategies to re-muscularize the heart. Many fate mapping experiments have shown there is very little evidence for stem cell populations residing in the heart that may significantly contribute to myocardial repair [98, 99]. However, one exciting avenue to re-muscularize the heart is to utilize the transplantation of stem cell derived cardiomyocytes [100]. This work has been taken through non-human primate studies showing that after infarction, the transplantation of hiPSC-CMs is able to re-muscularize the heart and partially restore function [101]. While this solution currently has limitations situated around: cell maturation, arrhythmogenesis and immunosuppression, this currently leads the field in terms of a clinical solution. An interesting alternative approach is the transdifferentiation of cells into cardiomyocytes. Since there is large scar tissue that is formed after a MI, the hope would be to transdifferentiate the residing fibroblasts into cardiomyocytes [102, 103]. However, the main limitation with transdifferentiation is that the efficiency of the reprogramming is very limited. As a result, not enough cells actually get reprogrammed into cardiomyocytes leading to poor functional changes.

Finally, there is one more avenue to pursue to bring about cardiac regeneration: promoting the endogenous cardiomyocytes to proliferate. The ideal situation would be to deliver factors to

the heart that would promote endogenous repair without having to inject any cells, no immunosuppressants and avoid virally infecting a patient with direct reprogramming factors. Much work has been done in this area to identify pathways in model organisms, like the zebrafish, that can promote cardiomyocyte proliferation [104]. While much work has been done in understanding the pathways that turn on during cardiac regeneration in model organisms, the initial events that start this process are not well understood. A better understanding of how a cardiomyocyte enters a proliferative state and why it retains that capacity in the adult state remain important questions that need to be answered to better develop therapies to treat human MI patients.

1.13 DISSERTATION OVERVIEW AND SIGNIFICANCE

The research in this thesis aimed at understanding the metabolic state of cardiomyocytes during development/maturation, a disease called mitochondrial tri-functional protein deficiency and regeneration. Chapter 1 described the current understanding and limitations in our knowledge of how metabolism shifts during cardiomyocyte maturation and de-differentiation, during regeneration, and how the metabolic state of a cardiomyocyte is perturbed in the fatty acid oxidation disorder mitochondrial tri-functional protein deficiency. Chapters 2 through 4 describe the rationale, scientific methods and results of the following three specific aims:

Aim 1: Generate a microRNA maturation cocktail to accelerate human stem cell derived cardiomyocyte maturation.

Aim 2: Elucidate the molecular mechanisms underlying mitochondrial tri-functional deficiency pathology in human stem cell derived cardiomyocytes.

Aim 3: Identify the early responding signals that pre-dispose a cardiomyocyte to re-enter the cell cycle and regenerate a damaged heart.

The work contained in the following three chapters have many implications in stem cell derived cardiomyocyte maturation and regeneration. The results found in aim 1 provided insight into stem cell derived cardiomyocyte maturation. We were able to screen seven microRNAs implicated in stem cell derived cardiomyocyte maturation and identified three novel microRNAs to combine with Let7 to bring about a robust maturation process. This microRNA maturation cocktail was termed MiMaC and consisted of the over-expression of Let7i and miR-452 and the knockout of miRs-122 and -200a. MiMaC was able to generate hiPSC-CMs that had greater cell size, force of

contraction, metabolic activity and the ability to utilize fatty acids. Furthermore, we identified a common predicted target of the knockout microRNAs used in MiMaC as the homeodomain-only protein (HOPX). HOPX overexpression was found to bring about hiPSC-CM cell size increase and on a transcript level the repression of cell cycle via the repression of nuclear kinetochore proteins. Our results in aim 2 resulted in the discovery of the initial precipitating factor leading to the pathological cardiac state found in mitochondrial tri-functional protein deficiency as being a cardiolipin remodeling defect. We then showed that mutations with HADHA correlated with cardiolipin remodeling defects. These data suggest that HADHA may have a direct role in remodeling the acyl-fatty acid side chains of cardiolipin and that mitochondrial tri-functional protein deficiency may have its disease etiology rooted in unstable cardiolipin management leading to mitochondrial dysfunction.

Finally, in aim 3, we identified that a pro-regenerative cardiomyocyte in adult zebrafish hearts and neonatal mouse hearts, is the result of a specific amino acid profile, high glutamine levels. We identified this cardiomyocyte state as being a "primed" state which is pro-regenerative. Furthermore, we identified one of the earliest signaling pathways that are engaged after cardiac injury as being the Wnt/β-catenin signaling pathways. We found that Wnt/β-catenin signaling drove Lin28 expression resulting in the de-differentiation of cardiomyocytes and also the activation of mTORC1. These data together show that a regenerating cardiomyocyte that has large amounts of glutamine are primed for regeneration and the combined amino acid and Wnt/β-catenin activation of mTORC1 to drive this regeneration process. This work provides insight into how cardiomyocytes mature and how their metabolism shifts during disease, maturation and regeneration.

Chapter 2. CREATING A MICRORNA COCKTAIL FOR HUMAN STEM CELL DERIVED CARDIOMYOCYTE MATURATION

Parts of this chapter is in the following manuscripts:

Fatty acid oxidation disorder gene TFPa/HADHA is required for cardiolipin re-modeling and mitochondrial proton gradient in human cardiomyocytes

Jason W. Miklas, Shiri Levy, Damien Detraux, Andrea Leonard, Kevin Beussman, Peter Hofsteen, Xiulan Yang, Jesse Macadangdang, Anup Madan, Deok-Ho Kim, Charles E. Murry, Nathan J. Sniadecki, Yuliang Wang, Hannele Ruohola-Baker

The transcriptional landscape of cardiac differentiation at single cell resolution

Clayton E Friedman, Quan Nguyen, Samuel W Lukowski, Abbigail Helfer, Han Sheng Chiu, Jason W. Miklas, Holly K Voges, Shengbao Suo Suo, Jing-Dong Jackie Han, Pierre Osteil, Guangdun Peng, Naihe Jing, Greg J Baillie, Anne Senabouth, Angelika N Christ, Timothy J Bruxner, Charles E Murry, Emily S Wong, Jun Ding, Yuliang Wang, James Hudson, Hannele Ruohola-Baker, Ziv Bar-Joseph, Patrick P L Tam, Joseph E Powell, and Nathan J Palpant

2.1   ABSTRACT

The ability to generate human cardiomyocytes from human induced pluripotent stem cells (hiPSC) provides an unprecedented opportunity to establish human in vitro cardiac models for disease modeling. Yet, the immaturity of hiPSC cardiomyocytes (hiPSC-CMs) prevents such technology from replacing animal models. An emerging area of hiPSC-CM maturation is in utilizing microRNAs (miRs) to change the hiPSC-CM gene profile to that of a mature myocyte. In this study, we performed a microRNA screen and identified four microRNAs, that when combined together, bring about robust hiPSC-CM maturation. This cocktail of microRNAs was termed MiMaC (MicroRNA Maturation Cocktail). MiMaC consists of two over-expression miRs: Let7 and -452 and two knock-out miRs: -122 and -200a. MiMaC was able to bring about an increase in hiPSC-CM cell size, twitch force, metabolic capacity and mature the hiPSC-CMs to the point where they can utilize fatty acids. Furthermore, we identified an intermediate cardiomyocyte maturation subgroup that appeared when miRs: Let7 and -452 were overexpressed in hiPSC-CMs. This intermediate group had a high up-regulation of oxidative phosphorylation genes, suggesting that metabolic re-arrangement may drive certain early aspects of cardiomyocyte maturation. Finally, we identified a common target of the knock-out microRNAs of MiMaC as HOPX. We generated a conditional over-expression line of HOPX to drive hiPSC-CM maturation. We found that HOPX over-expression led to an increase in area, in inhibition of cell cycle genes and a repression of serum response factor associated genes. We have now generated a scalable and robust platform to mature hiPSC-CMs termed MiMaC. This technology will significantly accelerate the fields ability to study cardiac disease in vitro utilizing hiPSC-CMs to better elucidate novel therapies.

2.2   RATIONALE

The heart's inability to naturally replace damaged tissue is a leading cause of death worldwide. The potential for utilizing human pluripotent stem cell derived cardiomyocytes (hPSC-CMs) for regeneration and modeling cardiac insult and disease may improve cardiac related therapeutic applications if factors that drive their maturation are uncovered.

Pluripotent stem cell derived cardiomyocytes (hPSC-CM) provide a means to study human disease *in vitro* but are limited due to their immaturity, representative of fetal cardiomyocytes (FCM) instead of adult cardiomyocytes (ACM) [105, 106]. Due to the lack of knowledge in how committed cardiomyocytes transition from an immature FCM to a mature ACM, many cardiac diseases with postnatal onset have been poorly characterized [107-111].   During cardiogenesis, FCMs go through developmental states and once past cardiomyocyte commitment exhibit: exit of cell cycle, cessation of spontaneous beating, utilization of lactate, and then at the post-natal stage utilization of fatty acids as the principal energy source [112-115].

Current approaches to mature hPSC-CMs toward ACM focus on prolonged culture [14], physically stimulating the cells with either electrical [17] or mechanical stimulation [15] or by 2D surface pattern cues to direct cell orientation [116]. An emerging area of hPSC-CM maturation is in manipulating microRNAs (miRs) [13, 117, 118]. We have shown that overexpressing just one miR, Let-7, can accelerate human embryonic stem cell derived cardiomyocytes (hESC-CM) maturation towards an ACM-like state [13]. However, no maturation regimen has been able to mature hPSC-CMs to an adult state.

To better understand the biological changes that occur during human cardiac maturation we conducted a microRNA screen where we found many significantly regulated miRs during the *in vitro* transition between Day20 hPSC-CMs and 1-year matured hPSC-CMs. We chose the

highest up-regulated family of miRs to study from the screen: the Let-7 family of miRs [13]. We showed that the overexpression of just one miR, Let7i or Let7g, drove a robust, albeit incomplete, maturation response in hPSC-CMs. We saw hallmarks of cardiomyocyte maturation such as: myocyte hypertrophy, increased transcript expression of structural, calcium handling and ion channel genes, an increased ability to oxidize fatty acids and an increased action potential duration. However, since the OE of just one miR was insufficient to bring about full cardiomyocyte maturation, we sought to combine multiple miRs to bring a more robust and full maturation response.

We performed a screen and identified multiple miRs that alone were able to bring about certain aspects of hPSC-CM maturation. This included, cell size, field potential duration, metabolic activity and twitch force. From this screen, the top 4 miRs were chosen to combine together to generate a MicroRNA Maturation Cocktail we termed MiMaC. This MiMaC cocktail consisted of two overexpression miRs: Let7i and -452 and two KO miRs: -122 and -200a. We found that MiMaC was able to bring about a robust hPSC-CM maturation.

Many fundamental transcriptional and epigenetic regulators have been studied during cardiac development [119-121] and disease [122] yet, there are limited studies for post cardiomyocyte commitment maturation. So far, studies to understand the transition of the glycolysis-dependent fetal heart to oxidative metabolism in the adult heart have been mostly related to the peroxisome proliferator-activated receptor (PPAR/estrogen-related receptor/PPARγ coactivator-1α (PGC1α) circuit [123-125]. However, it is currently unknown as to what other factors act upstream or in synergy with this pathway in controlling cardiac energetics.

We sought to identify a novel regulator of post committed cardiomyocyte maturation and found that a common predicted target of MiMaC's KO miRs was HOPX. HOPX is a

homeodomain protein that lacks the conserved residues required for DNA binding. Studies in mice have shown that this protein may interact with SRF and modulates SRF-dependent cardiac-specific gene expression and cardiac development. HOPX has been shown to modulate BMP4 signaling during cardiac development through the repression of Wnt signalling to bring about commitment of cardiomyoblasts [126]. We found that HOPX was able to regulate cardiomyocyte size, repress cell cycle genes and repress serum response factor gene loci in hiPSC-CMs when conditionally over-expressed for two weeks. These findings show that HOPX is a novel regulator of cardiomyocyte maturation and that MiMaC, in part, acts through HOPX to bring about hiPSC-CM maturation.

2.3   SCIENTIFIC METHODS

2.3.1   *hESC and hiPSC and cardiac differentiation*

The hESC line RUES2 (NIHhESC-09-0013) and hiPSC line WTC #11, previously derived in the

Conklin laboratory [127], were cultured on Matrigel growth factor-reduced basement membrane

matrix (Corning) in mTeSR media (StemCell Technologies).   A monolayer-based directed

differentiation protocol was followed to generate hESC-CMs and hiPSC-CMs, as done previously

[128]. hiPSC-CM cardiolipin assay was done with a small molecule monolayer-based directed

differentiation protocol, as done previously [129]. 15 days after differentiation hPSC-CMs were

enriched for the cardiomyocyte population using a lactate selection process [130]. We generated

cardiomyocyte populations ranging from 40-60% that were then enriched to 75-80%

cardiomyocytes after 4 days of lactate enrichment.

microRNA overexpression and knockout

We used LentiCrisprV2 plasmid (Addgene 52961) to KO microRNAs-141, -200a, -205

and -122. gRNAs for each miR that had either the protospacer adjacent motif (PAM) NGG cut

site adjacent or in the seed region of the mature microRNA were chosen to test. gRNAs can be

found in Supplement Table S12. The global reduction of each miR was assessed via TaqMan RT-

qPCR with probes specific against the mature form of each respective miR.

We used the pLKO.1 TRC vector (pLKO.1 - TRC cloning vector was a gift from David Root

(Addgene plasmid # 10878) to OE a microRNA [131]. The genomic sequence 200bp up- and

down-stream of the mature microRNA was amplified and purified. Primers for each microRNA

can be found in Supplemental Table S15. The amplicons were cloned between AgeI and EcoRI

sites of pLKO.1 TRC vector under the human U6 promoter.

2.3.2   *Viral particle production*

HEK 293FT cells were plated one day before transfection. On the day of transfection, the OE or KO plasmid of choice was combined with packaging vectors psPAX2 (psPAX2 was a gift from Didier Trono Addgene plasmid # 12260) and pMD2.G (pMD2.G was a gift from Didier Trono Addgene plasmid # 12259) in the presence of 1μg/μL of polyethylenimine (PEI) per 1μg of DNA. Medium was changed 24 hours later and the lentiviruses were harvested 48 and 72 hours after transfection. Viral particles were concentrated using PEG-it (System Biosciences, Inc).

2.3.3   *hiPSC-CM transduction and selection*

hiPSC-CMs were transduced on day 14 post-induction in the presence of hexadimethrine bromide (Polybrene, 6μg/ml). Lentivirus was applied for 17-24 hours and then removed. Cells were cultured for an additional two weeks. Lactate selection was employed to obtain an enriched population of cardiomyocytes [130]. Puromycin selection was used to select for cells that have positively incorporated the vector. After two weeks of culture, cells were harvested for end point analysis. For the MiMaC group, hiPSC-CMs were transduced with a lower dose of the four different lentiviruses concurrently while controls were transduced with both control vectors: pLKO.1 and the LentiCRISPRv2 empty vector.

2.3.4   *Immunocytochemistry and morphological analysis*

Cells were fixed in 4%(vol/vol) paraformaldehyde, blocked for an hour with 5% (vol/vol) normal goat serum (NGS), and incubated overnight with primary antibody in 1% NGS, followed by secondary antibody staining in NGS. Measurements of CM area were performed using Image J software. Quantification of mitotracker intensity were performed using Image J software and following previously published methods on co-localization quantification [132]. Analysis was

done on a Leica TCS-SPE Confocal microscope using a 40x or 63x objective and Leica Software. Primary antibodies used were: αActinin 1:250 Sigma A7811 anti-mouse, HADHA 1:250 abcam ab54477 anti-rabbit, ATP Synthase β 1:250 abcam ab14730 anti-mouse, Titin 1:300 Myomedix TTN-9 (cTerm) anti-rabbit, GFP 1:300 Invitrogen A-11122 anti-rabbit. Secondary antibodies and other reagents used were: DAPI at a concentration of 0.02μg/mL, phalloidin alexa fluor 568 1:250, alexa fluor 488 or 647-conjugated goat anti-mouse and anti-rabbit secondary antibodies 1:500 (Molecular Probes). MitotrackerCMTMRos Life technologies (M7510) used at a final concentration of 300nM in RPMI with B27 plus insulin supplement, incubated with cells for 45 minutes prior to fixation.

2.3.5 *Micro-electrode array*

Electrophysiological recording of spontaneously beating cardiomyocytes was collected for 2 minutes using the AxIS software (Axion Biosystems). After raw data collection, the signal was filtered using a Butterworth band-pass filter and a 90μV spike detection threshold. Field potential duration was automatically determined using a polynomial fit T-wave detected algorithm.

2.3.6 *Microposts force of contraction and beat rate*

Arrays of polydimethylsiloxane (PDMS) microposts were fabricated as previously described [133]. The tips of the microposts were coated with mouse laminin (Life Technologies), and cells were seeded onto the microposts in Attoflour® viewing chambers (Life Technologies) at a density of approximately 75,000 per cm^2 in RPMI medium with B27 supplement and 10% fetal bovine serum. The following day, the media was removed and replaced with serum-free RPMI medium, which was exchanged every other day. Once the cells resumed beating (typically 3 to 5 days after seeding), contractions of individual cells were imaged (at a minimum of 70 FPS) using

a Hamamatsu ORCA-Flash2.8 Scientific CMOS camera fitted on a Nikon Eclipse Ti upright microscope using a 60x water immersion objective. Prior to imaging, the cell culture media was replaced with a Tyrode buffer containing 1.8 mM Ca2$^+$, and a live cell chamber was used to maintain the cells at 37 °C throughout the imaging process. A custom-written matlab code was used to track the deflection, Δ_i, of each post i underneath an individual cell, and to calculate the total twitch force, $F_{twitch} = \sum_{i=1}^{\# posts} k_{post} \times \Delta_i$ [133], where $k_{post} = 56.5 \ ^{nN}/_{\mu m}$ and the spacing between posts was 6 μm.

2.3.7   *Seahorse Assay*

The Seahorse XF96 extracellular flux analyzer was used to assess mitochondrial function as previously described [13]. The plates were pre-treated with 1:60 diluted Matrigel reduced growth factor (Corning). At around 28 days after differentiation, cardiomyocytes were seeded onto the plates with a density of 50,000 cells per XF96 well. The seahorse assays were carried out 3 days after the seeding onto the XF96 well plate. One hour before the assay, culture media was exchanged for base media (unbuffered DMEM (Seahorse XF Assay Media) supplemented with sodium pyruvate (Gibco/Invitrogen, 1mM) and with 25mM glucose (for MitoStress assay), 25mM glucose with 0.5mM Carnitine for Palmitate assay. Injection of substrates and inhibitors were applied during the measurements to achieve final concentrations of 4-(trifluoromethoxy) phenylhydrazone at 1μM (FCCP; Seahorse Biosciences), oligomycin (2.5μM), antimycin (2.5μM) and rotenone (2.5μM) for MitoStress assay; 200mM palmitate or 33μM BSA, and 50μM Etomoxir (ETO) for palmitate assay. The OCR values were further normalized to the number of cells present in each well, quantified by the Hoechst staining (Hoechst 33342; Sigma-Aldrich) as measured using fluorescence at 355nm excitation and 460nm emission. Maximal OCR is defined as the

change in OCR in response to FCCP compared to OCR after the addition of oligomycin. ATP production was calculated as the difference between the basal respiration and respiration after oligomycin. Proton leak was calculated as the difference between respiration after oligomycin and after antimycin & rotenone. Cellular capacity to utilize Palmitate as an energy source was calculated as the difference between the average OCR after second palmitate addition and the final respiration value before the second addition of palmitate. The reagents were from Sigma, unless otherwise indicated.

2.3.8   *RNA-sequencing*

Day-30 hiPSC-CMs were harvested for RNA preparation and genome wide RNA-seq (>20 million reads). RNA-seq samples were aligned to hg19 using Tophat, version 2.0.13 [134]. Gene-level read counts were quantified using htseq-count [135] using Ensembl GRCh37 gene annotations. Genes with total expression above 1 normalized read count across RNA-seq samples in each binary comparison were kept for differential analysis using DESeq [136]. Princomp function from R was used for Principal Component Analysis. TopGO R package [137] was used for Gene Ontology enrichment analysis. To assess the effects of miR perturbation on cardiac maturation pathways, each condition was compared against their empty vector (EV), and up-regulated genes (>1.5 fold change) and down-regulated genes were identified (< -1.5 fold change). A hypergeometric test was performed on up- and down-regulated genes separately for enrichment against a curated set of pathways that are beneficial for cardiac maturation, resulting in a m by n matrix, where m is the number of pathways (m=7) and n is the number of conditions (n=6, including EV). The negative log10 of the ratio between enrichment p-value for up- and down-regulated genes were calculated to represent the overall net "benefit" of a treatment: large positive value (>0) means the treatment results in more up-regulation of genes in cardiac maturation pathways than down-regulation of

these genes, and more negative values means the treatment results in more down-regulation of genes in cardiac maturation pathways.

2.3.9   *Single cell RNA-sequencing*

10x genomics was used to obtain single cell RNA-Seq data. Cells were processed using the Chromium Single Cell 3 Reagents Kit (v2 chemistry) (10x genomics) and the manufacturer's protocol was followed. Raw single cell RNA-seq data is processed through the CellRanger pipeline from 10X Genomics. Output of the CellRanger pipepline is further analyzed using Seurat R package [138]. Cells with more than 40% of reads mapped to mitochondrial genes, less than 200 detected genes or less than 2000 Unique Molecular Identifiers (UMIs) are removed. Remaining cells are scaled by number of UMIs and % mapped to mitochondrial genes. Clusters are identified with *FindClusters* function in Seurat with resolution parameter 0.4. Genes detected in at least 25% of cells in either cluster and have false discovery rate<0.1 are defined as differentially expressed. Expression values are normalized for each gene across all cells plotted in the heat maps (i.e., Z-scores). Human in vivo maturation markers are based on genes up-regulated in adult heart compared to fetal heart in the Roadmap Epigenomics Project [139]. Moue in vivo maturation markers are based on genes up-regulated in the in vivo cardiomyocyte single cell RNA-seq data from Delaughter et al. [140]. Gene Ontology enrichment is performed using the TopGO package [137].

2.3.10   *Glucose and fatty acid media*

The base media which we are calling Glucose Media, is RPMI supplemented with B27 with insulin. The fatty acid media is the glucose media with oleic acid conjugated to BSA (Sigma

O3008): 12.7µg/mL, linoleic acid conjugated to BSA (Sigma L9530): 7.05µg/mL, sodium palmitate (Sigma P9767) conjugated to BSA (Sigma A8806): 52.5µM and L-carnitine: 125µM.

2.3.11   *Box plots*

The 'x' in each box plot denotes the average value while the horizontal bar denotes the median value, no outlier values are shown. * denotes P<0.05.

2.3.12   *Bar graphs*

Bar graphs show the mean±SEM. Bar graphs which do not show SEM are generated from RNA-Sequencing data that had one or two samples sequenced.

2.3.13   *STRING analysis*

Protein association maps were generated using STRING version 10.5. In each diagram, genes connected to one another have an association with one another. There are three action effects: arrow –> positive, --| - negative and line with a circle on the end – unspecified. There are also eight different action types that are denoted by line color: green – activation, blue – binding, cyan – phenotype, black – reaction, red – inhibition, purple – catalysis, pink – post-translational modification and yellow – transcriptional regulation. Kmeans clustering was used to identify the significantly changed genes due to MiMaC for: muscle structure development and extracellular matrix organization. Markov Clustering Algorithm (MCL) was used to identify genes MiMaC had down-regulated to control cell division.

2.3.14   *Statistical analysis*

Statistical analysis was performed on experiments with an N equal or greater to 3. P values were calculated using student t-test or one-way ANOVA. For student t-test a Shapiro-Wilk normality

test was performed. For one-way ANOVA a Kolmogorov-Smirnov normality test was performed. For multiple comparisons, the Holm-Sidak method was used. For one-way ANOVA analysis that failed the normality test, ANOVA a Kruskal-Wallis one-way ANOVA of Variance on Ranks was performed. For multiple comparisons, the Dunn's method was used. All statistical tests used an $\alpha=0.05$.

2.3.15 *HOPX OE-line creation*

$1x10^6$ WTC hiPSCs were transfected with 0.5μg AAVS1-TALEN, 0.5μg AAVS1-TALEN and 4μg of HOPX-NLS-eGFP or 4μg of NLS-eGFP to generate the HOPX OE line and the HOPX negative control (NC) line using Amaxa Lonza Human stem cell Kit #2. The cells were then plated with 5mM Rocki onto matrigel in mTeSR. Two days following the nucleofection, the cells were selected for Puromycin 0.5μg/ml for 2 days. The sequence for the HOPX-NLS-eGFP construct can be found below.

Table 2-1: Quantitative RT-qPCR primers for human genes

Gene Name	Forward Primer	Reverse Primer
MYL2	TGTCCCTACCTTGTCTGTTAGCCA	ATTGGAACATGGCCTCTGGATGGA
TNNC1	TGGTTCGGTGCATGAAGGAC	GTCGATGTAGCCATCAGCATT
GAPDH	CTGGGCTACACTGAGCACC	AAGTGGTCGTTGAGGGCAATG
NPPA	CAACGCAGACCTGATGGATTT	AGCCCCCGCTTCTTCATTC
HOPX-GFP	AGTGCAGATCCGTCACAGAC	GCTGAACTTGTGGCCGTTTA

2.3.16 *HOPX-NLS-eGFP construct sequence*

HOPX-NLS-GFP

ATGTCGGCGGAGACCGCGAGCGGCCCCACAGAGGACCAGGTGGAAATCCTGGAGTA

CAACTTCAACAAGGTCGACAAGCACCCGGATTCCACCACGCTGTGCCTCATCGCGGC

CGAGGCAGGCCTTTCCGAGGAGGAGACCCAGAAATGGTTTAAGCAGCGCCTGGCAA

AGTGGCGGCGCTCAGAAGGCCTGCCCTCAGAGTGCAGATCCGTCACAGACGGTGGT

CCAAAGAAGAAGCGGAAGGTCGGTGGTACCATGGTGAGCAAGGGCGAGGAGCTGT

TCACCGGGGTGGTGCCCATCCTGGTCGAGCTGGACGGCGACGTAAACGGCCACAAG

TTCAGCGTGTCCGGCGAGGGCGAGGGCGATGCCACCTACGGCAAGCTGACCCTGAA

GTTCATCTGCACCACCGGCAAGCTGCCCGTGCCCTGGCCCACCCTCGTGACCACCCT

GACCTACGGCGTGCAGTGCTTCAGCCGCTACCCCGACCACATGAAGCAGCACGACT

TCTTCAAGTCCGCCATGCCCGAAGGCTACGTCCAGGAGCGCACCATCTTCTTCAAGG

ACGACGGCAACTACAAGACCCGCGCCGAGGTGAAGTTCGAGGGCGACACCCTGGTG

AACCGCATCGAGCTGAAGGGCATCGACTTCAAGGAGGACGGCAACATCCTGGGGCA

CAAGCTGGAGTACAACTACAACAGCCACAACGTCTATATCATGGCCGACAAGCAGA

AGAACGGCATCAAGGTGAACTTCAAGATCCGCCACAACATCGAGGACGGCAGCGTG

CAGCTCGCCGACCACTACCAGCAGAACACCCCCATCGGCGACGGCCCCGTGCTGCT

GCCCGACAACCACTACCTGAGCACCCAGTCCGCCCTGAGCAAAGACCCCAACGAGA

AGCGCGATCACATGGTCCTGCTGGAGTTCGTGACCGCCGCCGGGATCACTCTCGGCA

TGGACGAGCTGTACAAGTAA

2.4   RESULTS

2.4.1   *Screening microRNAs for hPSC-CM maturation*

To better understand the biological changes that occur during human cardiac maturation we had previously conducted a miR screen where we found many significantly regulated miRs during the *in vitro* transition between Day-20 (D20) hPSC-CMs and 1-year matured hPSC-CMs [13]. We cross-referenced this list to *in vivo* miR-sequencing data of human fetal to adult ventricular myocardium [141, 142]. We previously found the highest up-regulated family of miRs, Let-7, could be overexpressed in hESC-CMs to drive a robust, albeit incomplete, maturation response [13]. We sought to build off this finding by combining multiple miRs together with Let-7 to rapidly mature hPSC-CMs by promoting a more complete adult like transcriptome. We chose the top 15 up- and down-regulated miRs from the screen and identified the top 200 predicted targets (TargetScanHuman) for each miR [143]. Using each miR's predicted targets, pathway analysis was performed using GeneAnalytics software to determine which miRs were affecting pathways associated with cardiomyocyte maturation. These included glucose and/or fatty acid metabolism, cell growth and hypertrophy and cell cycle. Many down-regulated miRs were associated with maintenance of a pluripotent state and were not chosen to screen for cardiomyocyte maturation. Six miRs were chosen based on the pathway analysis to assess for their CM maturation potency: three up-regulated miRs (miR-452, -208b and -378e) and three down-regulated miRs (miR-122, -200a, and -205) (Figure 2-1A).

The three candidate highly up-regulated miRs chosen were miR-378e [144], -208b [145] and -452. The family of 378 miRs was chosen due to their high expression level in matured CMs and involvement in cardiac hypertrophy. MiR-378e and -378f share the same seed region and we chose to focus on miR-378e as the representative miR for the 378 family. Mir-208b was chosen

due to its predicted involvement in both metabolic and cardiac hypertrophic pathways. Furthermore, miR-208b is an intronic miR in the gene myosin β-heavy chain (MYH7) and has been reported to have roles in specifying slow muscle fibers while repressing fast muscle fiber gene programs in mouse hearts [146]. MiR-452 was the second highest up-regulated miR, after Let-7, and was found to have predicted targets associated with metabolism.

The three candidate highly down-regulated miRs chosen were miR-200a, -122 and -205. MiR-141 and -200a share the same seed region and are involved in both hypertrophy and metabolism pathways. We chose miR-200a as the representative miR to study. The other two highly down-regulated miRs, miR-205 and miR-122, showed the greatest degree of down-regulation.

2.4.2 *Functional analysis of candidate microRNAs*

These six miRs were assessed using four functional tests to determine hPSC-CM maturation: cell area, force of contraction, metabolic capacity and electrophysiology. WT D15 hiPSC-CMs were transduced with a lentivirus to either OE a miR or KO a miR using CRISPR/Cas9. Cells were then lactate selected to enrich for the cardiomyocyte population and puromycin selected to enrich for the population containing the viral vector. Functional assessment was performed after two weeks of miR perturbation on D30 (Figure 2-1B).

An important feature of cardiomyocyte maturation is increase in cell size. We found that out of the tested miRNAs, only miR-208b OE brought a significant increase in cell area (EV: $2891\mu m^2$, 208b: $5802\mu m^2$, $P<0.05$) (Figure 2-1C and Figure 2-2A). Immature hPSC-CMs spontaneously beat at a high rate and have a short field potential duration when studied by extracellular micro-electrodes. Using micro-electrode arrays, we assessed if any of the OE miRs increased the field potential duration to a physiologically relevant length. Out of the tested

miRNAs, only miR-452 OE increased the corrected field potential duration (cFPD) to a more adult like duration (cFPD, EV: 296ms, 452: 380ms) (Figure 2-1D). One of the hallmarks of cardiomyocyte maturation is the increase in contractile force generated by the cell. We performed single cell force of contraction analysis using a micropost platform [13, 133, 147]. Out of the tested miRNAs, only the KO of miR-200a brought about a significant increase in force of contraction (EV: 30.8nN, miR-200a: 51.7nN, $P<0.05$) (Figure 2-1E and Figure 2-2B). Finally, we assessed the metabolic capacity of miR treated hPSC-CMs. Cardiomyocytes are a metabolically demanding cell type necessitating mitochondria that have a high capacity for ATP synthesis. Out of the tested miRNAs, only the KO of miR-122 brought about a significant increase in maximum oxygen consumption rate (OCR) indicating more active mitochondria (miR-122 KO: 1.35 fold change compared to EV, $P<0.001$) (Figure 2-1F and Figure 2-2C).

2.4.3 *Bioinformatic analysis of candidate microRNAs*

RNA-Sequencing was performed after alterations of some of the miRs (miR-378e OE, -208b OE, -452 OE, -122 KO or -205 KO) to assess their global transcriptional impact in hPSC-CMs. To determine if each miR was able to generate a differential effect on a global transcript level we analysed the samples using principal component analysis (PCA). In each sample, approximately 11,000 expressed protein-coding genes with an aggregated expression of at least three FPKM across all samples were used for PCA. PCA showed that each miR was able to bring a significant change from their respective controls (Figure 2-2D). MiR-452 OE had the largest separation on PC1 while miR-122 KO had the largest separation on PC2. This suggests that each of these two miRs have a robust influence on the hPSC-CM transcriptional profile. Furthermore, since none of the miRs clustered with one another, each miR was capable of inducing a unique expression signature.

Each miR's function was then analyzed in a more targeted manner by specifically examining pathways that are essential for cardiac maturation. A pathway enrichment heat map of how each miR influenced seven different pathways chosen as hallmarks of cardiomyocyte maturation (Figure 2-2E). MiR-122 KO had an up-regulation of cell cycle and fatty acid metabolism genes. MiR-452 OE showed an up-regulation of cardiac hypertrophy, electrophysiology and cytoskeleton. MiR-208b OE showed a strong up-regulation of cardiac identity along with cell cycle and electrophysiology genes. Finally, miR-378e OE showed an up-regulation of electrophysiology genes while miR-205 KO showed poor up-regulation of cardiac maturation related pathways. This heat map reinforces that each miR has a unique influence on cardiomyocyte maturation, as each miR brought about a different set of pathway enrichment. Furthermore, based on the heat map data miR-205 KO had a poor ability to bring about cardiomyocyte maturation while miRs-122 KO, -452 OE and -208b OE all showed a strong ability to influence hallmark pathways of cardiomyocyte maturation.

From these data, we generated a MicroRNA Maturation Cocktail we termed MiMaC, consisting of: Let7i OE, miR-452 OE, miR-122 KO, and miR-200a KO. Let7i was chosen due to our previous study showing the potency of this miR to bring about cardiomyocyte maturation [13]. From each of the functional assays, we chose a miR that brought a significant increase in maturation to generate a cocktail that consisted of the smallest number of miRs.

2.4.4   *Functional assessment of MiMaC*

To assess MiMaC treated hPSC-CM maturation we performed force of contraction, cell area and metabolic assays (Figure 2-3A). MiMaC treated hiPSC-CMs had a statistically significant increase in twitch force (mean force: 36 nN, $P = 0.002$) as compared to control cells (mean force: 24 nN) (Figure 2-3B,C). MiMaC treated hiPSC-CMs also had a statistically significant increase in power

generated (mean power: 38 fW, $P = 0.016$) as compared to control cells (mean power: 22 fW) (Figure 2-3D).

MiMaC treated hPSC-CMs had a statistically significant increase in cell area. Using hiPSC-CMs, MiMaC treated CMs had a mean area of 3022 μm^2, $P < 0.001$, as compared to control cells which had a mean area of 2389 μm^2 (Figure 2-3E,F). In addition to MiMaC's effect on hiPSC-CM, MiMaC also significantly increased the cell area of treated hESC-CMs (Figure 2-4A). One of the hallmarks of cardiomyocyte maturation is gaining the ability to utilize FAs to generate ATP. Immature hPSC-CMs are unable to utilize long chain fatty acids for ATP production via β-oxidation. To assess whether MiMaC treated hPSC-CMs could oxidize long chain FAs, we acutely challenged the cells with palmitate and measured if there was an increase in OCR. Both MiMaC treated hESC-CMs and hiPSC-CMs were able to utilize palmitate significantly greater than control CMs (Figure 2-3G and Figure 2-4B).

2.4.5   *Transcriptional assessment of MiMaC*

To gain a better understanding of how MiMaC was affecting the transcriptome of hiPSC-CMs we performed RNA-Sequencing comparing D30 EV control CMs to D30 MiMaC treated CMs. Pathway enrichment analysis using Hallmark gene set (Supplemental Table S1) showed that many cell maturation and muscle processes were up-regulated such as: myogenesis and epithelial mesenchymal transition [148]. The top down-regulated pathways were associated with cell cycle, a key feature of cardiomyocyte maturation. Using STRING Analysis, we determined the network of significantly up-regulated and interconnected genes associated with two pathways: myogenesis and epithelial mesenchymal transition (Figure 2-4C). STRING Analysis was also used to show the significantly down-regulated and interconnected genes associated with the mitotic spindle and

G2M checkpoint (Figure 2-4D). These findings show that the MiMaC tool is able to promote a more mature transcriptome in hiPSC-CMs.

2.4.6   *scRNA-Sequencing analysis of miR treated CM maturation*

To utilize the MiMaC tool to provide further insight into underlying mechanisms of cardiomyocyte maturation and to garner a better understanding of how each miR that constitutes MiMaC behaves in CM maturation, we performed single cell RNA-Sequencing (scRNA-Seq) on five groups of miR treated CMs: EV, Let7i & miR-452 OE, miR-122 & -200a KO, MiMaC and MiMaC + FA. Unbiased clustering was performed to determine how the miR perturbations changed CMs; we found five subgroups (Figure 2-3L) and used the Chi-square test to assess whether the miR perturbations resulted in enrichments in these five clusters (Figure 2-3M). The EV group was enriched in clusters 0 and 3, Let7i and miR-452 OE group was enriched in clusters 0 and 1, miR-122 and -200a KO group was enriched in clusters 0 and 3 and MiMaC and MiMaC + FA were enriched in clusters 1 and 2. Cluster 4 mainly consisted of cells with poor read counts and was not analyzed further. Characterizing the cell fate in each subgroup showed the majority of cells were cardiomyocytes with a very small subset of cells in cluster 1 displaying fibroblast (ENC1, DCN and THY1) and epicardial markers (WT1, TBX18) (Figure 2-4F). These data indicate that our lactate enrichment protocol successfully generated highly enriched cardiomyocyte populations.

To rank which clusters had a higher degree of cardiomyocyte maturation we assessed the scRNA-Seq clusters in two different ways. First, we assessed the genes highly up- and down-regulated in the MiMaC enriched cluster, cluster 2, along with cardiac markers and oxidative phosphorylation genes (Figure 2-3N and Supplemental Table S2) [140]. Next, we examined *in vivo* human cardiac maturation markers in the identified clusters (Figure 2-3O and Supplemental Table S3). We found that cluster 2 had genes associated with myofibril structural proteins highly

up-regulated and ribosomal and ECM adhesion genes down-regulated (Figure 2-3N). The mean expression levels of the in vivo maturation marker genes were significantly higher in cluster 2 as compared to the other clusters (Figure 2-3O; $P < 2 \times 10^{-16}$, using linear mixed effects model). Based on these findings, we ranked each cluster from least mature to most mature as cluster: $0<1<3<2$. Cluster 2, the most mature CM cluster enriched for the MiMaC treated CMs, showed the highest expression of HOPX, a gene that is up-regulated in maturation and is the predicted target of the down-regulated miRs in MiMaC (Figure 2-4G and Supplemental Table S4). Importantly, these data indicated that the observed transcriptional maturation mirrors normal *in vivo* cardiomyocyte maturation (Figure 2-4O).

Finally, we assessed the addition of fatty acids with MiMaC to increase cardiomyocyte maturation. Three long chain fatty acids, palmitate, linoleic and oleic acid were added to the basal cardiac media used. We found the MiMaC + FA cells were enriched in cluster 2. While some studies have shown lipotoxicity with particular FAs, our analysis showed no increase in transcripts indicative of apoptosis (Supplemental Table S5) [149]. These data indicate that the MiMaC was essential to bring about a robust transcriptional maturation of our hiPSC-CMs and that it was necessary to incorporate all four microRNAs together to bring about this robust maturation response.

2.4.7   *scRNA-Seq reveals an intermediate cardiomyocyte maturation stage*

After unbiased analysis of the miR treated CMs it was clear each miR combination resulted in enrichment of different states of CM maturation. Interestingly, cardiomyocyte cluster 1, enriched for Let7i and miR-452 OE, showed a robust up-regulation of OXPHOS and Myc target genes but was not yet significantly increased in most cardiomyocyte maturation markers (Figure 2-3N-O and Figure 2-43H,I; Supplemental Table S6). Hence treatment of Let7i and miR-452 OE created an

intermediate maturity CM in which the metabolic maturation was the leading force. These data suggest a possible intermediate stage from a fetal like CM to a more mature CM which requires transient up-regulation of OXPHOS genes.

2.4.8 *HOPX is a novel regulator of CM maturation*

To better understand the molecular mechanisms that are critical for cardiac maturation, the overlapping predicted targets of the chosen six miRs were determined. We had previously studied the predicted targets of Let7, insulin receptor-pathway and PRC2 function, and their role in cardiomyocyte maturation [13], however, we have not studied the targets of the down-regulated miRs. We found that all three down-regulated miRs during maturation had five common predicted targets. One of these predicted targets, homeobox protein (HOPX) (Figure 2-5A), is important for cardiomyoblast specification [126], yet no work on this transcriptional regulator has addressed the later process, human cardiomyocyte maturation. HOPX expression was up-regulated in *in vitro* (D30/D20 3.9 fold, *P*=0.04 and 1-Yr/D20 7.7 fold, *P*=0.002) (Figure 2-5B), *in vivo* (adult vs fetal 3 fold, *P*=0.0046) (Figure 2-5C) and MiMaC (D30MiMaC/D30EV 2.3 fold, *P*=0.004) cardiomyocyte maturation (Figure 2-5D). To analyze how our MiMaC miRs might individually regulate HOPX expression during maturation, we analyzed HOPX levels in miR-122 KO and Let7i OE hiPSC-CMs. We found HOPX was up-regulated 6.8 fold in D30 miR-122 KO hiPSC-CMs while Let7i OE matured hiPSC-CMs had no effect on HOPX expression (Figure 2-6A). These data indicate that Let7i OE maturation does not govern HOPX cardiac maturation pathways. This highlighted the necessity of combining multiple miRs together to generate a robust maturation effect in hPSC-CMs and that HOPX seems to be a strong candidate for post-committed cardiomyocyte maturation.

2.4.9   *HOPX OE regulates cardiomyocyte growth and cell division*

To assess HOPX OE in cardiomyocyte maturation, we generated an iPSC line that conditionally overexpressed HOPX fused with a nuclear localization signal (NLS) and enhanced green fluorescent protein (eGFP) termed HOPX OE. The overexpression of HOPX was controlled by a tetracycline promoter. A corresponding control iPSC line of NLS-eGFP under the control of a tetracycline promoter was also generated termed negative control (NC) (Figure 2-5E,F and Figure 2-6B).

We performed RNA-Sequencing on CMs that had 2 weeks of HOPX OE or just eGFP OE (NC) and determined the differentially expressed genes between these two groups. GO term analysis showed that many of the up-regulated processes were related to cell growth and maturation while many of the down-regulated processes were associated with cell cycle (Figure 2-5G). To better understand the genes involved in these two processes we performed STRING analysis to assess how these networks of genes were related to one-another. This showed that the differentially expressed up-regulated genes associated with cell growth in the HOPX OE group generated a highly-interconnected network (Figure 2-5H). We then generated four clusters using Kmeans clustering: regulation of cell growth, regulation of growth (via insulin-like growth factor pathway), cell development and renin-angiotensin regulation of aldosterone production, a classic pathway for cardiac hypertrophy [150]. Functionally, we assessed if the HOPX OE group had any morphological changes due to the up-regulated of cell growth genes. We found that CM cell area significantly increased after two weeks of HOPX OE (HOPX: 9989 μm^2 NC: 2362 μm^2 *P*<0.001) (Figure 2-5I and Figure 2-6C).

Using STRING analysis, we showed that the differentially expressed genes associated with cell division in the HOPX OE group generated a highly-interconnected network with key cell cycle

genes highly down-regulated and one up-regulated inhibitor of cell cycle (cyclin-dependent kinase inhibitor 1C) (Figure 2-5J) which, also re-capitulated the cell cycle repression finding we found with MiMaC treated hiPSC-CMs. We then generated four clusters using Kmeans clustering: regulation of mitotic cell cycle, cell division, inhibition of cilia and ubiquitin protein. Representative cell cycle genes, BUB1, MKI67 and CENPE, are down-regulated while the inhibitor of many G1 cyclin/cdk complexes, CDKN1C, is significantly up-regulated in the HOPX OE condition (Figure 2-5K). These data suggest that HOPX OE is a driver of exit from cell cycle and cardiomyocyte hypertrophy.

2.4.10   *HOPX regulates cell cycle via SRF genes*

HOPX is a homeodomain protein that does not bind DNA but rather is recruited to locations in the genome by serum response factor (SRF). HOPX in turn recruits histone deacetylase (HDAC) and removes acetylation marks resulting in the silencing of genes (Figure 2-7A). HOPX OE led to a significant down-regulation of 294 SRF targets (hypergeometric test p-value is 1.31×10^{-5}) while the group of SRF targets that were up-regulated was not significant (hypergeometric test p-value is 0.99) (Figure 2-7B and Supplemental Table S6). Clearly, HOPX OE had successfully led to the repression of many SRF target genes.

We validated using qPCR a known SRF target gene that should be repressed during cardiomyocyte maturation, natriuretic peptide precursor A (NPPA). After two weeks of HOPX OE, NPPA was significantly repressed, while cardiac troponin C, a non-SRF cardiac gene was unaffected by HOPX OE. The ventricular isoform of myosin light chain, MYL2, which is activated as ventricular cardiomyocytes mature, increases 1.87-fold in expression after two weeks of HOPX OE (Figure 2-7C).

To better understand what role HOPX may have in repressing SRF target genes during normal cardiomyocyte maturation we determined the SRF target genes in common between HOPX OE Vs. NC and the human adult Vs. fetal myocardium (ventricular myocardium) transitions. There were 294 SRF targets lower in HOPX OE vs. NC and 564 SRF targets lower in adult Vs. fetal myocardium. 76 SRF targets were common between the two groups and formed a significant group of genes (hypergeometric test p-value is 5.44×10^{-24}) (Figure 2-7D). Assessing these 76 genes via GO term analysis showed a strong association with repression of cell cycle (Figure 2-7E). Using STRING analysis, we determined the network of connected genes out of the 76 genes in common and ran Kmeans clustering to generate 4 clusters (Figure 2-7F). We found the majority of the genes fell into two cell cycle clusters (mitotic cell cycle and cell cycle), the third cluster was associated with DNA repair and the fourth cluster associated with muscle development. Finally, we wanted to determine the network of SRF regulated cell cycle genes that was in common between the HOPX OE line and adult cardiomyocytes (Figure 2-7G). This network identified, at least in part, the way in which HOPX directly regulates SRF cell cycle genes to mature a cardiomyocyte through its exit from cell cycle. Using MCL clustering, one cluster was found showing that all genes were associated with cell cycle with 7 of the 10 genes associated with the spindle machinery. These data indicate that, at least partly MiMaC acts through HOPX, repressing SRF cell cycle targets.

2.5   DISCUSSION

Many tools have been generated to mature hPSC-CMs which include: electrical and/or mechanical stimulation [15, 17, 151], cell microenvironment [12, 152, 153] and culture time [14]. However, none of these methods directly affect maturation aspects that allow the analysis of FA metabolism. Building off our previous work studying the role of Let-7 in hPSC-CM maturation [13], we developed a microRNA maturation cocktail (MiMaC) that was able to mature hPSC-CM size, force of contraction and metabolism. MiMaC can facilitate the study of cardiac diseases including metabolic cardiac diseases in hPSC-CMs. Furthermore, we used MiMaC system to better understand the late development, maturation processes [119-121]. Importantly, we find a common microRNA target, HOPX, as a novel, critical regulator of cardiomyocyte maturation.

Previous studies have shown an increase in metabolic gene expression when cardiomyocytes develop from fetal to adult stage, metabolic remodeling [154]. Increase of OXPHOS gene expression may indicate an increase in mitochondrial copy number or biosynthesis of a more mature mitochondria, or both [155]. Our scRNA-seq studies discovered a novel, intermediate cardiomyocyte sub-group with a high metabolic gene expression for OXHPOS and Myc targets. These data suggest a possible intermediate stage from a fetal like CM to a more mature CM which, requires transient up-regulation of OXPHOS genes. Since Parkin is upregulated at this stage as well (Supplemental Table S11), these data support the hypothesis that quality control type mitophagy of fetal stage mitochondria and biosynthesis of mature mitochondria takes place in MiMaC induced cardiomyocyte maturation. This is similar to the previously shown mitophagy mediated response via Parkin during perinatal mouse heart development [155]. Importantly, this intermediate stage in maturation was also observed in MTP/HADHA mutant cardiomyocytes, prior to development of the pathological state. Further

dissection of this stage will allow mechanistic understanding of the regulation of this process both in normal and disease states.

The molecular mechanisms that govern cardiomyocyte maturation, the process upon which a committed cardiomyocyte grows and matures from a fetal cardiomyocyte to an adult cardiomyocyte, are not well understood. Many fundamental transcriptional and epigenetic regulators have been studied during cardiac development [119-121] and disease [122] yet, there are limited studies for post committed cardiomyocyte maturation. We identified a critical regulator of cardiomyocytes, HOPX, as a common predicted target of the microRNA maturation cocktail. HOPX has previously been identified as a regulator of cardiomyocyte hypertrophy [156] and cell cycle [157]. Overexpression of HOPX in the mouse ventricle led to pathological hypertrophic growth while null mouse ventricles for HOPX showed an increased number of cardiomyocytes, suggesting that HOPX expression is required to facilitate cardiomyocyte exit from the cell cycle. Accordingly, we showed that hiPSC-CM cellular size is up-regulated and cell cycle is down-regulated due to HOPX overexpression. Furthermore, for the first time using transcriptomics, we have identified the SRF target genes that are down-regulated in the presence of HOPX overexpression in hiPSC-CMs. These SRF targets show a strong enrichment for cell cycle regulators, specifically repressing G1/S transition and spindle/kinetochore machinery to induce an exit of cell cycle and promote hypertrophic growth. Therefore, we propose that the microRNA maturation cocktail accelerates maturation partly by repressing cell cycle through HOPX.

Together, this study has generated a tool to mature hPSC-CMs for *in vitro* cardiac disease modeling and understanding the basic biology/molecular mechanisms of cardiomyocyte maturation. With this tool, we can now study cardiac diseases, such as metabolic fatty acid oxidation disorders, to bring about new insight and molecular understanding of human cardiac

biology and pathology. These efforts are done in the hope to generate robust human cardiac cells

to utilize for the discovery of novel therapies.

2.6   FIGURES
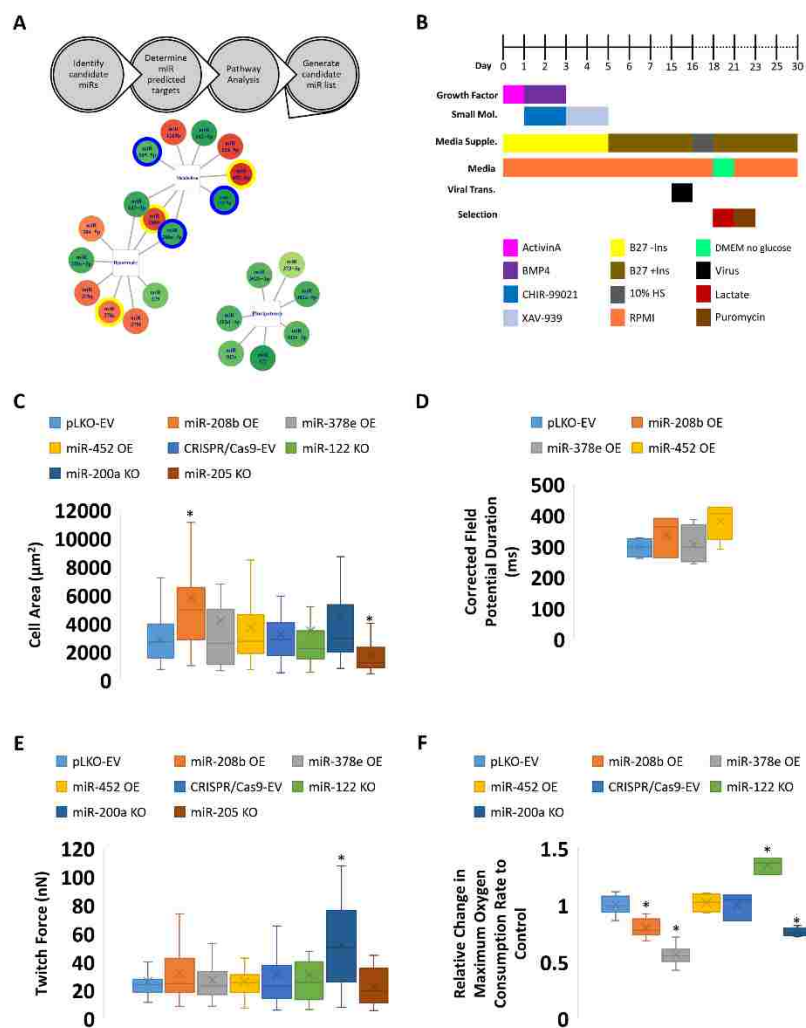
Figure 2-1: Cardiomyocyte maturation microRNA screen.

A) Schematic of the workflow performed to determine candidate microRNAs to screen for cardiomyocyte maturation. B) Schematic of the workflow performed to generate microRNA transduced stem cell derived cardiomyocytes. C) Cell area analysis of microRNA treated hiPSC-CMs. MicroRNA-208b OE lead to a significant increase in cell area while miR-205 KO led to a significant decrease. D) Micro-electrode array analysis of microRNA treated hiPSC-CMs corrected field potential duration (cFPD). MiR-452 OE led to a longer cFPD. E) Single cell twitch

force analysis using a micro-post assay. MiR-200a KO led to a significant increase in twitch force of hiPSC-CMs. F) Seahorse analysis of the maximum change in oxygen consumption rate (OCR) due to FCCP after oligomycin treatment of microRNA treated hiPSC-CMs. MiR-122 KO led to a significant increase in maximum OCR while miR-208b OE, -378e OE and -200a KO led to significant decreases in maximum OCR.
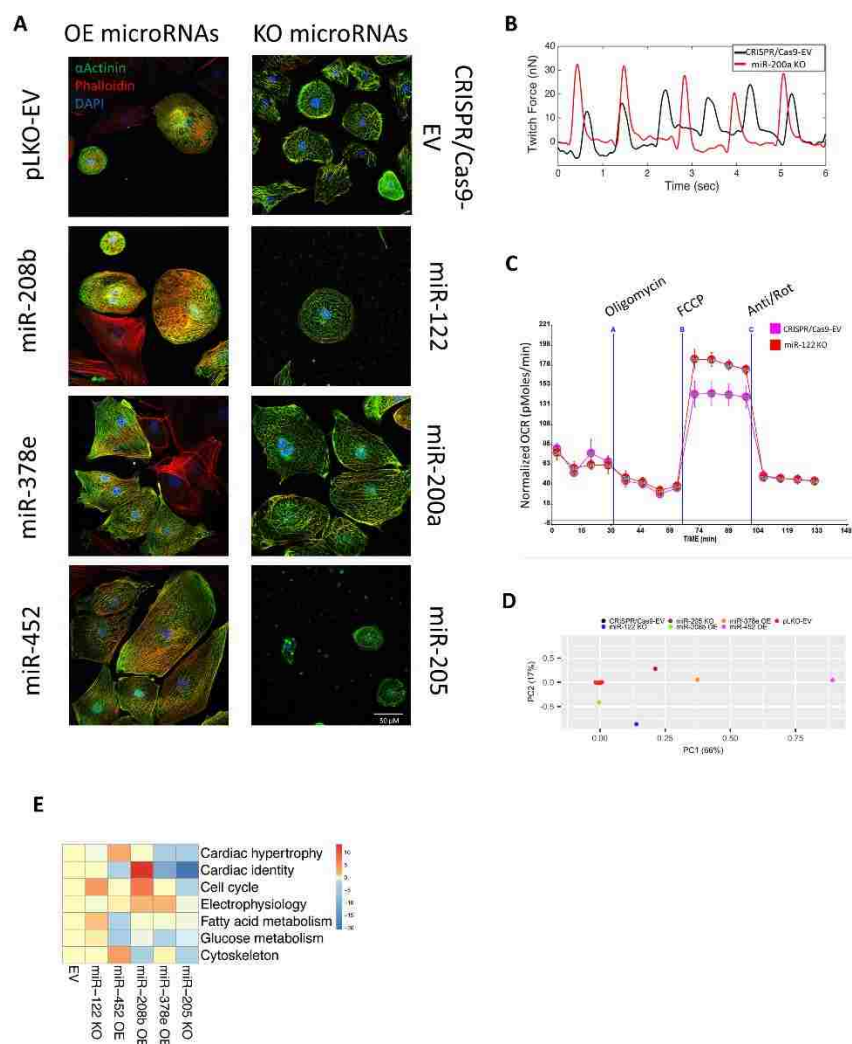
Figure 2-2: Identification of microRNAs that govern the maturation of hPSC-CMs.
A) Representative confocal microscopy images for the six screened miRs and their respective controls. Green denotes the cardiac structural protein αActinin, red denotes phalloidin which stains F-actin and blue denotes DAPI which stains cell nuclei. B) Representative force trace for a control hPSC-CM and a miR-200a KO treated hPSC-CM. C) KO of miR-121 led to a significant increase in maximum oxygen consumption rate. Representative trace of the mitostress assay is shown. D) Principal component analysis (PCA) of RNA-Sequencing data for the OE or KO of a

single microRNA in Day-30 hPSC-CMs. E) Heatmap showing seven pathways that are associated with hPSC-CM maturation and how each individual microRNA's perturbation of hPSC-CM transcriptome influences the expression of each pathway. Red indicates genes up-regulated by the treatment show more significant enrichment in the pathway than genes down-regulated by the treatment, blue means the opposite.
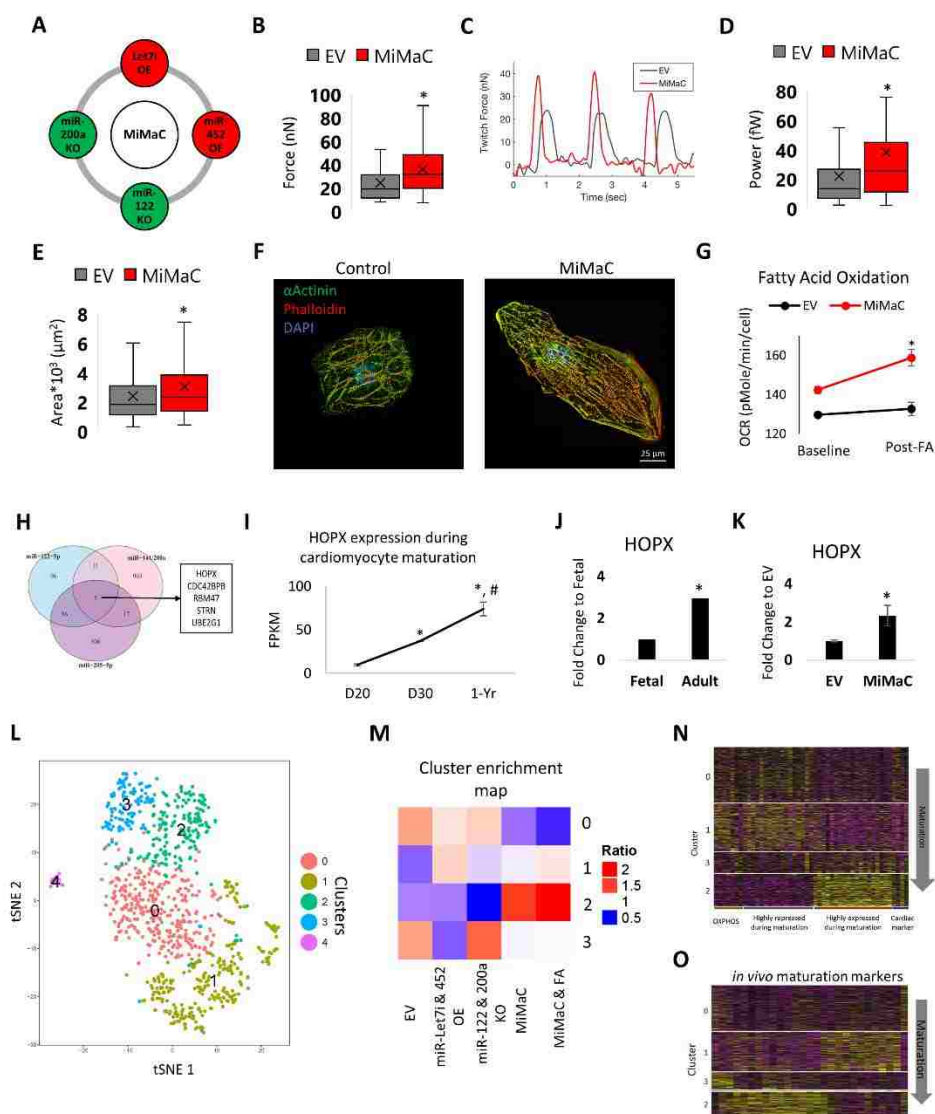
Figure 2-3: MiMaC accelerates hiPSC-CM maturation.

A) Schematic of the four microRNAs combined to generate MiMaC. B) Single cell force of contraction assay on micro-posts showed that MiMaC treated hiPSC-CMs led to a significant increase in twitch force. C) Representative trace of a EV (control) and a MiMaC treated hiPSC-CM. D) Single cell force of contraction assay on micro-posts showed that MiMaC treated hiPSC-CMs led to a significant increase in power. E) Cell size analysis showed that MiMaC treated

hiPSC-CMs led to a significant increase in area. F) Representative confocal microscopy images of EV and MiMaC treated hiPSC-CMs. αActinin (green), phalloidin (red) and DAPI are shown. G) Seahorse analysis of fatty acid oxidation capacity showed that MiMaC treated hiPSC-CMs matured to a point where they could oxidize palmitate for ATP generation while controls cells were not able to utilize palmitate. MiMaC hiPSC-CMs had a significant increase in OCR due to palmitate addition. H) Venn diagram of KO microRNA predicted targets and the identification of HOPX as a common predicted targeted between all KO miRs screened for cardiomyocyte maturation. I) Plot of HOPX expression from RNA-Sequence data during cardiomyocyte maturation. HOPX expression is significantly higher in D30 and 1-year hESC-CMs and 1-year hESC-CMs have statistically significantly higher HOPX as compared to D30 hESC-CMs. * denotes significance vs D20. # denotes significance vs D30. J) HOPX expression in adult human ventricle tissue is significantly higher than fetal human ventricular tissue. Plotted using RNA-sequencing data. K) RT-qPCR of HOPX expression of HOPX showed that MiMaC treated hiPSC-CMs at D30 had a statistically significant higher level of HOPX as compared to EV control D30 hiPSC-CMs. L) Single cell RNA-Seq tSNE plot of unbiased clustering of microRNA treated hPSC-CMs. M) Cluster plot detailing which treatment groups are enriched in each cluster. N) Heatmap of maturation categories based on MiMaC cluster. O) Heatmap of *in vivo* human maturation markers that are up-regulated with maturation (yellow).
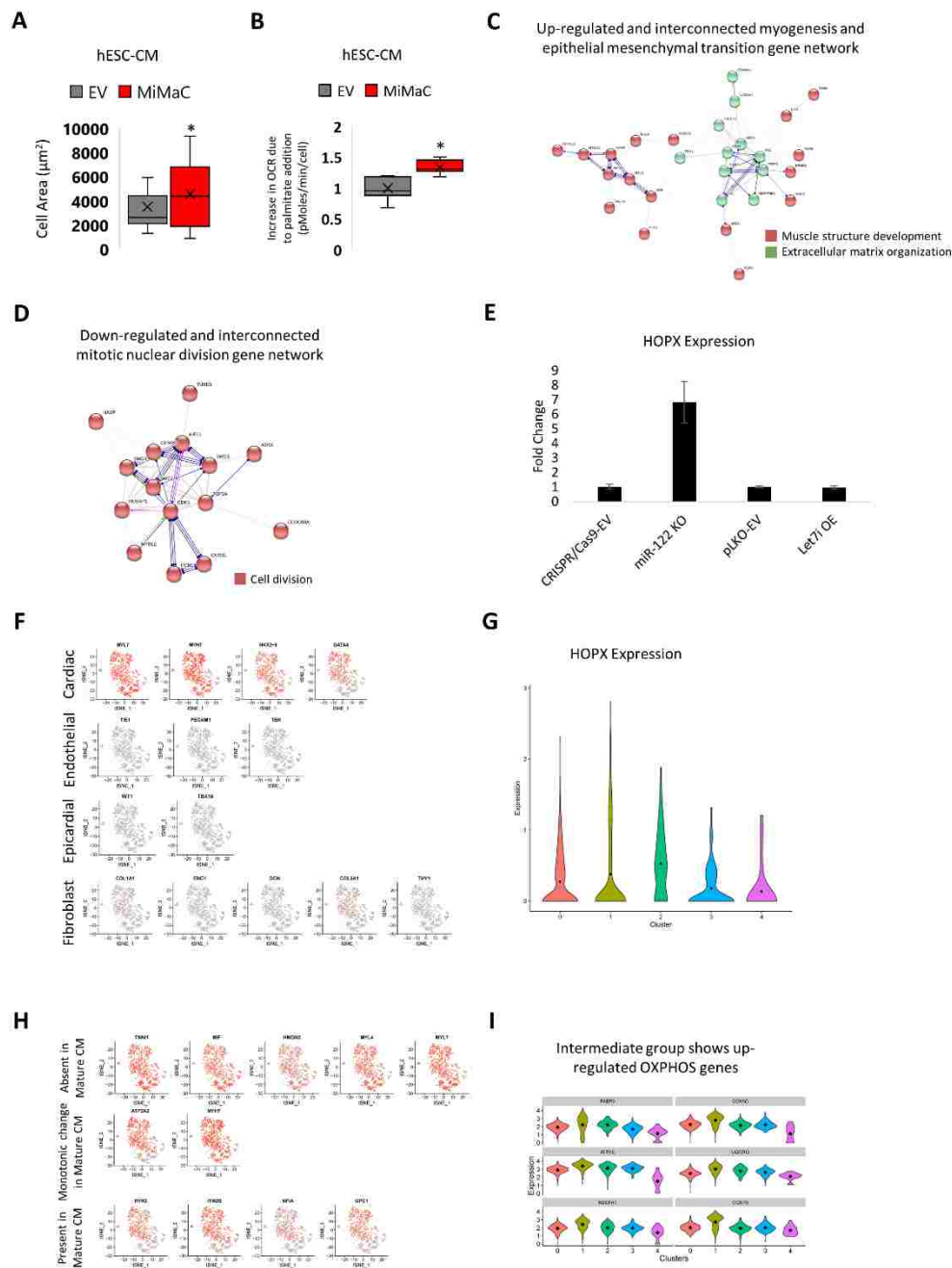
Figure 2-4: MiMaC treated hPSC-CMs show an increase in cell size, ability to use fatty acids and a more mature transcriptome.

A) MiMaC treated hESC-CMs showed a statistically significant increase in cell area as compared to control EV hESC-CMs.   B) MiMaC treated hESC-CMs were able to utilize the fatty acid palmitate to generate ATP. MiMaC treated hESC-CMs had a statistically significant increase in

oxygen consumption due to the presentation of palmitate. C) String analysis plot of up-regulated and interconnected myogenesis and epithelial mesenchymal transition genes. Two clusters of genes are highlighted: red – muscle structure development, green – extracellular matrix organization. D) String analysis plot of down-regulated and interconnected mitotic nuclear division gene network. One cluster of genes are highlighted: red – cell division. E) Knockout of miR-122 and not Let-7i leads to up-regulation of HOPX. RT-qPCR analysis of HOPX expression in miR-122 KO hiPSC-CM and Let-7i OE hiPSC-CM and their respective controls. F) tSNE plots of cell lineage markers show the majority of cells are cardiomyocytes. G) Violin plot of HOPX expression. H) Set of genes that change during cardiomyocyte maturation show the intermediate cluster is less mature. I) Set of OXPHOS genes up-regulated in cluster 2, the intermediate maturation group.
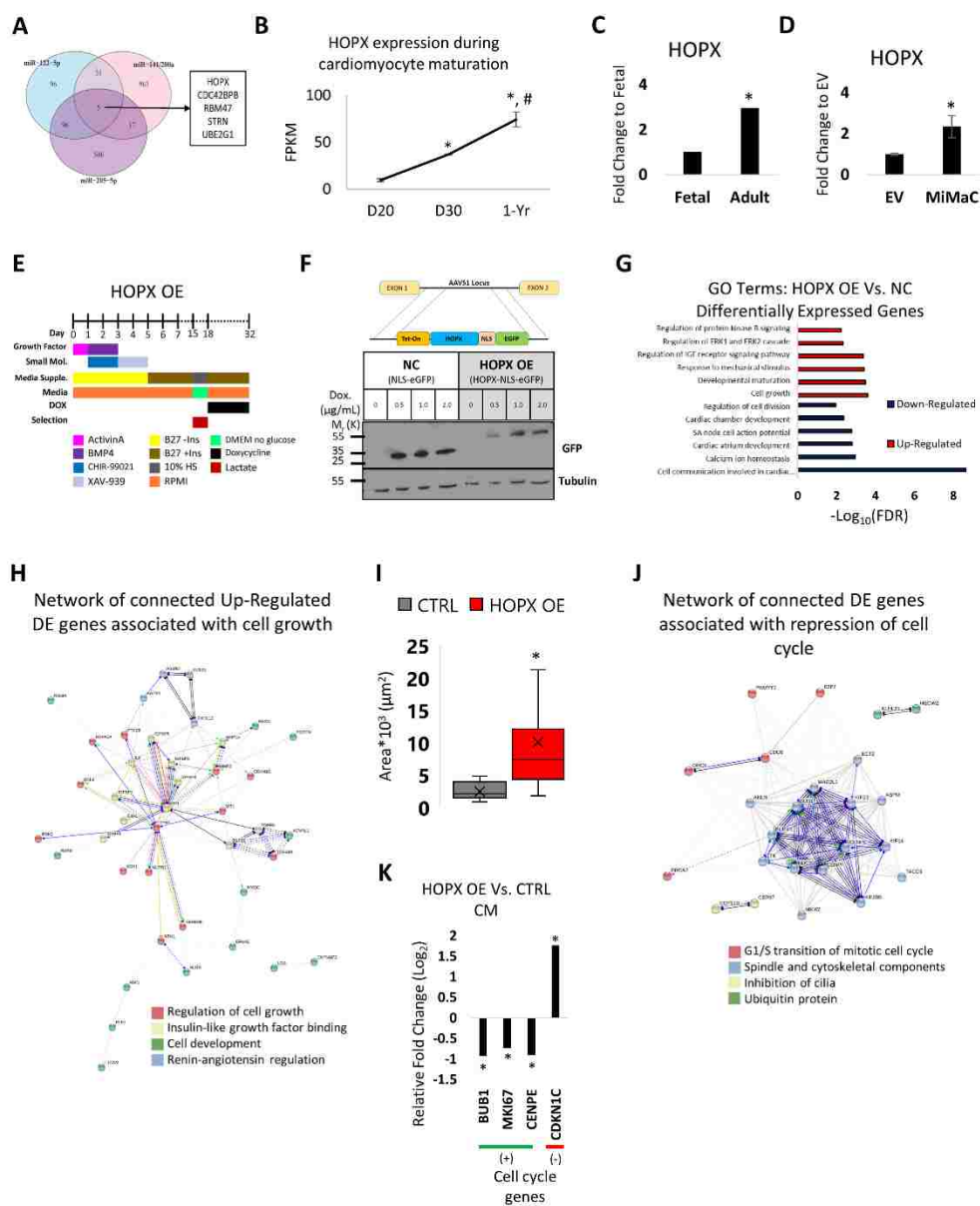
Figure 2-5: HOPX is a key regulator of cardiomyocyte maturation of cell cycle exit and growth.

A) Venn diagram of KO microRNA predicted targets and the identification of HOPX as a common predicted targeted between all KO miRs screened for cardiomyocyte maturation. B) Plot of HOPX expression from RNA-Sequence data during cardiomyocyte maturation. HOPX expression is

significantly higher in D30 and 1-year hESC-CMs and 1-year hESC-CMs have statistically significantly higher HOPX as compared to D30 hESC-CMs. * denotes significance vs D20. # denotes significance vs D30. C) HOPX expression in adult human ventricle tissue is significantly higher than fetal human ventricular tissue. Plotted using RNA-sequencing data. D) RT-qPCR of HOPX expression of HOPX showed that MiMaC treated hiPSC-CMs at D30 had a statistically significant higher level of HOPX as compared to EV control D30 hiPSC-CMs. E) Schematic of HOPX OE experimental set-up. F) Schematic diagram of the conditionally expressed HOPX-NLS-EGFP construct (NLS – nuclear localization signal, EGFP – enhanced green fluorescent protein). Below is a western of control (NLS-eGFP) termed NC and the HOPX OE iPSC lines at different concentrations of doxycycline. Western is blotted against GFP and house keeping protein tubulin. G) List of GO terms of HOPX OE vs. NC control hiPSC-CMs. H) String analysis plot of up-regulated and interconnected cell growth gene network. Four clusters of genes are highlighted: red – regulation of cell growth, yellow – insulin-like growth factor binding, green – cell development and blue – renin-angiotensin regulation. I) Cell size analysis showed that HOPX OE treated hiPSC-CMs led to a significant increase in area. J) String analysis plot of interconnected genes associated with repression of cell cycle. Four clusters of genes are highlighted: red – G1/S transition of mitotic cell cycle, blue – spindle and cytoskeletal components, yellow – inhibition of cilia and green – ubiquitin protein. K) Fold change of cell cycle genes from RNA-Sequencing data for HOPX OE vs. NC hiPSC-CMs. Green bar represents positive regulators of cell cycle while the red bar represents negative regulators of cell cycle.
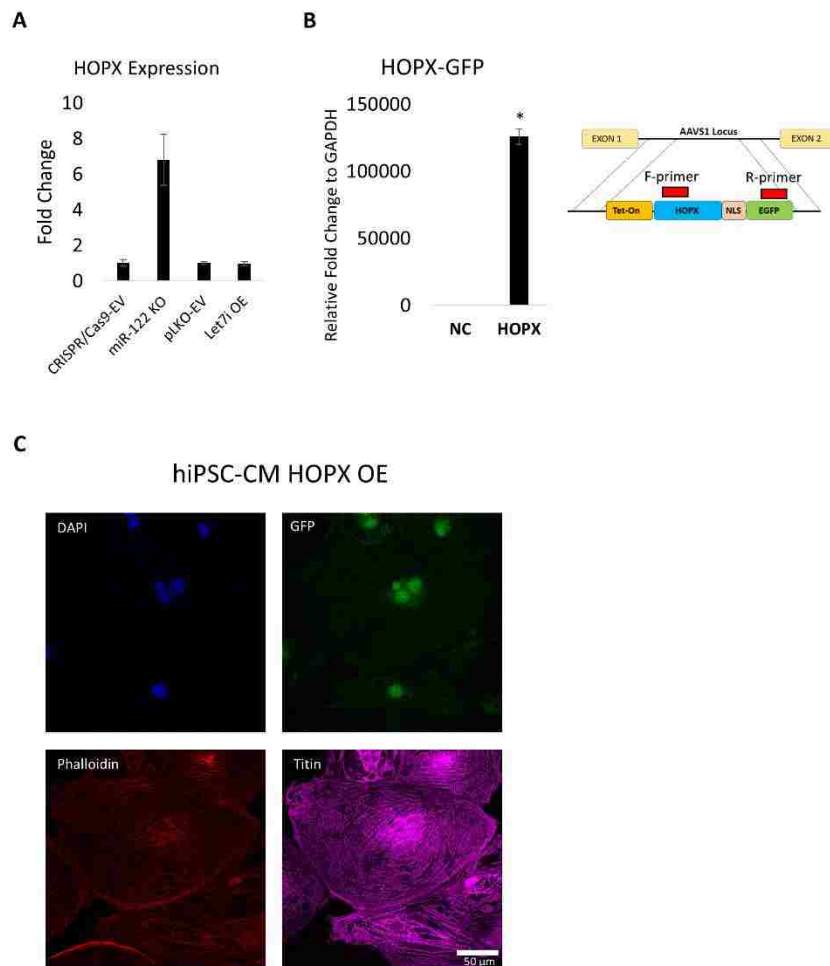
Figure 2-6: HOPX is a key regulator of cardiomyocyte maturation.

A) Knockout of miR-122 and not Let-7i leads to up-regulation of HOPX. RT-qPCR analysis of HOPX expression in miR-122 KO hiPSC-CM and Let-7i OE hiPSC-CM and their respective controls. B) FACs data for the LOF HOPX line differentiation efficiency. C) HOPX-NLS-eGFP construct is robustly expressed in doxycycline treated hiPSC-CMs. RT-qPCR for the expression of the HOPX-NLS-eGFP construct in doxycycline treated HOPX OE hiPSC-CMs and NC hiPSC-CMs. Primer locations indicated in schematic. No detection of the HOPX-NLS-eGFP construct is found in the NC sample. D) Representative confocal image of HOPX OE hiPSC-CMs at D32

after two weeks of doxycycline treatment. Blue – DAPI, green – anti-GFP, red – phalloidin and pink – titin.
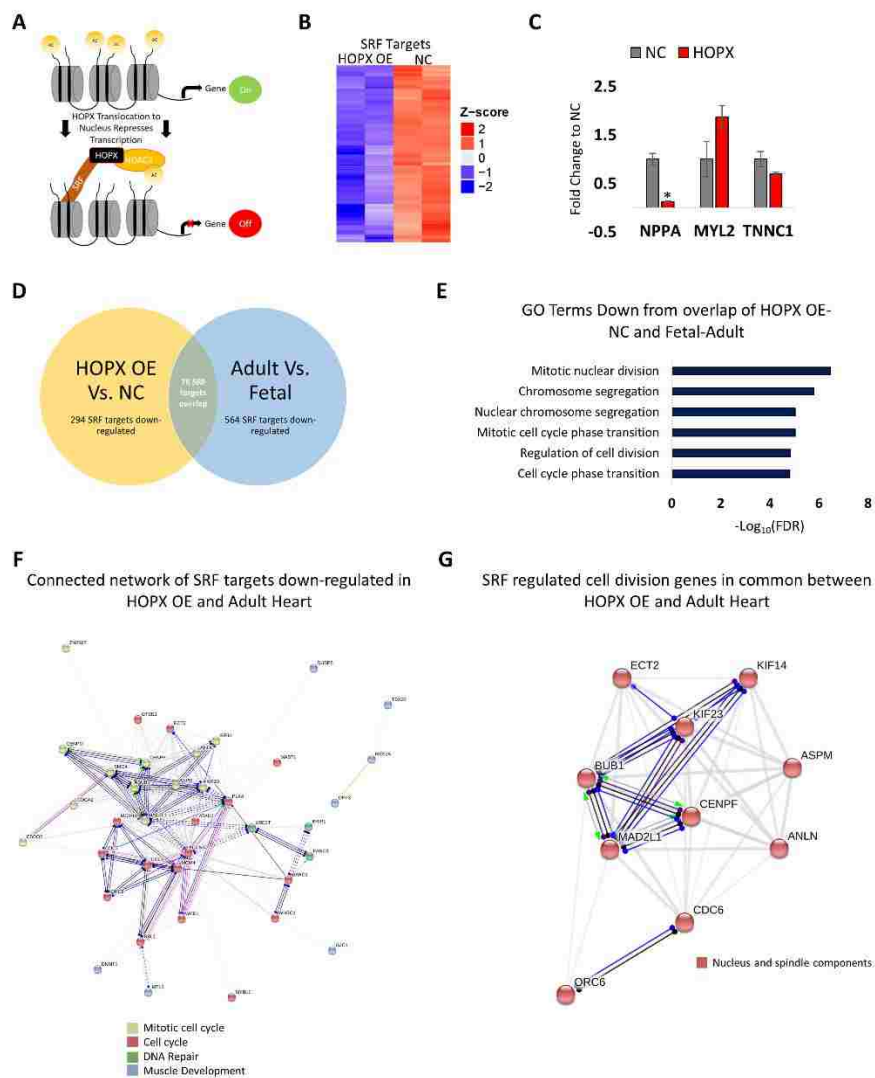
Figure 2-7: HOPX OE leads to down-regulation of SRF genes regulating cell cycle.
A) Schematic of how HOPX is localized to DNA via serum response factor (SRF) to then recruit histone deacetylase such as HDAC2 to repress SRF genes by removing acetylation marks. B) Heatmap showing the down-regulation of SRF targets in the HOPX OE group as compared to NC hiPSC-CMs. C) RT-qPCR analysis of NC hiPSC-CM and HOPX OE hiPSC-CM showing a significant down-regulation of gene NPPA. D) Venn diagram showing the number of SRF down-regulated genes in the HOPX OE vs. NC group, the human adult ventricular myocardium vs. fetal myocardium and the overlap of SRF-down-regulated genes between these two transitions. E) List

of down-regulated GO terms for the overlap of HOPX OE vs. NC hiPSC-CMs and human adult vs. fetal ventricle SRF targets. F) String analysis plot of down-regulated and interconnected SRF targets in HOPX OE and human adult ventricle. Four clusters of genes are highlighted: yellow – mitotic cell cycle, red – cell cycle, green – DNA repair and blue – muscle development. G) String analysis plot of down-regulated SRF cell division genes in common between HOPX OE and human adult ventricle. One cluster was highlight: red – nucleus and spindle components.

Chapter 3. FATTY ACID OXIDATION DISORDER GENE TFPA/HADHA IS REQUIRED FOR CARDIOLIPIN RE-MODELING AND MITOCHONDRIAL PROTON GRADIENT IN HUMAN CARDIOMYOCYTES

Parts of this chapter is in the following manuscripts:

Fatty acid oxidation disorder gene TFPa/HADHA is required for cardiolipin re-modeling and mitochondrial proton gradient in human cardiomyocytes

Jason W. Miklas, Shiri Levy, Damien Detraux, Andrea Leonard, Kevin Beussman, Peter Hofsteen, Xiulan Yang, Jesse Macadangdang, Anup Madan, Deok-Ho Kim, Charles E. Murry, Nathan J. Sniadecki, Yuliang Wang, Hannele Ruohola-Baker

3.1 ABSTRACT

Mitochondrial trifunctional protein deficiency, due to mutations in hydratase subunit A (HADHA), results in sudden infant death syndrome (SIDS) with no cure. To reveal the disease etiology, we generated stem cell-derived cardiomyocytes from HADHA-deficient hiPSCs and accelerated their maturation via a novel, engineered MicroRNA Maturation Cocktail (MiMaC) that upregulated the epigenetic regulator, HOPX. Fatty acid challenged MiMaC treated HADHA mutant cardiomyocytes manifested the disease phenotype: defective calcium dynamics and repolarization kinetics which resulted in a pro-arrhythmic state. Single cell RNA-seq revealed a novel cardiomyocyte developmental intermediate, based on metabolic gene expression. This intermediate gave rise to mature-like cardiomyocytes in control cells but, mutant cells transitioned to a pathological state with reduced mitochondrial proton gradient, cisternae structure and membrane dynamics. The mutant mitochondria lacked mature tetra[18:2] cardiolipin which HADHA maintains. This study reveals that TFPa/HADHA, a MLCL-AT-like enzyme, is required for cardiolipin remodeling and functional mitochondria in human cardiomyocytes.

3.2 RATIONALE

One of the hallmarks of cardiomyocyte maturation is the capability to use fatty acids as a substrate to generate ATP. Immature cardiomyocytes can perform glucose oxidation while mature cardiomyocytes can perform glucose as well as fatty acid oxidation to generate ATP. Mitochondrial trifunctional protein (MTP/TFP) deficiency is a result of impaired fatty acid oxidation (FAO) due to mutations in hydroxyacyl-CoA dehydrogenase/3-ketoacyl-CoA thiolase/enoyl-CoA hydratase subunit A (HADHA/LCHAD) or subunit B (HADHB) [28].

Mitochondrial trifunctional protein (MTP) deficiency results in sudden unexplained infant death, Reye-like syndrome, cardiomyopathy and/or skeletal myopathy [158, 159]. [28]. A major phenotype of MTP-deficient newborns is sudden infant death syndrome (SIDS), which manifests after birth once the child begins nursing on lipid-rich breast milk. Defects in FAO have a role in promoting a pro-arrhythmic cardiac environment, however, the exact mechanism of action is not understood, and there are no current therapies [38, 160].

Since many infants die soon after birth, it is a difficult disease to study and develop pharmacological interventions. Similarly, homozygous deficient mice in MTP suffer early neonatal death [56]. Previous studies point towards cardiac lesions caused by HADHA mutation or the potential for arrhythmogenic intermediary metabolites of fatty acids, such as long-chain acylcarnitines, causing arrhythmias [45, 56]. Thus, while it is clear that defects in fatty acid oxidation have a role in SID, the exact mechanism of action is not understood.

In this study we analyzed mitochondrial tri-functional protein deficiency by generating stem cell-derived cardiomyocytes from HADHA-deficient human induced pluripotent stem cells (hiPSCs) and accelerated their maturation by our engineered microRNA maturation cocktail that upregulates the epigenetic regulator, homeobox protein (HOPX). Fatty acid (FA) challenged

HADHA mutant cardiomyocytes showed aberrant calcium handling, delayed repolarization and erratic beating suggesting a pro-arrhythmic state. These pathological cardiac manifestations were a result of the underlying mitochondrial pathology which presented as mitochondrial dysfunction due to proton gradient loss, lack of normal cisternae and swelling of the mitochondria. The mechanism underlying this pathological state was identified as a mis-regulation of cardiolipin homeostasis due to the loss of tetra[18:2] cardiolipin species as a result of the HADHA mutation. These data revealed the essential dual role of HADHA in fatty acid beta-oxidation and as an acyl-transferase in cardiolipin remodeling for cardiac homeostasis.

3.3 METHODS

3.3.1 *HADHA line creation*

Using LentiCrisprV2 plasmid [161] (lentiCRISPRV2 was a gift from Feng Zhang (Addgene plasmid # 52961) two different gRNAs targeted to Exon 1 of HADHA were designed using CRISPRScan [162]. Sequences for the gRNAs can be found in Supplemental Table S12. The gRNA and Cas9 expressing plasmids were transiently transfected into the WTC line using GeneJuice (EMD Millipore). 24 hours after transfection, WTCs were puromycin selected for two days and then clonally expanded. DNA of the clones was isolated, the region around the targeting guides was PCR amplified (see guides in Supplemental Table S12) and sequenced to determine the insertion and deletion errors generated by CRISPR-Cas9 system in exon 1 of HADHA. Western analysis was performed to determine the levels of HADHA protein in HADHA mutants. 31 clones were sent for sequencing from gRNA1 experiment, 6 clones (19%) had no mutations while 25 clones (81%) were found to have mutations. 24 clones were sent for sequencing from gRNA2, 1 clone had no mutations (4%) while 23 clones (96%) were found to have mutations. Two of the mutant lines were analyzed further in this study.

3.3.2 *CRISPR off-target*

The potential off targets of the HADHA gRNA were identified using Crispr-RGEN's Cas-OFFinder tool [163]. The top predicted off targets were then amplified by GoTaq PCR and sequenced. Off-target primers can be found in Supplemental Table S13. Sequencing for primer pair #1 can be found in Supplemental Figure 1E.

3.3.3   *Protein extraction and western blot analysis*

Cells were lysed directly on the plate with a lysis buffer containing 20mM Tris-HCl pH 7.5, 150mM NaCl, 15% Glycerol, 1% Triton X-100, 1M β-Glycerolphosphate, 0.5M NaF, 0.1M Sodium Pyrophosphate, Orthovanadate, PMSF and 2% SDS [164]. 25U of Benzonase Nuclease (EMD Chemicals, Gibbstown, NJ) was added to the lysis buffer right before use. Proteins were quantified by Bradford assay (Bio-rad), using BSA (Bovine Serum Albumin) as Standard using the EnWallac Vision. The protein samples were combined with the 4x Laemmli sample buffer, heated (95°C, 5min), and run on SDS-PAGE (protean TGX pre-casted 4%-20% gradient gel, Bio-rad) and transferred to the Nitro-Cellulose membrane (Bio-Rad) by semi-dry transfer (Bio-Rad). Membranes were blocked for 1hr with 5% milk and incubated in the primary antibodies overnight at 4°C. The membranes were then incubated with secondary antibodies (1:10000, goat anti-rabbit or goat anti-mouse IgG HRP conjugate (Bio-Rad) for 1hr and the detection was performed using the immobilon-luminol reagent assay (EMD Millipore). Primary antibodies are as follows: Alpha tubulin antibody Cell Signalling Technologies (2144) 1:2000, Beta tubulin Promega (G7121) anti-mouse 1:4000, Beta Actin Cell Signalling Technologies (4970) 1:4000, HADHA Abcam (ab54477 anti-rabbit 1:1000, UCP3 Abcam (ab3477) anti-rabbit 1:200, SLC25A4 (ANT1) Sigma (SAB2105530) anti-rabbit 1:1000, OXPHOS MitoSciences (MS604/G2830) anti-mouse 1:1000, anti-GFP Invitrogen (A-11122) anti-rabbit 1:1000.

3.3.4   *Immunocytochemistry and morphological analysis*

Cells were fixed in 4%(vol/vol) paraformaldehyde, blocked for an hour with 5% (vol/vol) normal goat serum (NGS), and incubated overnight with primary antibody in 1% NGS, followed by secondary antibody staining in NGS. Measurements of CM area were performed using Image J

software. Quantification of mitotracker intensity were performed using Image J software and following previously published methods on co-localization quantification [132]. Analysis was done on a Leica TCS-SPE Confocal microscope using a 40x or 63x objective and Leica Software. Primary antibodies used were: αActinin 1:250 Sigma A7811 anti-mouse, HADHA 1:250 abcam ab54477 anti-rabbit, ATP Synthase β 1:250 abcam ab14730 anti-mouse, Titin 1:300 Myomedix TTN-9 (cTerm) anti-rabbit, GFP 1:300 Invitrogen A-11122 anti-rabbit. Secondary antibodies and other reagents used were: DAPI at a concentration of 0.02μg/mL, phalloidin alexa fluor 568 1:250, alexa fluor 488 or 647-conjugated goat anti-mouse and anti-rabbit secondary antibodies 1:500 (Molecular Probes). MitotrackerCMTMRos Life technologies (M7510) used at a final concentration of 300nM in RPMI with B27 plus insulin supplement, incubated with cells for 45 minutes prior to fixation.

3.3.5 *Calcium transient analysis method*

Cardiomyocytes were plated on Matrigel coated round glass coverslips. The cardiomyocytes were incubated for 25 minutes at 37°C with 1mM Fluo-4 AM (Life Technologies, F14201) in Tyrode's buffer (1.8mM $CaCl_2$, 1mM $MgCl_2$, 5.4mM KCl, 140mM NaCl, 0.33mM NaH_2PO_4, 10mM HEPES, 5mM glucose, pH to 7.4). The substrate was then transferred to a 60mm Petri dish fresh with pre-warmed Tyrode's buffer for imaging. Samples were imaged using a Hamamatsu ORCA-Flash2.8 Scientific CMOS camera fitted on a Nikon Eclipse Ti upright microscope. Videos were taken with a 40x water-immersion objective at a framerate of at least 20 frames per second. The fluorescence power was adjusted to ensure adequate capture of fluorescence change during depolarization without bleaching, and the same fluorescence power was used for all experiments. The cardiomyocytes were biphasically stimulated at 5 V/cm with carbon electrodes (Ladd

Research, 30250) at either 0.5Hz or 1Hz, and at least 5 beats were captured during each video for analysis.

Videos were analyzed with a custom MATLAB code; calcium transients were obtained finding the cell boundary and averaging the fluorescence within the boundary for each video frame. The background fluorescence was determined automatically for each video frame and subtracted from the calcium transients. The calcium transients were then analyzed to find the peak fluorescence (F), baseline fluorescence (F_0), time to peak (T_{peak}), and time to 50% and 90% relaxation (T_{50R}, T_{90R}). The rates to peak, 50%, and 90% relaxation (R_{peak}, R_{50R}, R_{90R}) were calculated by dividing the respective fluorescence change by the respective time. An exponential decay function ($e^{-t/\tau}$) was fit to the relaxation between 10% and 90% relaxation to determine the relaxation coefficient, τ. All of these measurements were obtained for at least 4 beats in each video and averaged for comparison.

3.3.6 *Transmission electron microscopy*

Cells were fixed in 4% glutaraldehyde in sodium cacodylate buffer, post fixed in osmium tetroxide, en bloc stained in 1% uranyl acetate, dehydrated through a series of ethanol, and embedded in Epon Araldite. 70nm sections were cut on a Leica EM UC7 ulta microtome, and viewed on a JEOL 1230 TEM.

3.3.7 *Elamipretide (SS-31)*

SS-31 came from Stealth BioTherapeutics and was dissolved in PBS. A final concentration of 1nM was used in experiments.

3.3.8 *Box plots*

The 'x' in each box plot denotes the average value while the horizontal bar denotes the median value, no outlier values are shown. * denotes P<0.05.

3.3.9 *Bar graphs*

Bar graphs show the mean±SEM. Bar graphs which do not show SEM are generated from RNA-Sequencing data that had one or two samples sequenced.

3.3.10 *Statistical analysis*

Statistical analysis was performed on experiments with an N equal or greater to 3. P values were calculated using student t-test or one-way ANOVA. For student t-test a Shapiro-Wilk normality test was performed. For one-way ANOVA a Kolmogorov-Smirnov normality test was performed. For multiple comparisons, the Holm-Sidak method was used. For one-way ANOVA analysis that failed the normality test, ANOVA a Kruskal-Wallis one-way ANOVA of Variance on Ranks was performed. For multiple comparisons, the Dunn's method was used. All statistical tests used an $\alpha=0.05$.

3.3.11 *Targeted cardiolipin analysis using LC-MS/MS*

Immediately before extraction, each cell pellet was dissolved in 40μL DMSO and the membranes were disrupted by sonication. Cells were subjected to sonication using 3 cycles consisting of 20 seconds on, 10 seconds off. Care was taken to keep the cells on ice during sonication. After shaking, the suspension was transferred into a 2mL glass LC vial.

For cardiolipin extraction, an extraction mixture consisting of 20mL chloroform/methanol mix (2:1 v/v) and 30μL internal standard solution (5mg PC(18:0/18:1(9Z)) (Avanti Polar Lipids,

Inc., Alabaster, AL) was prepared. Next, 600µL of the extraction mixture was added to the samples, followed by vortexing and incubation at -20°C for 20 minutes. The samples were then sonicated in an ice bath for 15 minutes. Purified water (100µL) was added, and the samples were shaken for 30 minutes at room temperature. After centrifugation at 12,000×g for 10 minutes at 4°C. The bottom phase was transferred to a new glass LC vial and dried under vacuum. The residue was then reconstituted by adding 150µL acetonitrile/isopropanol/H_2O (65:30:5, v/v/v), and centrifuged at 20,000×g for 10 minutes at 4°C. The supernatant was transferred to individual glass vials for MS analysis.

For targeted cardiolipin measurements, 2µL of each prepared sample was injected into a 6410 Agilent Triple Quad LC-MS/MS system for analysis using an electrospray ionization source and negative ionization mode. Chromatographic separation was achieved on an Agilent 300 SB-C8 RRHD column (1.8µm, 2.1×50mm). The mobile phase A was 10mM ammonium acetate in acetonitrile/H_2O (6:4, v/v), and mobile phase B was 10mM ammonium acetate in isopropyl alcohol/acetonitrile/H_2O (90:10:1, v/v/v). The mobile phase composition changed from 60% A to 1% A over the 12 minute separation, followed by a rapid increase to 60% A and equilibration to prepare for the next injection. The total experimental time for each injection was 20 minutes. The flow rate was 0.26mL/min, the auto-sampler temperature was 4°C, and the column compartment temperature was set to 55°C. Targeted MS/MS data were acquired using multiple-reaction-monitoring (MRM) mode. MassHunter Workstation Software Quantitative Analysis for QQQ B.07.00 (Agilent) was used to integrate extracted MRM peaks.

3.4   RESULTS

3.4.1   *Generation of mitochondrial trifunctional protein deficient cardiomyocytes*

To recapitulate the cardiac pathology of mitochondrial trifunctional protein deficiency (Figure 3-1A) on the cellular level *in vitro*, we used CRISPR/Cas9 to generate mutations in the gene HADHA of human iPSCs. From our wild type (WT) hiPSC line, that serves as our isogenic control, we generated multiple HADHA mutation hiPSC lines using two different guides targeting exon 1 of HADHA (Figure 3-2A,B). We then chose to study a knockout (KO) HADHA (HADHA^KO) and compound heterozygote (HADHA^Mut) hiPSC lines that were generated using gRNA1.

Examining the DNA sequence of the HADHA^KO line showed a homozygous 22bp deletion which resulted in an early stop codon in exon 1 (Figure 3-1B and Figure 3-2C). The HADHA^Mut line had a 2bp deletion and 9bp insertion on the first allele and a 2bp insertion on the second allele (Figure 3-1C and Figure 3-2D). Both lines showed no off-target mutations on the top three predicted sites (Figure 3-2E). The mutations found in the HADHA^Mut line resulted in a predicted early stop codon on both alleles (Figure 3-2F). However, when we examined the protein in each line we found that HADHA was expressed in the WT hiPSC line, not expressed in the HADHA^KO line and was still expressed, to a lower degree, in the HADHA^Mut line (Figure 3-1D). We then examined the transcript of HADHA expressed in WT and HADHA^Mut lines. We found the WT line expressed the full length HADHA transcript from exon 1-20 while the HADHA^Mut line skipped exons 1-3 and expressed HADHA exons 4-20 (Figure 3-1C). It is possible that the mutations generated at the intron-exon junction induced an alternative splicing event and a new transcript since there is no known transcript of HADHA from exon 4-20 (Figure 3-2G). The observed reduction in the HADHA mutant molecular weight (Figure 3-1D) supports this

hypothesis. The expressed HADHA[Mut] protein skips the expression of exons 1-3, 60 amino acids, generating a truncated ClpP/crotonase domain which likely compromises the mitochondrial localization and protein folding of the enzyme pocket resulting in the inability to stabilize enolate anion intermediates during FAO (Figure 3-2H).

Using a monolayer directed differentiation protocol [128] we generated human induced pluripotent stem cell derived cardiomyocytes (hiPSC-CMs) from the three lines. We found that the reduction or loss of HADHA did not hinder the ability to generate cardiomyocytes (Figure 3-1E). To assess the functional phenotype of our MTP deficient cardiomyocytes, we performed a Seahorse Assay to measure the increase in oxygen consumed due to the presentation of a long chain FA, palmitate. We expected MTP deficient CMs to display a hindered ability to utilize long chain FAs in comparison to the WT CMs. However, we found that all CMs, even the control CMs, were unable to utilize long chain FAs (Figure 3-1F). hiPSC-CMs are immature cells representative of a FCM rather than an ACM which is why they are unable to utilize FAs as a substrate for ATP production [13, 114, 165]. Consequently, we needed to generate a tool to mature our hiPSC-CMs so that they could utilize FAs allowing us to then assess the functional phenotype of our MTP deficient CMs.

3.4.2 *MTP/HADHA Deficient CMs display reduced mitochondrial function*

The generation of the MiMaC tool allowed us to study HADHA CM disease etiology. Since immature hPSC-CMs were unable to oxidize fatty acids, it was necessary to mature the HADHA Mut and KO CMs with MiMaC, which brings about fatty acid oxidation in WT CMs. First, we assessed the maximum OCR of WT, HADHA Mut and KO CMs. MiMaC treated WT CMs had a statistically significant increase in maximum OCR (2.2 fold change) as compared to control cells

(Figure 3-3A,B). Interestingly, control and MiMaC treated HADHA Mut CMs had maximum OCR similar to control WT-CMs while the KO CMs had depressed maximum OCR.

Next, we assessed whether MiMaC treated HADHA Mut and KO CMs could utilize palmitate for ATP production. Only MiMaC treated WT CMs showed a statistically significant increase in oxygen consumption due to palmitate addition (Figure 3-3C). WT control CMs along with control and MiMaC treated HADHA Mut and KO CMs were unable to utilize FAs. These data show that MiMaC treated CMs have the capacity to utilize long chain FAs, however, MiMaC treated HADHA Mut and KO CMs are unable to do so. MiMaC was essential to assess the FAO limitations of the HADHA Mut and KO CMs.

The HAHDA KO CMs displayed a more severe metabolic phenotype since both allele copies of HAHDA had an early stop codon. However, the HADHA Mut CMs, which are a compound heterozygote which resulted in the loss of the mitochondrial localization signal, displayed a less severe metabolic phenotype. We moved forward studying the HADHA Mut CMs in depth to better understand the molecular mechanism governing cardiac MTP deficiency etiology.

3.4.3   *Abnormal calcium handling of HADHA Mut CMs*

MTP deficient infants can present with sudden, initially unexplained death after birth [56]. It is possible that the stress of lipids, the main substrate for ATP production found in a mother's breast-milk, is what precipitates the early infant death due to MTP deficiency. We chose to utilize a combination of three long chain fatty acids supplemented to our base cardiac media which contains glucose (Glc+FA media): palmitate, oleic and linoleic acid, since these FAs are the most abundant in the serum of breastfed human infants [166]. Palmitate, as a fatty acid substrate, is one of the most abundant fatty acids circulating during the neonatal period, representing 36% of all long-

chain free fatty acids [167]. While challenging CMs with FAs can lead to lipotoxicity, we have carefully developed a concentration and combination of three fatty acids that do not result in lipotoxicity (Figure 3-4A) [168, 169]. Moreover, other groups in the field of hPSCS-CM maturation have also found that carefully chosen and fully conjugated FAs stimulate aspects of CM maturation [170].

To better understand the way in which MTP deficient CMs may be precipitating an arrhythmic state leading to SIDS, we measured calcium transients in our WT and HADHA Mut CMs (Figure 3-3D and Figure 3-4B). We found, the fold change in calcium being cycled was significantly higher in WT CMs as compared to HADHA Mut CMs (WT CM: 2.03, Mut CM: 1.55, $P<0.001$) (Figure 3-3E) with no change in calcium rise velocity (Figure 3-4C). This suggested calcium was being cycled from the cytosol and stored in an aberrant manner in HADHA Mut CMs. When examining the tau-decay constant, we found HADHA Mut CMs had a higher average value (WT CM: 0.63 s, Mut CM: 0.76 s) (Figure 3-3F). This suggested the rate at which calcium was being pumped back into the sarco/endoplasmic reticulum was slower in the HADHA Mut CMs.

3.4.4 *Delayed repolarization and beat rate abnormalities in HADHA Mut CMs*

Since HADHA Mut CMs cultured in Glc+FA media exhibited abnormal calcium cycling, we assessed whether or not these CMs also exhibited abnormal electrophysiology. We determined membrane potential changes using a voltage sensitive fluorescent dye, Fluovolt. We found that while HADHA Mut CMs had no change in the maximum change in voltage amplitude or the rate of depolarization (Figure 3-3G,H and Figure 3-4D,E), significant differences were observed when examining repolarization rates. We found that the time to wave duration (WD) 50% (WD50) and 90% (WD90) were significantly longer in the HADHA Mut CMs as compared to WT CMs (Figure

3-3I and Figure 3-4F). These data suggest that the HAHDA Mut CMs cultured in Glc+FA result in impaired repolarization. This phenotype can be caused by the observed abnormal calcium dynamics due to impaired cycling of calcium back into the sarcoendoplasmic reticulum.

Since HADHA Mut CMs cultured in Glc+FA media exhibited defective calcium handling and electrophysiology, we assessed whether these CMs exhibited beat rate abnormalities. We tracked the spontaneous beating of HADHA Mut CMs cultured in Glc or Glc+FA media for 12D to quantify beat rate abnormalities. HADHA Mut CMs cultured in the Glc+FA media displayed abnormal beat rate variability as the time between beats was not even (Figure 3-3J). Quantifying these findings, we found that the HADHA Mut CMs in Glc+FA media had a significantly higher beat interval (Figure 3-4G) and a significantly higher change in beat-to-beat interval (ΔBI) (Figure 3-3K). These data suggest that HADHA Mut CMs in Glc+FA media beat on average slower and the time between beats was more variable. Furthermore, we quantified the percentage of ΔBI that were greater than 250ms and on average the HADHA Mut CMs in Glc+FA had a higher percentage of potentially arrhythmic ΔBIs (Figure 3-4H) [171]. Finally, we generated a Poincaré plot with fitted ellipses (95% confidence interval) around each group's beat interval data (Figure 3-3L). A narrow and elongated ellipse suggested uniform beat intervals while a more rounded ellipse suggested beat rate abnormalities. Taking the ratio of the major to minor axis of each ellipse we found that the HADHA Mut Glc condition had a ratio of 4.36 while the HADHA Mut Glc+FA condition had a ratio of 3.12 indicating that the HADHA Mut Glc+FA condition had a more rounded ellipse meaning more beat-to-beat variability in these CMs.

3.4.5   *Single cell RNA-sequencing identifies HADHA Mut CM subpopulations*

Single cell RNA-Sequencing was performed to better understand how the HADHA Mut CM population was behaving when challenged with FAs. A tSNE plot detailing each of the sequenced

cell groups showed a clear distinction between WT and HADHA Mut CMs, with a small but significant overlap (Figure 3-5A). When performing unbiased clustering, 6 clusters were found: 0 HADHA Mut CMs non-replicating, 1 an intermediate maturation population of WT and Mut CMs, 2 HADHA Mut CMs replicating, 3 healthy CMs, 4 fibroblast like population, 5 epicardial like population (Figure 3-5B,C and Figure 3-6A).

To assess degree of maturation and disease state we categorized each cluster based on the key categories described previously (Figure 2-3N). Up-regulated genes in cluster 3 were associated with myofibril assembly and striated muscle cell development while down-regulated genes in cluster 3 were associated with ribosomal proteins and ECM associated proteins. Interestingly, a subset of both WT and HADHA Mut CMs were identified in an intermediate CM maturation cluster, cluster 1, as described above (Figure 2-3L, Figure 3-5D). This cardiac population had a high up-regulation of OXPHOS and Myc target genes (Figure 3-6B). WT cells that further developed from this intermediate state were identified in the more mature CM state, cluster 3. HADHA Mut cells, however, entered two different pathological states of disease. We postulate that first, HADHA Mut cells lose many highly expressed and repressed cardiac markers along with cell cycle inhibitor CDKN1A, as seen in cluster 0 (Figure 3-6C). Finally, very diseased HADHA Mut CMs in cluster 2 up-regulate genes that should be highly repressed in mature CMs, and activate cell cycle genes (Figure 3-5D, Figure 3-6C,D and Supplemental Table S7). We benchmarked these stages of maturation and disease progression against *in vivo* mouse and human maturation markers and found a similar trend for maturation, disease progression and loss of cardiac identity (Figure 3-5E and Figure 3-6E-G).

Examining significantly changed hallmark pathways between HADHA Mut CM clusters and the WT CM cluster we found OXHPOS, cardiac processes and myogenesis, being depressed

in the mutant cells (Supplemental Table S8, S9). Furthermore, while WT CMs show strong expression of cell cycle repressor CDKN1A, both HADHA Mut CM populations lost this expression. Cluster 2, the replicating HADHA Mut CMs, had an up-regulation of DNA replication, G2M checkpoint and mitotic spindle genes (Supplemental Table S9). Moreover, genes that are expressed in replicating and/or endocycling cells such as MKI67 and RRM2 were expressed only in cluster 2 HADHA Mut CMs (Figure 3-6C). To address potential pathological outcomes of the abnormal cell cycle marker increase, we analyzed the number of nuclei per cell in HADHA mutant CM. Importantly, we observed a significant increase of the nuclei per cell in HAHDA Mut CMs as compared to WT CMs (Chi square test $P<0.001$) (Figure 3-5F,G). The majority of WT CMs were mono- or bi-nucleated which is the healthy state found *in vivo* for nuclei number in CMs [172]. However, the number of mono-nucleated HADHA Mut CMs was significantly reduced while the number of bi- and multi-nucleated HADHA Mut CMs were increased suggesting a pathological state in the HADHA Mut CMs [173]. These data support the surprisingly high cell cycle transcript expression we found in a subpopulation of HADHA Mut CMs (cluster 2). While we showed a pathological multi-nucleation in HADHA mutant CM, it is also possible that this phenotype is accompanied with pathological cell replication and polyploidization. These data suggest multiple stages of disease state.

We postulate three different states of pathology in HADHA Mut CMs challenged with FAs: intermediate state::non-replicating CM state::replicating CM state. Cluster 1 showed an intermediate state of CM maturity, characterized by elevated OXPHOS and Myc target genes (Supplemental Table S10). Importantly, both WT and HADHA CMs are found in cluster 1, suggesting that the HADHA CMs only manifest pathological phenotypes that separate them from wild type cells later in development, during maturation process, similar to seen in human

development. However, cluster 0 only contained HADHA mutant CM and showed a pathological state with depressed cell cycle repressors along with depressed metabolic and cardiac structural genes. Finally, cluster 2 was the most pathological having repressed metabolic and cardiac genes and upregulated cell cycle genes [174].

We performed unbiased metabolic pathway analysis, screening 68 metabolic pathways and found HADHA Mut CM clusters, 0 and 2, displayed reduced metabolic pathway gene expression in comparison to WT CM, cluster 3 (Figure 3-5H,I). Specifically, OXPHOS was one of the most down-regulated pathways followed by cholesterol metabolism and fatty acid oxidation. Interestingly, in cluster 2 there were two highly up-regulated metabolic pathways: nucleotide interconversion and folate metabolism, two key metabolic processes involved in DNA synthesis (Figure 3-5J). Since HADHA Mut CMs displayed disrupted expression of cardiac identify genes along with a down-regulation of many metabolic pathways including fatty acid and OXPHOS genes, we next wanted to examine the mitochondria and myofibrils of these cells.

Sarcomere degradation and aberrant mitochondrial activity of HADHA Mut and KO CMs When HADHA Mut and KO CMs were cultured in glucose-media alone, no obvious defects were observed in HADHA Mut and KO compared to the WT CMs (Figure 3-7A,B). However, when cultured 6-12 days in FA media, sarcomere and mitochondrial defects manifested in the HADHA Mut and KO CMs, while the WT CMs appeared normal (Figure 3-7C,D and Figure 3-8A). After 12D of Glc+FA media treatment, WT CMs had healthy myofibrils while the HADHA Mut and KO CMs showed sarcomere dissolution, as α-actinin staining became punctate and actin filaments were difficult to detect (Figure 3-7D and Figure 3-8A). Since HADHA Mut and KO CMs displayed a loss of sarcomere structure after being challenged with FAs we next began to assess mitochondrial health since the HADHA Mut and KO CMs were unable to process long chain FAs.

We first stained for mitochondria using ATP Synthase beta subunit to assess the presence of a mitochondrial network. We found that both the WT and HADHA Mut CMs had many connected mitochondria while the KO CMs had lost their mitochondrial network to small, more circular mitochondria. To assess the functionality of these mitochondria, we analyzed the mitochondrial proton gradient via mitotracker orange staining. After 12-days of Glc+FA rich media, HADHA Mut CMs had highly depressed mitochondrial membrane proton gradient while the HADHA KO CMs had severely disrupted mitochondrial networks (Figure 3-7D and Figure 3-8A,B).

To better assess the sarcomere and mitochondrial disease phenotype we performed transmission electron microscopy (TEM) on WT and HADHA Mut CMs after 12D of Glc+FA exposure (Figure 3-8C). WT CMs showed abundant myofibrils, clear Z bands but indistinct A-bands and I-bands, and no M-lines, indicating an intermediate, normal stage of CM myofibrillogenesis. Furthermore, WT CMs showed healthy mitochondria with good cristae formation. In contrast, HADHA Mut CMs showed poor myofibrils with a disruption of Z-disk structure replaced by punctate Z-bodies [175] and disassembled myofilaments in the cytoplasm. Interestingly, HADHA Mut CM mitochondria were small and swollen with very rudimentary cristae morphology (Figure 3-8C) [176]. Quantifying the WT and HADHA Mut CM mitochondria revealed HADHA Mut mitochondria were smaller in area and more rounded as compared to WT mitochondria (Figure 3-7E,F and Figure 3-8D,E). Finally, examining complex I-V proteins showed that HADHA Mut CMs had depressed complex I-IV protein expression in Glc+FA conditions (Figure 3-7G). These data show HADHA Mut CMs lose sarcomere structure and mitochondrial membrane potential and morphology while KO CMs lose sarcomere structure and mitochondrial network stability when exposed to FAs. The loss of complex I-IV and mitochondrial structure in HADHA Mut CMs suggested critical structural components of the

mitochondria were either disrupted or misprocessed. We next wanted to examine one phospholipid that is critical to mitochondrial homeostasis, cardiolipin (CL).

3.4.6   *Loss of HADHA function leads to abnormal cardiolipin formation and depletion of tetra [18:2] cardiolipin*

Cardiolipin is a phospholipid essential for optimal mitochondrial function and homeostasis as it maintains electron transport chain function along with other functions [63, 64]. CL is the major phospholipid of the mitochondrial inner membrane that is synthesized in the mitochondria and is dynamically remodeled during postnatal development and disease [66, 67]. The most abundant species of CL in the human heart is tetralinoleoyl-CL (tetra18:2) [68]. In cardiac diseases such as diabetes, ischemia/reperfusion and heart failure, or in more specific Tafazzin mutant in Barth syndrome, tetra18:2 CL levels decrease [69-72]. Using targeted lipidomics, we found that HADHA Mut CMs challenged with FAs showed a robust decrease of tetra18:2 CL, along with the significant depletion of the majority of other CL species (Figure 3-8F,G). Furthermore, the relative amount of monoylysocardiolipin (MLCL) [18:2] [18:2] [18:2] was the most abundant CL species in the mutant CMs (Figure 3-86F). This immature form of CL and its abundance is reminiscent of Barth syndrome patients, who have an inability to mature MLCL to CL [93]. Two species of interest, tetra18:1 CL and [18:1][18:1][18:2][18:2] CL showed significant enrichment in the HADHA Mut CMs (Figure 3-8G). Interestingly, [18:1][18:1][18:2][18:2] CL is specifically depleted in Barth syndrome patients who have a mutation in tafazzin [177, 178]. This may suggest that one avenue of CL remodeling has been hindered due to the HADHA mutation and instead, is more heavily relying upon tafazzin mediated remodeling of CL.

It has been previously shown that the HADHA protein has a similar enzymatic function to monolysocardiolipin acyltransferase (MLCL AT) [61]. MLCL AT transfers mainly unsaturated

fatty acyl chains to lyso-CL. It therefore seems plausible that HADHA has a direct role in remodeling cardiolipin to produce mature tetra[18:2] CL species in cardiomyocytes. Once tetra[18:2] CL species begin to deplete, the CM can fall into a pathological state of mitochondrial disarray. These data suggest that a mutation in the HADHA enzyme results in increased levels of MLCL and production of abnormal cardiolipin species. Lack of correct cardiolipin species can be causal for mitochondrial defects and pathology seen in HADHA CMs.

3.4.7 *SS-31 rescues aberrant proton leak in HADHA Mut CMs chronically exposed to FAs*

To better understand the pathological state of HADHA Mut and KO CMs exposed to chronic FAs we functionally assessed their mitochondria. We found that the maximum OCR of Glc+FA treated HADHA Mut and KO CMs were significantly depressed as compared to WT cells (Mut CM: 190 pmoles/min/cell, KO CM: 125 pmoles/min/cell, WT CM: 359 pmoles/min/cell, $P<0.05$) (Figure 3-8H). Furthermore, HADHA Mut CMs displayed reduced oxygen dependent ATP production (Mut CM: 51 pmoles/min/cell, KO CM: 43 pmoles/min/cell, WT CM: 93 pmoles/min/cell, $P<0.05$) (Figure 3-8I). Since we observed exposure to FAs led to a reduction in mitochondrial membrane potential, reducing ATP production, we postulated that this may be due in part to an increased proton leak [179, 180]. We showed by testing the difference in OCR between repressing ATP synthase (oligomycin treatment) and repressing the electron transport chain (antimycin, rotenone) that HADHA Mut and KO CMs had a significantly higher proton leak than WT CMs (Mut CM: 7.66 pmoles/min/cell, KO CM: 10.52 pmoles/min/cell, WT CM: 3.64 pmoles/min/cell, $P<0.05$). Previous studies have revealed that elamipretide (SS-31), a mitochondrial-targeted peptide can prevent mitochondrial depolarization, the proton leak [181]. Interestingly, a 1nM treatment of HADHA Mut cardiomyocytes with elamipretide (SS-31) rescued the increased proton leak in Glc+FA challenged Mut CMs (Figure 3-8J). These data suggest that HADHA Mut and

KO CMs exposed to FAs resulted in reduced mitochondrial capacity due in part to increased proton

leak.

3.5   DISCUSSION

We have generated the first human MTP deficient cardiac model *in vitro* utilizing MiMaC matured hiPSC-CMs and discovered that a TFPα/HADHA defect in long-chain FAO results in disease like erratic beating suggesting a pro-arrhythmic state. We further showed a mechanism of action; mutations in HADHA resulted in abnormal composition of the prominent phospholipid, cardiolipin due to its acyl-CoA transferase activity [61]. Abnormal CL composition results in defective mitochondrial cisternae and highly reduced mitochondrial proton gradient. These mitochondrial defects manifested as sarcomere dissolution, defective calcium handling and electrophysiology. Delayed calcium storage and repolarization contributed to the uneven cardiomyocyte beating patterns, which in turn can precipitate tissue level arrhythmia seen in MTP deficient newborns with SIDS.

Using pluripotent stem cell derived cardiomyocytes we searched for the etiology of the arrhythmia observed in patients with HADHA mutations, causing MTP deficiency. Importantly, hiPSC derived HADHA mutant cardiomyocytes recapitulated the arrhythmic phenotype observed in patients, emphasizing the utility of hiPSC-CMs for modeling human disease. To better understand the cause of the arrhythmia, we dissected the phenotypes using fatty acid challenged HADHA cardiomyocytes and identified a potential clue for the disease progression, cardiolipin. One novel therapeutic intervention that rescued part of the HADHA mutant phenotype was SS-31. SS-31 is a mitochondrial targeted peptide that has been shown to bind cardiolipin and prevent cardiolipin conformation changes under stress such as peroxidation [182]. SS-31 has been shown to inhibit mitochondrial depolarization and swelling in cardiac cells and islets and rescue cardiolipin defects in cardiomyocytes [181, 183]. Since we found that SS-31 rescued the increased proton leak in FA challenged HADHA CMs, and since abnormal CL species are observed in

HADHA mutant, we propose cardiolipin defects precipitate our observed mitochondrial dysfunction.

Cardiolipin is a critical component of the mitochondrial inner membrane. It is an atypical phospholipid composed of four (instead of two) acyl chains that are connected with a glycerol moiety. This atypical structure of cardiolipin results in a conical shape that is thought to be critical for inner mitochondrial membrane structure and function [62]. In particular, cardiolipin has been shown to function in organizing the electron transport chain (ETC) higher order structure, important for ETC activity, and acts as a proton trap on the outer leaflet of the inner mitochondrial membrane [65]. Hence, the reduction of the mature form of CL results in mitochondrial abnormalities such as proton gradient loss, ETC depression resulting in depressed ATP production and abnormal mitochondrial architecture [64].

Pathological remodeling of CL has been implicated in the mitochondrial dysfunction observed in diabetes, heart failure, neurodegeneration, and aging [64, 83]. However, the pattern and composition of abnormal CL species in the case of HADHA mutant was more specific than seen previously in heart failure or diabetes, suggesting that HADHA may be directly involved in CL processing. Interestingly, previous studies using HeLa cells have suggested HADHA exhibits acyl-CoA transferase activity upon monolysocardiolipin (MLCL) for its remodeling into cardiolipin [61]. As such, these data suggest that defects in HADHA directly cause impaired cardiolipin remodeling resulting in the inability to produce and possibly maintain the acyl chain composition of mature cardiolipin [84]. However, the exact contribution of this acyltransferase to physiological CL remodeling has been unclear [61]. We now report that in our FA challenged human HADHA mutant cardiomyocytes MLCL became the most abundant cardiolipin while mature tetra[18:2] cardiolipin was depleted and mitochondrial activity was compromised, similar

to seen previously in Tafazzin mutant causing Barth's syndrom [184]. These data for the first time establish the exact contribution of HADHA acyltransferase to physiological CL remodeling in human cardiomyocytes.

Barth syndrome, an X-linked cardiac and skeletal mitochondrial myopathy due to mutations in the gene tafazzin (TAZ), has a similar disease etiology and cardiac manifestation as MTP deficiency [184, 185]. Tafazzin is a transacylase which is essential for the remodeling of MLCL to mature cardiolipin [186]. Both HADHA and TAZ play key roles in generating mature cardiolipin and both diseases have similar pathological phenotypes including sudden unexplained death due to ventricular arrhythmias [184]. CL- [18:1][18:1][18:2][18:2], which are specifically reduced in abundance in TAZ mutants, showed an increased abundance in our HAHDA Mut CMs. This suggests that since mutant HADHA is not able to remodel CL, TAZ becomes the preferred enzyme which, results in abnormal accumulation of TAZ mediated MLCL remodeled CL species. These data suggest a linear or parallel relationship between the two enzymes in cardiolipin processing in human cardiomyocytes.

Here we have shown that FA exposure to MTP deficient CMs leads to abnormal cardiolipins pattern that result in severe mitochondrial defects and calcium abnormalities that pre-dispose CMs to erratic beating in HADHA Mut CMs. We identified SS-31 as a novel therapy to rescue the proton leak phenotype of FA challenged HADHA Mut CMs. This suggests that SS-31, or other cardiolipin affecting compounds, may serve as a potential treatment to help mitigate aspects of mitochondrial dysfunction in MTP deficiency and potentially other cell autonomous defects of FAO disorders.

3.6   FIGURES
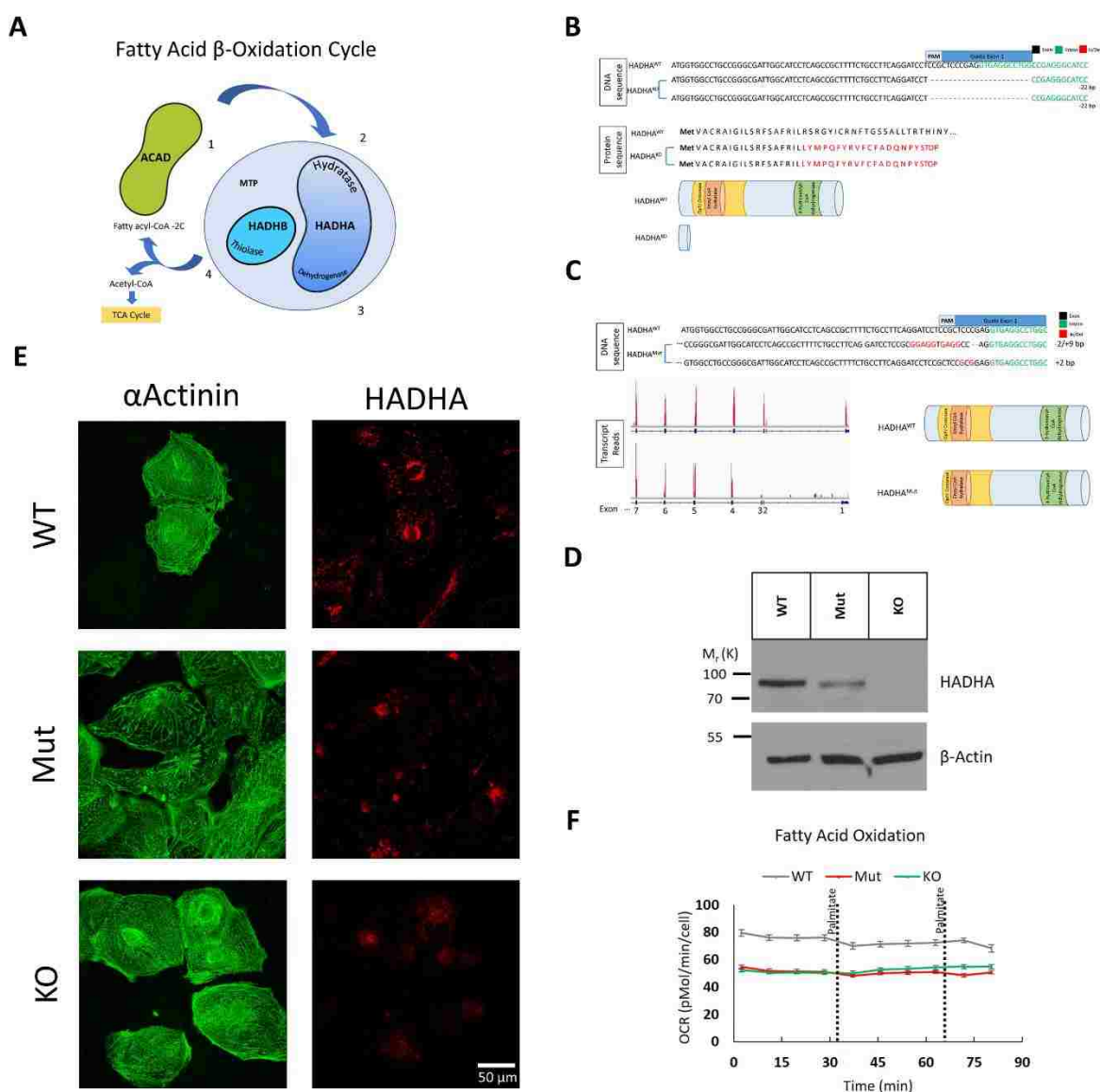
Figure 3-1: Generation of HADHA Mutant and Knockout stem cell derived cardiomyocytes. A) Schematic of fatty acid beta-oxidation detailing the four enzymatic steps. B) Schematic of HADHA KO DNA and protein sequence from WTC iPSC line showing a 22bp deletion which resulted in an early stop codon. C) Schematic of HADHA Mut DNA and protein sequence from WTC iPSC line showing a 2bp deletion and 9bp insertion on the first allele and a 2bp deletion on

the second allele. RNA-Sequencing read counts show that the HADHA Mut expresses exons 4-20 resulting in a truncated protein. D) Western analysis of HADHA expression and housekeeping protein β-Actin in WTC iPSCs. E) Confocal microscopy of WT, HADHA Mut and HADHA KO hiPSC-CMs for the cardiac marker αActinin (green) and HADHA (red). F) Seahorse analysis trace of fatty acid oxidation capacity of WT, HADHA Mut and HADHA KO hiPSC-CMs.
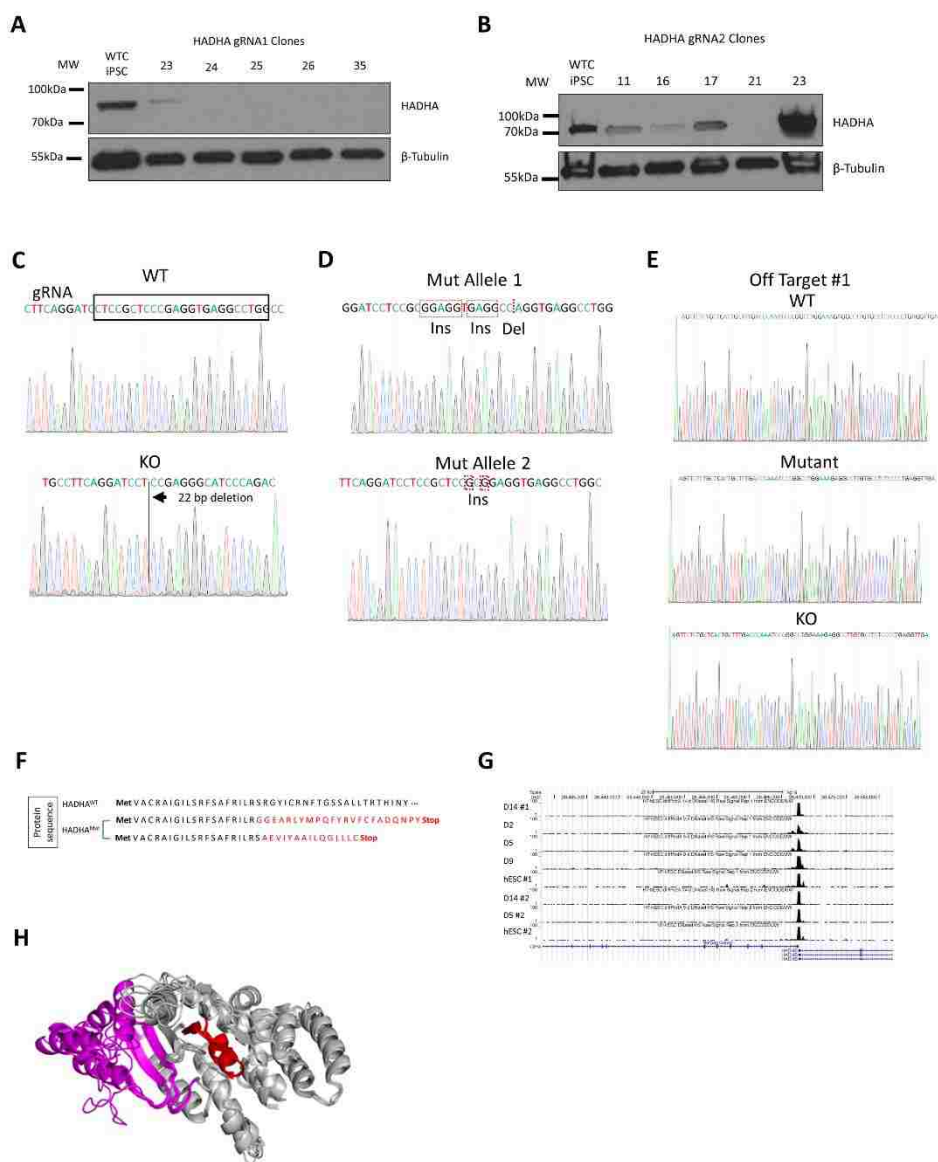
Figure 3-2: HADHA iPSC clone analysis.

A) Western of five clones generated from gRNA1 induction of HADHA mutations. B) Western of five clones generated from gRNA2 induction of HADHA mutations.HADHA iPSC mutation characterization. C) Chromographs of WTC iPSC WT and HADHA gRNA1 clone #35 (KO). D) Chromograph of clone #23 (mutant, each allele shown). WT iPSC shows the gRNA region in the red box. KO shows the position of the 22bp deletion. E) Chromographs of WTC iPSC WT, HADHA mutant and HADHA KO off-target #1 PCR amplification. F) Predicted protein sequence

of HADHA Mut (clone #23). G) DNA-Seq. data showing the location of H3K4me3 marks indicating transcription start site. HADHA is expressed in the stem cell state and throughout stem cell derived cardiomyocyte differentiation at D2, 5, 9 and 14 with only one region in exon 1 for the TSS. H) HADHA protein model of exons 1-11 (half the protein) showing exons 1-3 in purple, exons 4-11 in grey and the enoyl-CoA hydratase catalytic pocket in red.
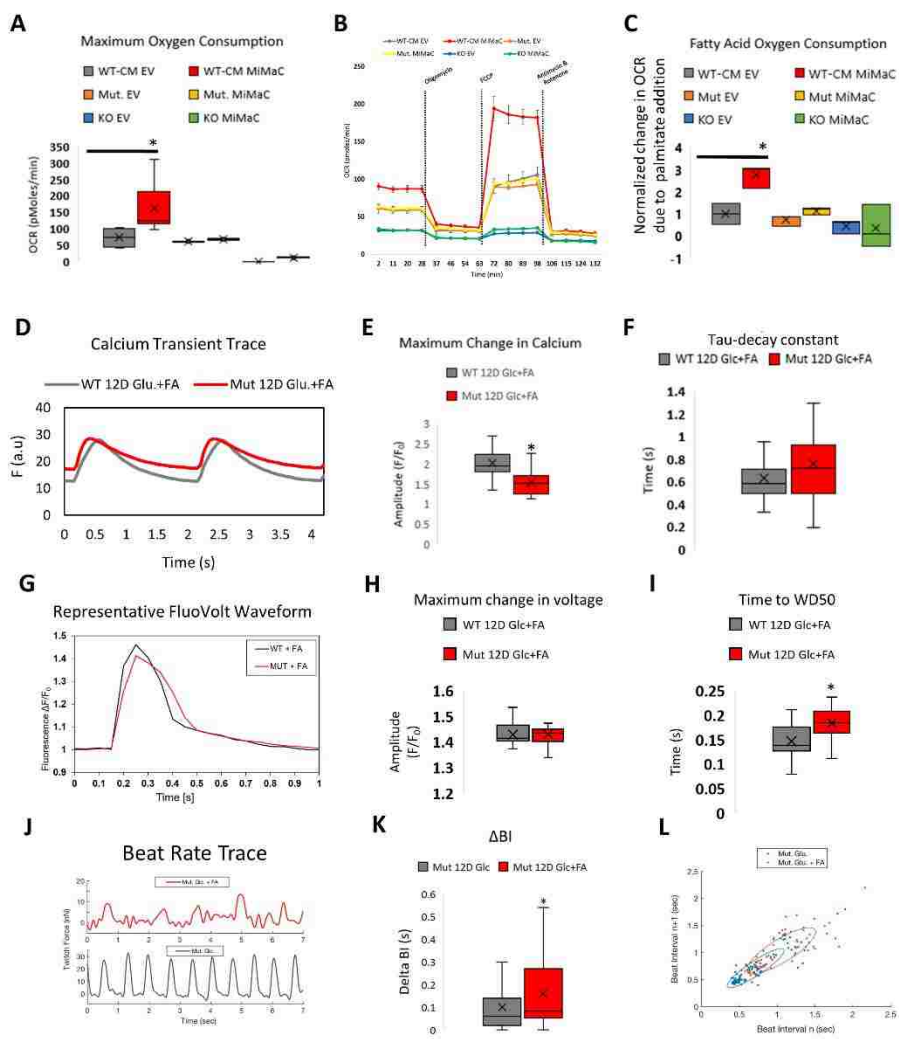
Figure 3-3: Fatty acid challenged HADHA Mut CMs displayed elevated cytosolic calcium levels leading to increased beat rate irregularities.

A) Seahorse mitostress assay to analyze maximum oxygen consumption rate after oligomycin and FCCP addition. MiMaC treated CMs showed a significant increase in maximum OCR compared to control EV CMs. B) Representative trace of the mitostress assay. C) Seahorse analysis of fatty acid oxidation capacity showed that MiMaC treated hiPSC-CMs matured to a point where they could oxidize palmitate for ATP generation while controls cells were not able to utilize palmitate. MiMaC hiPSC-CMs had a significant increase in OCR due to palmitate addition. Both MiMaC treated Mut and KO hiPSC-CMs were unable to oxidize palmitate. D) Representative trace of the

change in fluorescence during calcium transient analysis. E) Quantification of the maximum change in fluorescence during calcium transients. Mut CMs as compared to WT CMs after 12D of Glc+FA media treatment had a statistically significantly lower change in calcium. F) Quantification of the tau-decay constant. Mut CMs as compared to WT CMs after 12D of Glc+FA media treatment had a higher tau-decay constant. G) Representative trace of the change in fluorescence during Fluovolt, action potential, analysis. H) Quantification of the maximum change in fluorescence during action potential. I) Time to wave duration 50% is significantly longer in Mut CMs as compared to WT CMs after 12D of Glc+FA media treatment. J) Representative beat rate trace of Mut CM in Glc or Glc+FA media. K) Quantification of the change in beat interval (ΔBI). Mut CMs in Glc+FA media as compared to Mut CMs in Glc media had a statistically significant higher ΔBI. L) Poincaré plot showing ellipses with a 95% confidence interval for each group. The more rounded ellipse of the Mut Glc+FA condition shows that these cells had a greater beat to beat instability as compared to Mut Glc CMs.
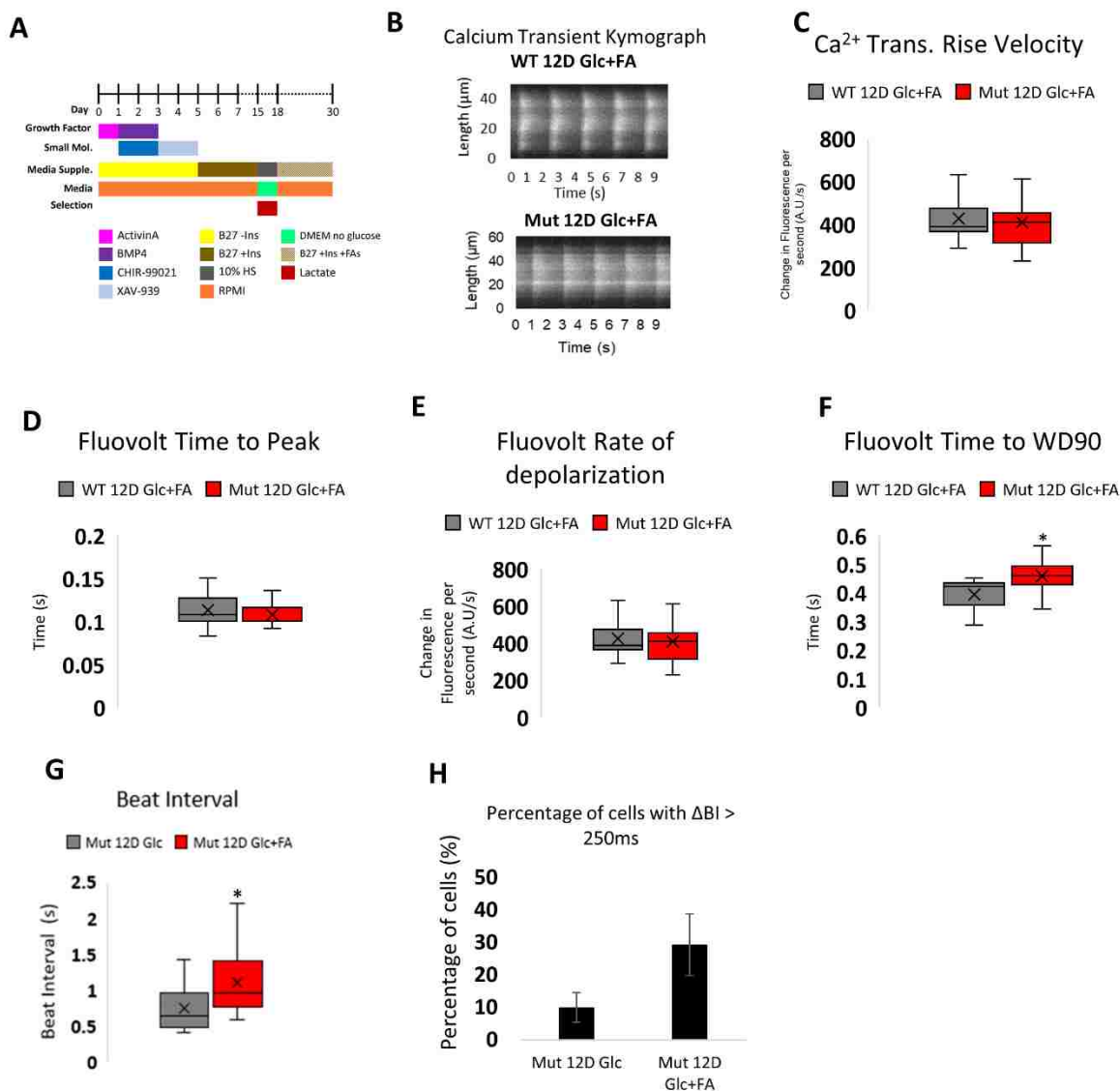
Figure 3-4: HADHA Mut hiPSC-CMs have abnormal calcium, electrophysiology and beat rates.

A) Schematic of fatty acid treatment of WT and Mut hiPSC-CMs. B) Representative kymograph of WT and Mut CMs after 12D of Glc+FA media   C) Quantification of the rate of calcium release, calcium rise velocity. D) Quantification of the time to reach maximum depolarization. E) Quantification of the rate of maximum depolarization. F) Time to wave duration 90% is significantly longer in Mut CMs as compared to WT CMs after 12D of Glc+FA media treatment.

G) Quantification of the beat interval. Mut CMs in Glc+FA media as compared to Mut CMs in Glc media had a statistically significant higher beat interval. H) Quantification of the number of cells with a ΔBI greater than 250ms suggesting an erratically beating cell. Mut CMs after 12D of Glc+FA media as compared to Mut CMs in Glc media had a higher percentage of cells with ΔBI's greater than 250ms.
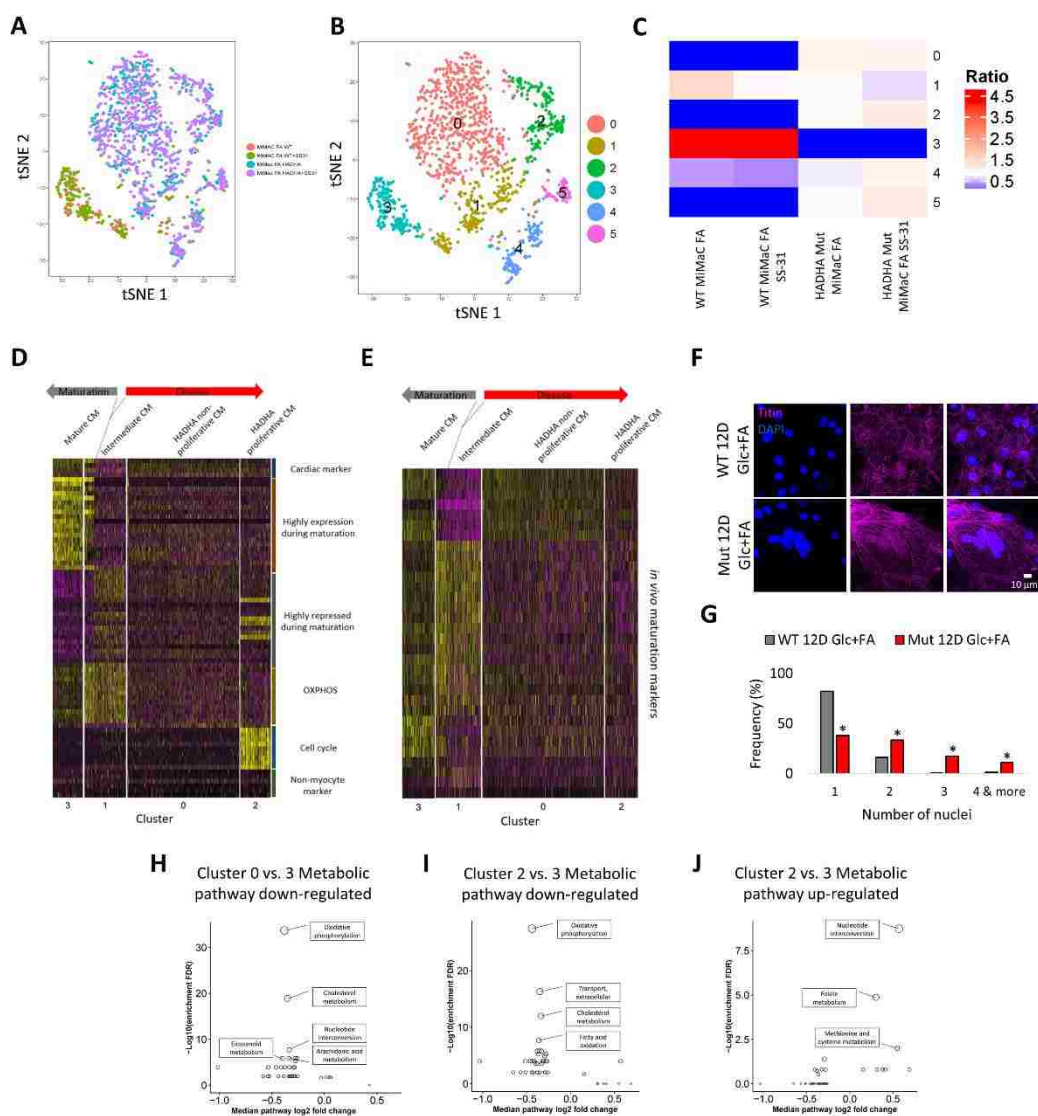
Figure 3-5: scRNA-Seq reveals multiple disease states of fatty acid challenged HADHA Mut CMs.

A) Single cell RNA-sequencing tSNE plot of WT compared to HADHA Mut CMs shows a clear distinction between these two groups. Four conditions of D30 CMs: 6 days of FA treated MiMaC WT CM, 6 days of FA and SS-31 MiMaC WT CMs, 6 days of FA treated MiMaC HADHA Mut CMs and 6 days of FA and SS-31 treated MiMaC HADHA Mut CMs. B) Unbiased clustering revealed 6 unique groups. C) Heatmap detailing the enrichment of conditions in each cluster. D) Heatmap of maturation categories based on MiMaC cluster. E) Heatmap of *in vivo* mouse

maturation markers that are up-regulated with maturation. F) Confocal microscopy showing that HADHA Mut CMs have more nuclei than WT CMs. Blue – DAPI and pink – Titin. G) Histogram of the frequency of cells with either 1, 2, 3 or 4 or more nuclei. HADHA mutant CMs have a significant number of cells with 3 or more nuclei. H) Down-regulated metabolic pathways in cluster 0 (non-replicating HADHA CMs) as compared to cluster 3 (WT CMs). I) Down-regulated metabolic pathways in cluster 2 (endoreplicating HADHA CMs) as compared to cluster 3 (WT CMs). J) Up-regulated metabolic pathways in cluster 2 (endoreplicating HADHA CMs) as compared to cluster 3 (WT CMs). Metabolic bubble plot circle size is proportional to the statistical significance. The smaller the p-value, the larger circle. Adjusted p-value 0.01 used as cut-off.
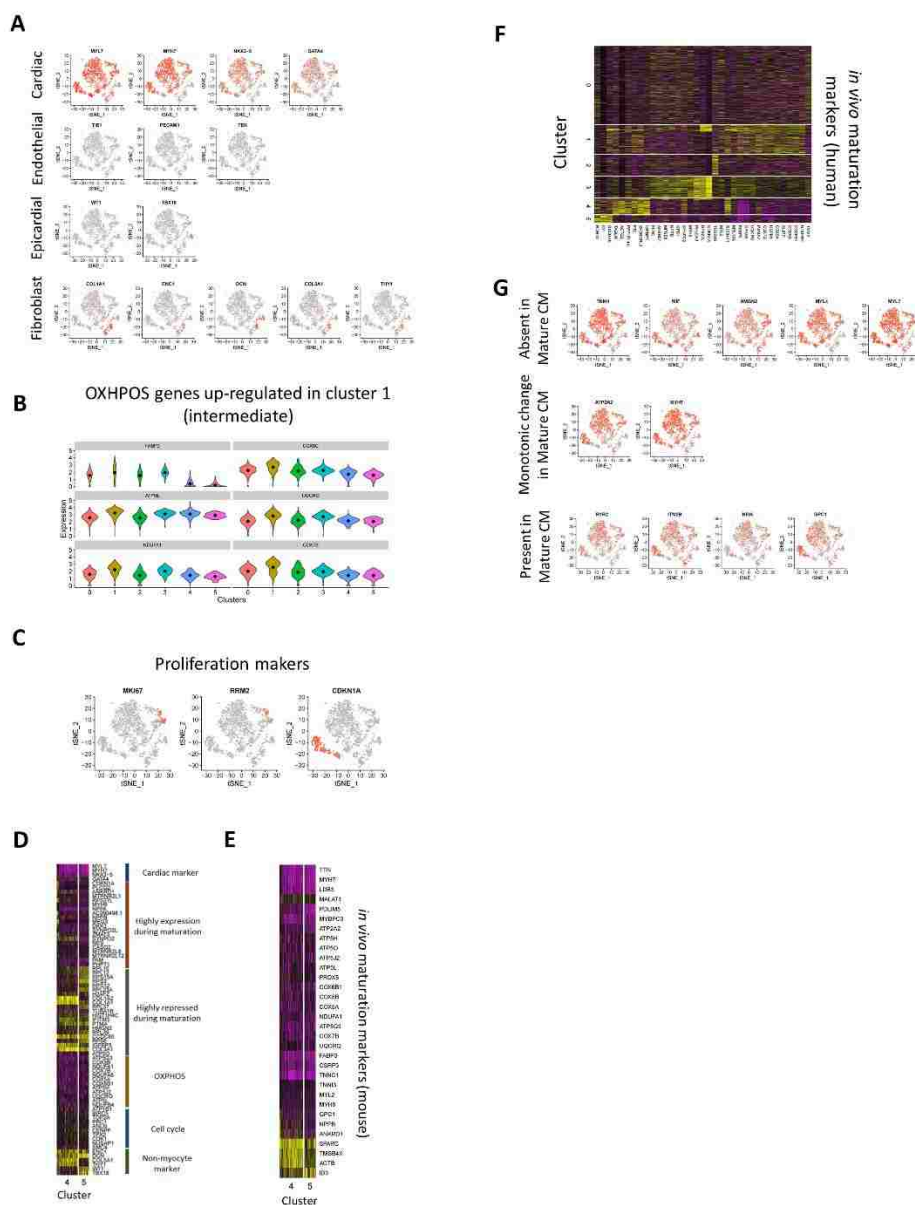
Figure 3-6: Single Cell RNA-Sequencing elucidates HADHA CM subpopulations.
A) tSNE plots of cell lineage markers. B) Set of OXPHOS genes up-regulated in cluster 2, the intermediate maturation group. C) tSNE plots showing HADHA Mut CMs lose cell cycle repressor CDKN1A and a subset of HADHA Mut CMs gain markers for proliferation: MKI67 and RRM2. D) Heatmap of maturation categories based on MiMaC cluster. E) Heatmap of *in vivo* mouse maturation markers that are up-regulated during mouse cardiac maturation. F) Heatmap of

in vivo maturation markers that are up-regulated during human cardiac maturation. G) Set of genes changing during cardiomyocyte maturation show the intermediate cluster is less mature.
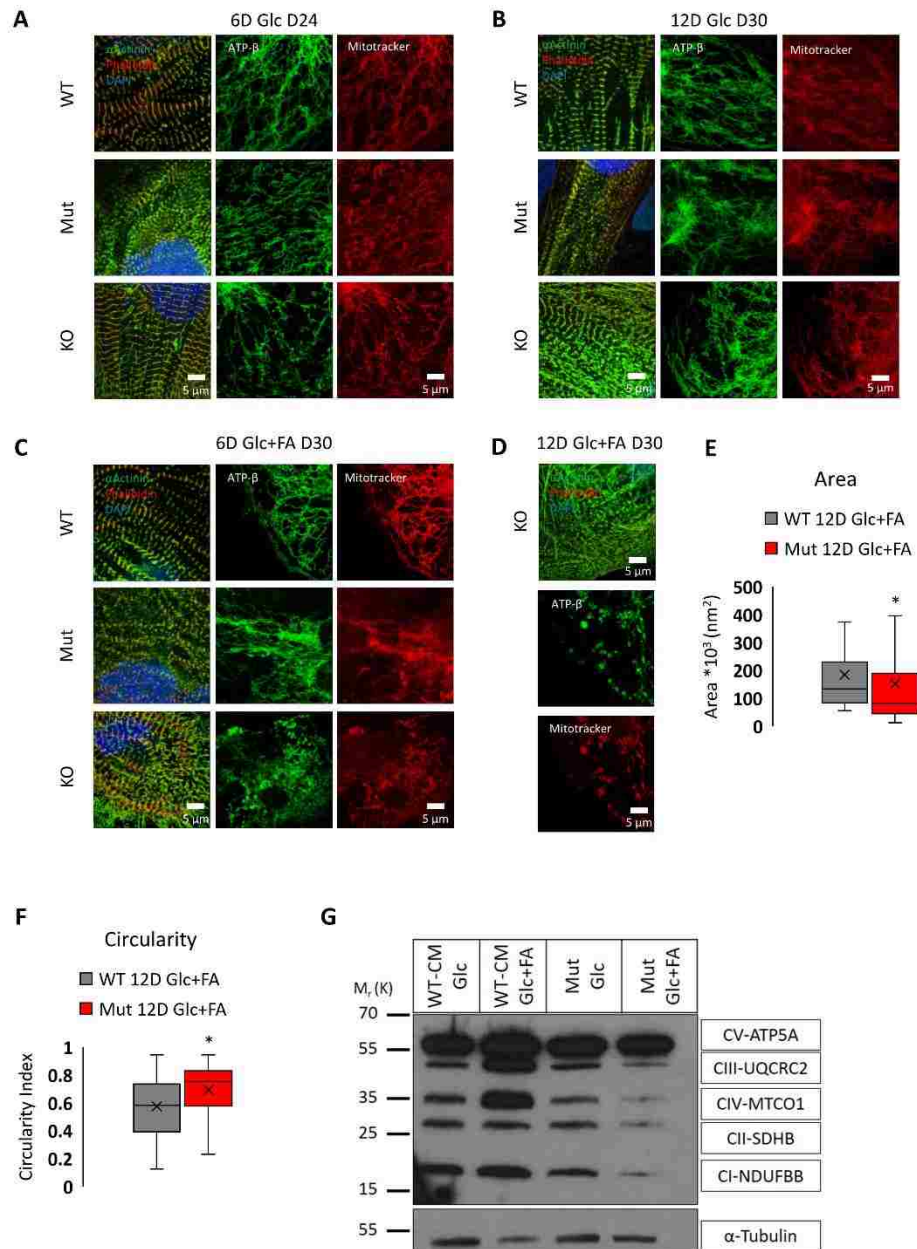
Figure 3-7: HADHA Mut hiPSC-CMs after 6D of glucose and fatty acid media treatment show mild sarcomere and mitochondrial defects.

A) Representative confocal images of D24 WT, HADHA Mut and HADHA KO hiPSC-CMs cultured in glucose media. Myofibril staining of αActinin (Green) and actin (phalloidin – red) show no abnormalities. Mitochondrial staining with ATP synthase β subunit (green) and mitochondrial potential gradient shown via mitotracker staining (red) show no mitochondrial

abnormalities. B) Representative confocal images of D30 WT, HADHA Mut and HADHA KO hiPSC-CMs cultured in glucose media. Myofibril staining of αActinin (Green) and actin (phalloidin – red) show no abnormalities. Mitochondrial staining with ATP synthase β subunit (green) and mitochondrial potential gradient shown via mitotracker staining (red) show no mitochondrial abnormalities. C) Representative confocal images of WT, HADHA Mut and KO hiPSC-CMs after 6D of glucose and fatty acid media treatment. After 6D of glucose and fatty acid media treatment WT hiPSC-CMs display normal sarcomere and mitochondria. After 6D of glucose and fatty acid media treatment HADHA Mut and KO hiPSC-CMs display signs of sarcomere disruption as seen in the less defined αActinin staining and the beginnings of loss of mitochondrial proton gradient as seen from the mitotracker staining in the mutant. ATP synthase β subunit (green) shows normal mitochondrial networks in both the WT and HADHA Mut hiPSC-CMs while there are the beginnings of loss of mitochondrial network in the HADHA KO hiPSC-CMs. D) Representative confocal images of HADHA KO hiPSC-CMs after 12D of glucose and fatty acid media treatment. After 12D of glucose and fatty acid media treatment HADHA KO hiPSC-CMs display severely disrupted sarcomere and mitochondria structure. E) Quantification of mitochondria area in WT and HADHA Mut CMs shows small mitochondria size in Mut CMs. F) Quantification of mitochondria circularity index in WT and HADHA Mut CMs shows rounder mitochondria in Mut CMs. G) HADHA Mut hiPSC-CMs show a reduction in complex I-IV proteins after 12D of glucose and fatty acid media treatment. Western analysis of complex I-V of the electron transport chain for WT and HADHA Mut hiPSC-CMs cultured either in glucose or glucose and fatty acids for 12D.
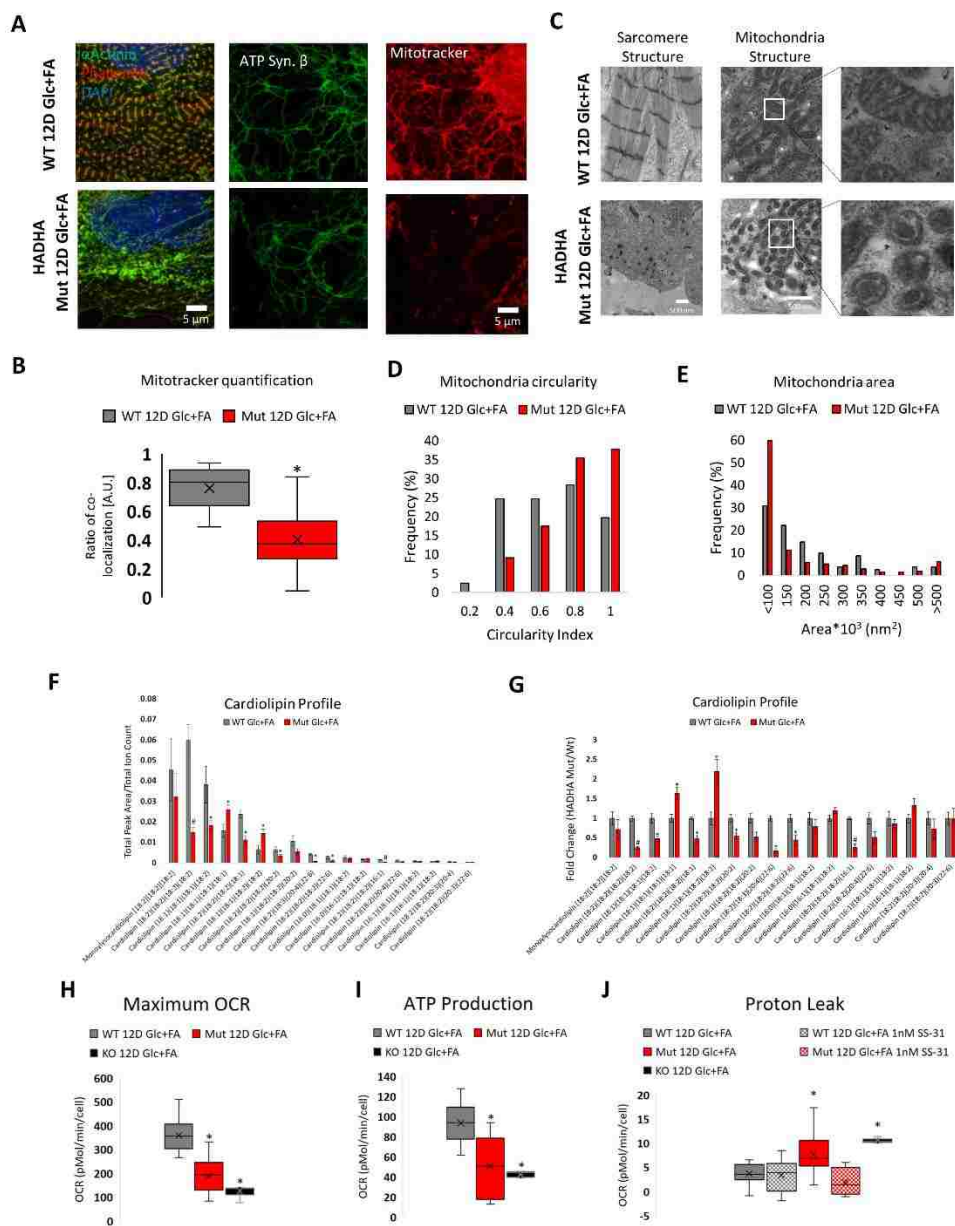
Figure 3-8: Fatty acid challenged HADHA Mut CMs displayed swollen mitochondria with severe mitochondrial dysfunction.

A) Representative confocal images of WT and Mut CMs in 12D of Glc+FA media. B) Quantification of mitotracker and ATP synthase β colocalization and intensity. C) Transmission electron microscopy images of WT and Mut CMs after 12D of Glc+FA media showing sarcomere and mitochondria structure. D) Histogram of mitochondria circularity index for WT and HADHA

Mut CMs after 12 days of Glc+FA media showed HADHA Mut CMs mitochondria are rounder. E) Histogram of mitochondria area for WT and HADHA Mut CMs after 12 days of Glc+FA media showed HADHA Mut CMs mitochondria are smaller. F) Abundances of different cardiolipin species in WT and HADHA Mut CMs. G) Relative abundance of different cardiolipin species in WT and HADHA Mut CMs. H) Quantification of maximum OCR from mitostress assay. Mut and KO CMs as compared to WT CMs after 12D of Glc+FA media had a significantly lower max OCR. I) Quantification of ATP production from mitostress assay, calculated as the difference between baseline OCR and OCR after oligomycin. Mut and KO CMs as compared to WT CMs after 12D of Glc+FA media had significantly lower ATP production. J) Quantification of proton leak from mitostress assay, calculated as the difference between OCR after oligomycin and OCR after antimycin & rotenone. Mut and KO CMs as compared to WT CMs after 12D of Glc+FA media had significantly higher proton leak. SS-31 treated Mut CMs after 12D of Glc+FA had a significantly lower proton leak and non-treated Mut CMs.

Chapter 4. AMINO ACID PRIMING OF MTOR IS ESSENTIAL FOR HEART REGENERATION

Parts of this chapter are in the following manuscript:

Amino acid priming of mTOR is essential for heart regeneration

Jason W. Miklas*, Peter Hofsteen*, Shiri Levy, Jeanot Muster, Aaron M. Robitaille, Lauren Abell, Jamie M. Goodson, Nicholas Strash, Inez Pranoto, Anup Madan, Michael T. Chin, Rong Tian, Yuliang Wang, Charles E. Murry, Randall T. Moon, Hannele Ruohola-Baker

* Equal authorship

4.1 ABSTRACT

For a short period of time in mammalian neonates, the mammalian heart can regenerate via cardiomyocyte proliferation. This regenerative capacity is largely absent in adults. In other organisms, including zebrafish, damaged hearts can regenerate throughout their lifespans. Many studies have been performed to understand the mechanisms of cardiomyocyte de-differentiation and proliferation during heart regeneration, however, the underlying reason why adult zebrafish and young mammalian cardiomyocytes are primed to enter cell cycle have not been identified. Here we show the primed state of a pro-regenerative cardiomyocyte is dictated by its amino acid profile and metabolic state. Adult zebrafish cardiomyocyte regeneration is a result of amino acid-primed mTOR activation. Zebrafish and neonatal mouse cardiomyocytes display elevated glutamine levels, predisposing them to amino acid-driven activation of mTORC1. Wnt/β-catenin signalling is an early responding pathway that results in the instigation of primed mTORC1 activation and later metabolic remodeling necessary for zebrafish cardiomyocyte maturation. Hence, we have identified a unique mTORC1 primed state shared by both zebrafish and mammalian regeneration competent cardiomyocytes.

4.2 RATIONALE

Cardiovascular disease is the leading cause of death worldwide. One of the major contributors to cardiovascular morbidity is myocardial infarctions (MI). While there have been improvements in treating the short-term pathologies associated with MI, many patients succumb to heart failure (HF) after five years. None of the current treatments for MI repair damage to the heart, but rather delay the onset of HF. Consequently, significant efforts are underway to develop strategies to re-muscularize the myocardium lost after MI [100].

After ischemic injury to the human heart, the lost myocardium is replaced by non-contractile scar tissue as cardiomyocytes that reside there have little proliferative capacity [187, 188]. In contrast, neonatal mouse hearts have the capacity to regenerate lost myocardium through cardiomyocyte proliferation [187-189]. However, the fully matured cardiomyocytes found in the adult mammalian heart lose their capacity to re-enter the cell cycle [190]. Cardiomyocyte maturation coincides with a metabolic switch from glycolysis to fatty acid oxidation, which functions to regulate the cell cycle. In non-regenerating species, during pathological states when regeneration attempts, but fails to occur, a reversion to a more naïve metabolic state is induced. Thus, understanding the molecular mechanisms regulating the metabolic state of cardiomyocyte maturation is likely to be important to developing new treatment options.

Zebrafish (*Danio rerio*) are a regenerative model organism used to study the molecular mechanisms regulating cardiac repair, since their cardiomyocytes retain the ability to re-enter the cell cycle after injury in the adult state [104, 191, 192]. Specifically, adult zebrafish cardiomyocytes de-differentiate to re-enter the cell cycle and then repopulate the lost myocardium [193]. Furthermore, the signaling events that control this regenerative process are complex, and include: the cross-talk between nerves and cardiomyocytes [194], notch signaling [195] and cell

cycle regulators such as Neuregulin1 [196] and Msp1 [197]. However, it is still unclear why adult zebrafish cardiomyocytes retain the potential to re-enter the cell cycle, and what other signaling pathways may contribute to this process.

A plethora of signaling pathways have been implicated in non-mammalian regeneration including: Activin, Bmp, Fibroblast growth factor (Fgf), Sonic hedgehog, Insulin-like growth factor (IGF), Notch, and retinoic acid (RA) [198, 199]. Here, we have focused on investigating the contributions of Wnt/β-catenin signaling and mechanistic target of rapamycin (mTOR) signalling to cardiomyocyte proliferation. The Wnt/β-catenin pathway is a conserved controller of cell fate and proliferation during embryonic development. Whereas, mTOR is a central regulator of growth and metabolism during the G1-phase of the cell cycle [200]. Interestingly, both pathways regulate zebrafish fin regeneration [198, 201]. Thus, we speculated that crosstalk between the Wnt and mTOR signaling networks would be important for promoting heart regeneration. Currently, the roles of Wnt and mTOR signaling have not been studied in the context of zebrafish heart regeneration. Furthermore, it is not clear whether there is an interaction between Wnt and mTOR signaling pathways during cardiac regeneration, and if these signaling pathways can be used to stimulate human cardiomyocyte proliferation. Here, we found that Wnt and mTORC1 signaling are up-regulated during cardiac regeneration. The inhibition of either of these pathways leads to decreased cardiomyocyte proliferation and scar formation. These findings implicate the Wnt-mTOR signaling axis as a potent mitogen activating pathway during zebrafish cardiac regeneration.

4.3 METHODS

4.3.1 *Zebrafish*

Wild-type (AB; Zebrafish International Resource Center, Eugene, OR, USA), Tg(*myl7:EGFP*) [202], hsWnt8:GFP [Tg(*hsp70l:Wnt8a-GFP*)[w34]] and *hsDKK:GFP* [Tg(*hsp70l:DKK1b-GFP*)[w32]] [201], s*iam:mCherry* [Tg(7xTCF.siam:nlsmCherry)] [203], TOP:dGFP [204] and vmhc:mCherry-NTR [Tg(vmhc:mCherry-Eco.NfsB)] [195] were used and maintained using standard procedures [205] in accordance with the Institutional Animal Care and Use Committee-approved protocols IACUC 2057-01 & 4364-02. Reverse osmosis system water is used and the water chemistry was adjusted to a temperature of 27.5°C, pH of 7.5, conductivity of 800 µS, hardness of 140 ppm, alkalinity of 35 ppm, dissolved oxygen content of 7.8 mg/L, and a total gas pressure of 101%. The average nitrate level is 55 ppm, the average nitrite level is 0.05 ppm, and the average ammonium level is 0.01 ppm. Larval feed starting at 5 dpf is a rotifer polyculture supplemented with the Zeigler larval diet, at 12 dpf live artemia is added to the diet, and at 60-90 dpf the fish are started on the Zeigler adult diet supplemented with live artemia once per day. The health status of the colony showedlow presence of *pseudoloma neurophilia* and an extremely low presence of *mycobacterium spp.* with no major clinical or subclinical findings of significance.

4.3.2 *Chemical ventricular cardiomyocyte ablation, surgical ventricular resection of the heart ventricle and young 3-day old heart isolation*

All chemical ventricular cardiomyocyte (VCM) ablation and ventricular resections were conducted on adult Zebrafish (~5-12 months old). For chemical mediated VCM ablation, fish were treated with 5 µM Metronidiazole (MTZ; Sigma) containing 0.1% dimethyl sulfoxide (DMSO) or vehicle control (0.1% DMSO) for 24 h protected from light. Following chemical treatment fish

were placed back in original aquaria and hearts were collected at 0 (prior to MTZ), 3, 7, 12 and 14 days post injury (dpi). Surgical ventricular resection was performed as previously described [197]. Briefly, zebrafish were anaesthetized in buffered 0.0168% tricaine methanesulfonate (MS-222), immobilized in a sponge, and skin posterior the heart cavity was opened to expose the apex of the heart ventricle. Bupivacaine was injected at the surgical site (1mg/kg) as a nerve block. Using microscissors, ~20% of the heart ventricle apex was resected, and the incision site was closed with VetBond. Following surgery, fish hearts were allowed to clot and returned to a draped static tank with an airstone for 24hr. The following day, fish were returned to their original aquaria until study termination. Larval hearts (72 hpf) were isolated and pooled as previously described [206, 207].

4.3.3   *Zebrafish heat shock*

Heterozygous Tg(*hsp70l:DKK1b-GFP*)[w32] and Tg(*hsp70l:Wnt8a-GFP*)[w34] fish were used to inhibit and induce canonical Wnt/β-catenin signalling respectively. Wnt8a and Dkk1b induction was achieved by exposing fish to water slowly increased from 28°C to 37°C. Fish remained at 37°C for 60 minutes, and were slowly brought back to normal water temperature. Fish were exposed to this heat shock protocol at least 4 hours prior to surgery and resumed daily heat shocks at 2 days post amputation.

4.3.4   *Gas chromatography-mass spectrometry*

GC-MS was conducted as previously described [208]. Briefly, frozen zebrafish heart tissue (20-25 mg) specimens were mixed with a 1.2mL mixture of cold methanol and chloroform (1:2 v/v; 4C) and homogenized using tissue teAror homogenizer and sonicated for 20 s. A further 800 μL cold chloroform/distilled water solution (1:1 v/v) was added, the sample was then vortexed and the set aside for 30 min on ice to separate the solvent layers. Next, after centrifugation (2000 rpm),

the aqueous (top) layer was separated and filtered using 1.5 mL 0.2 μm syringe filter and freeze dried.

To prepare the samples for GC/MS analysis, 30uL of 20mg/mL methoxyamine hydrochloride dissolved in pyridine was added to the dried aqueous metabolites, and samples were incubated at 37°C for 90 min. MTBSTFA (70 uL) was subsequently added and incubated at 37°C for 30 min. Samples were run on an Agilent 5977A Series GC/MSD system.

4.3.5   *Mouse heart isolation*

All animal experiments were performed with the approval of the Institutional Animal Care and Use Committee of the University of Washington. Mice with C57BL/6 background were purchased from Charles River. Mice were maintained on standard chow diet and water was available ad libitum in a vivarium with a 12-hr light-dark cycle at 22°C. Adult mice were anesthetized with sodium pentobarbital (150 mg/kg intraperitoneally) prior to heart isolation. Ventricles were removed and freeze clamped in liquid nitrogen. P0 and P7 mice were euthanized by decapitation. The hearts were removed and trimmed of atrial tissue, rinsed with PBS to remove blood, and snap frozen in liquid nitrogen. The hearts were stored at -80°C until analysis.

4.3.6   *RNA-sequencing and bioinformatics*

RNA-seq samples generated by this study and Bednarek et al ([209], accession number GSE71755) were aligned to Ensembl GRCz10 using Tophat ([134], version 2.0.13). Gene-level read counts were quantified using htseq-count [135] using Ensembl GRCz10 gene annotations. Genes with at least 10 normalized read counts summed across RNA-seq samples were kept for further analysis. *prcomp* function from R was used to for Principal Component Analysis. DESeq [136] was used for differential gene expression analysis. Genes with Benjamin- Hochberg adjusted

False Discovery Rate <0.1 and fold change >2 were considered differentially expressed. topGO R package [137] was used for Gene Ontology enrichment analysis.

4.3.7 *Proteomics*

Samples were analyzed as previously described [210]. Briefly, proteins were suspended in 1M urea, 50mM ammonium bicarbonate, pH 7.8, and heated to 50°C for 20min. Denatured proteins were reduced with 2mM DTT, alkylated with 15mM iodoacetamide, and digested overnight with trypsin. The resulting peptides were desalted on Waters Sep-Pak C18 cartridges. Peptides were separated using a heated 50°C 30cm C18 columns in a 180min gradient of 1% to 45% (vol/vol) acetonitrile with 0.1% (vol/vol) formic acid. Peptides were measured on a Thermo Scientific Lumos Orbitrap operated in data-dependent mode with the following settings: 60000 resolution, 400-1600 m/z full scan, Top Speed of 3 seconds, and a 1.8 m/z isolation window. Identification and label free quantification of proteins was done with MaxQuant 1.5 using a 1% false discovery rate (FDR) against the *Danio rerio* proteome dataset downloaded from Uniprot on July 1st, 2016. Peptides were searched using a 5ppm mass error and a match between run window of 2min. Proteins that were significantly regulated between conditions were identified in Perseus 1.4.1.3.

4.3.8 *Cell culture and cardiomyocyte directed differentiation*

Human embryonic stem cells (RUES2, Rockefeller University; hESC-09-0013) were maintained as previously described [210, 211]. Briefly, hESCs were plated on Matrigel (BD) coated tissue culture plates and maintained with irradiated mouse embryonic fibroblast conditioned media containing 5 ng/mL human bFGF (Peprotech, 100-18B). High density hESC directed differentiation towards cardiomyocyte was conducted as previously described [8]. Cardiomyocytes were harvested on day 25 of the protocol, pooled and randomly re-plated in a 24-

well tissue culture plates at a seeding density of 200k cells/well in 1 mL of RMPI (Invitrogen) containing B27 supplement. Cardiomyocytes were allowed to recover for 4 days until they were exposed to rWnt3A (100 ng/mL, R&D Systems) Rapamycin (200 nM), and XAV-939 (5 µM, Tocris) for 2 days prior to collection for flow cytometry.

4.3.9   *Reverse transcriptase-quantitative PCR*

RNA was isolated from young (3 days old), adult (~6 months old), and regenerating (3 and 7 dpi) zebrafish hearts as per manufacturers' protocol (TRIzol, ThermoFisher). Complementary DNA (cDNA) was synthesized using the Superscript III enzyme kit (Invitrogen). RT-qPCR was conducted using the sensimix SYBR PCR Kit (Bioline) on a 7900HT Fast-Real-Time PCR system (Applied Biosystems). Transcript abundance were normalized to the house keeping gene β-actin and primers are listed in Table 4-1.

4.3.10   *Western blotting*

Adult zebrafish hearts were collected at 0, 3, 7, 12, 14 dpi, washed in cold phosphate buffered saline (PBS), and flash frozen using liquid nitrogen. Human embryonic stem cell (hESC) derived cardiomyocytes (CM) were washed with ice cold PBS prior to collection and flash freezing. Hearts and hESC-CMs were lysed using ice cold cell lysis buffer (Cell Signaling, 9803) containing protease/phosphatase inhibitor cocktail (Cell Signaling, 5872) and cellular debris were separated by centrifugation. Protein concentration was quantified and normalized using a BCA Protein Assay Kit (ThermoFisher). Primary and secondary antibodies are listed in Table 4-2.

4.3.11 *In Situ hybridization*

Collected hearts and fixed in 4% PFA. Following fixation, hearts were saturated to 30% sucrose and mounted in OCT freezing media prior to cyro-sectioning. Sectional in situ hybridization was conducted against the Wnt8 riboprobe as described [212].

4.3.12 *Cardiomyocyte purity assay*

Cells were labeled for flow cytometry using cardiac troponin T (Thermo Scientific) or an IgG corresponding isotype control. Cells were analyzed using a BD FACSCANTO II (Beckton Dickinson, San Jose, CA) with FACSDiva software (BD Biosciences). Instrument settings were adjusted to avoid spectral overlap. Data analysis was performed using FlowJo (Tree Star, Ashland, Oregon).

4.3.13 *EdU (5-ethynyl-2'-deoxyuridine) assay*

Cardiomyocytes were exposed to 10 μM EdU (DMSO) for 24 h one day prior to collection for flow cytometry. Samples were trypsinized to obtain single cells and fixed for 10 min with 4% paraformaldehyde. Staining procedures for EdU incorporation were performed using the Click-iT EdU Flow Cytometry Cell Proliferation Assay kit using an Alexa Fluor 647 antibody (ThermoFisher).

4.3.14 *Transmission electron microscopy*

Hearts were fixed in 4% glutaraldehyde in sodium cacodylate buffer, post fixed in osmium tetroxide, en bloc stained in 1% uranyl acetate, dehydrated through a series of ethanol, and embedded in Epon Araldite. 70nm sections were cut on a Leica EM UC7 ulta microtome, and viewed on a JEOL 1230 TEM.

Table 4-1: qPCR primers

Gene	Forward Primer 5'-3'	Reverse Primer 5'-3'
gata4	GGCTCCTCTGAAGGTCAGTC	CAGGCTGTTCCACACTTCAC
nkx2.5	GGGATGGTAAACCGTGTCTG	TTGCTGTTGGACTGTGAAGG
β-actin	AAGCAGGAGTACGATGAGTC	TGGAGTCCTCAGATGCATTG
pdk2a	AGTTTGTCGCTGCTCTGGTC	ACTGGATTTGTGGCTCCATC
pdk2b	TGATAGAGGCGGTGGAGTTC	TACAGACGGGAGATGGGAAG
pdk3a	ATTCGTCAGCTCCAACATCC	ACACCATCTTAGCGGTTTCG
pdk4	TATCGACCCAAACTGTGACG	TCCACAGTTGCTCTCATTGC
myl7	ACCGGGATGGAGTTATCA	CTCCTGTGGCATTAGGG
cpt1b	ATGCTGCAGTATCGCCGTAA	GGAAACTTCTGAGTGTCATCTAGGA
cd36	GTCCAAACCTGTGTTGGTGC	CTAGGCTCAAAGGTGGCTCC

Table 4-2: Protein anti-bodies

Company	Protein	Catalogue number	anti	Dilution
Cell Signaling	S6	2217S	Rabbit	1:1000
Cell Signaling	c-Myc	5605S	Rabbit	1:1000
Cell Signaling	Axin1	2087S	Rabbit	1:1000
Cell Signaling	LEF1	2230S	Rabbit	1:1000
Cell Signaling	P-AKT	9271S	Rabbit	1:1000
Santa Cruz	PCNA	sc-56	Mouse	1:500
Active Motif	H3K27Me3	39158	Rabbit	1:1000
Cell Signaling	P-S6 (Ser235/236)	4858S	Rabbit	1:2000
Cell Signaling	GAPDH	5174S	Rabbit	1:5000
Cell Signaling	β-Actin	4970S	Rabbit	1:1000
Cell Signaling	β-Catenin	9562S	Rabbit	1:1000
Cell Signaling	α-Tubulin	2144S	Rabbit	1:1000
MitoSciences	Total OXPHOS (Complex I)	MS604	Mouse	1:1000
Cell Signaling	LRP6	3395S	Rabbit	1:1000
Cell Signaling	LRP6 pS1490	2568S	Rabbit	1:1000
Santa Cruz	MEF2	sc-313	Rabbit	1:500
Santa Cruz	MYH7	sc-53090	Mouse	1:500
ThermoFisher	SDHAF3 (ACN9)	PA5-24526	Rabbit	1:1000
Abcam	Lin28	ab46020	Rabbit	1:1000
Bio-Rad	Goat anti-mouse IgG HRP	1706516	Mouse	1:10,000
Bio-Rad	Goat anti-rabbit IgG HRP	1706515	Rabbit	1:10,000

4.4 RESULTS

Zebrafish (*Danio rerio*) are a regenerative model organism used to study the molecular mechanisms regulating cardiac repair, since their cardiomyocytes retain the ability to re-enter the cell cycle after injury in the adult state [104]. It is currently well understood that microRNAs (miRs), let-7a/c and miR-99/100, must be repressed in order for a cardiomyocyte to de-differentiate and re-enter the cell cycle [213]. However, the events that result in the down-regulation of these miRs are not understood, nor is it clear how other conditions predispose zebrafish cardiomyocytes to enter regeneration even in the adult state.

Using a transgenic chemically-induced ventricular cardiomyocyte (CM) ablation model (*vmhc:mCherry-NTR*) we identified the up-regulation of Lin28, a known protein that sequesters and inhibits the family of miRs let-7, 3-12 days after injury (Figure 4-1A,B). It has been previously shown that Lin28 is a target of Wnt/β-catenin signaling, suggesting that one of the earliest signaling events after myocardial insult would be Wnt/β-catenin signaling [214]. We used two different myocardial injury models, ventricle resection and chemical cell ablation, to test whether Wnt/β-catenin signalling, a pathway known to regulate cell cycle [215], is active shortly after injury. Following surgical partial resection of the ventricle apex [197] to stimulate cardiac regeneration [(3 and 7 days post amputation (dpa)], Wnt/β-catenin signalling reporter activity (TOP:dGFP [201, 204]) and Siam:mCherry [203]) and Wnt ligand expression (*wnt8a*) were increased along the resection plane of the ventricular myocardium as well as the epicardium while the uninjured myocardium showed no Wnt/β-catenin activity (Figure 4-2A,B) [201, 215]. We functionally tested the role of Wnt/β-catenin signalling during heart regeneration by inhibiting the pathway by genetic overexpression of an inducible Wnt co-receptor antagonist, Dickkopf 1 (hsDKK1b:GFP [201]). Inhibiting Wnt/β-catenin signalling blocked normal adult heart

regeneration, indicating that the pathway plays a critical role during endogenous heart regeneration (Figure 4-2C,D).

We further investigated Wnt/β-catenin activity in adult cardiomyocyte regeneration using a transgenic chemically-induced ventricular cardiomyocyte (CM) ablation model (*vmhc:mCherry-NTR*). This zebrafish line was engineered to express the enzyme nitroreductase (NTR) in ventricular myocytes, which generates a cytotoxic reduced form of the antibiotic metronidazole (MTZ), when given as a supplement to the fish water (Figure 4-1A) [195]. Wnt target genes, Lin28, Axin1 and c-Myc were significantly upregulated during two-week regeneration period after injury (Figure 4-1B,C), suggesting that similar to surgical ventricular apex resection, Wnt/β-catenin signalling was dramatically increased during regeneration after chemically induced injury. At 3 days post injury (dpi), due to the exposure of zebrafish to MTZ, we observed a dramatic increase in PCNA expression, an indication of increased cell division (Figure 4-1D). This regeneration requires Wnt/β-catenin activity, since genetically inhibiting Wnt/β-catenin signalling through overexpressing Dkk1b reduced Lin28 and c-Myc at 3 dpi (Figure 4-1E,F). In contrast, activating Wnt/β-catenin signalling by genetic Wnt8a overexpression increased PCNA and c-Myc protein levels at 3 dpi (Figure 4-1F). These results suggest that proliferation required during endogenous cardiac regeneration is dependent on Wnt/β-catenin signalling.

We next performed RNA-Sequencing on young zebrafish hearts (3-day old), adult, 3 dpi and 7 dpi hearts (Figure 4-3A) in an effort to shed light on mechanisms of cardiac regeneration. We first compared RNA-Sequencing datasets from our MTZ ventricular CM ablation model with those following cryoinjury from Bednarek *et al.* (Figure 4-4A-C) [216]. Principle component analysis (PCA) demonstrated our adult heart and 3 dpi heart samples clustered with those previously published indicating a high degree of similarity between the injury models (Figure

4-4C). Furthermore, we validated transcript abundance using a panel of genes by RT-qPCR (Figure 4-4A). We next conducted PCA to measure the variance within our samples. We found that the adult regenerating hearts (3 dpi, 7 dpi) clustered with young hearts along PC3 (Figure 4-3B) supporting the hypothesis that the adult heart re-activates an embryonic program during regeneration. Unbiased bioinformatics analysis revealed that young hearts and regenerating (3 dpi, 7 dpi) hearts displayed higher transcript levels of many Wnt ligands and targets compared to adult hearts (Figure 4-3C). Since the Wnt target, c-Myc, was up-regulated during the two-week regeneration period (Figure 4-1C), we assessed transcript abundance of Myc targets [217]. Many Myc targets were up-regulated in young hearts while being repressed in adult hearts (Figure 4-3D). Among these Myc-targets we identified cell cycle pathway genes that were up-regulated in young and 3 dpi hearts. Importantly, metabolic Myc-target genes, including many oxidative phosphorylation (OXPHOS) related pathways, were dramatically up-regulated in 7 dpi hearts (Figure 4-3D). These data suggest a role for Myc in the induction of cell proliferation and mitochondrial biogenesis or maturation (Figure 4-1C,F).

In addition to Myc-targets, we also performed genome wide unbiased global Gene Ontology (GO) enrichment analyses comparing all samples and identified ten significantly changed pathways that were associated with cardiac regeneration, maturation, and metabolic regulation (Figure 4-4D). Many metabolic and cardiac structural pathways were down-regulated at 3 dpi while at 7 dpi many metabolic pathways had been dramatically up-regulated. In particular, OXPHOS, the citric acid (TCA) cycle and fatty acid oxidation (FAO) were up-regulated at 7 dpi to levels higher than the uninjured adult heart (Figure 4-3E and Figure 4-4D). These data suggest that dramatic metabolic remodeling occurs during the first weeks of heart regeneration. Using metabolic pathway enrichment analysis, at 3 dpi we identified OXPHOS as the most down-

regulated metabolic pathway accompanied by FAO, glycolysis and TCA (Figure 4-4E). The levels of 3 dpi metabolic gene expression were similar to the levels observed in young hearts (Figure 4-3E). By 7 dpi however, OXPHOS was the highest up-regulated metabolic pathway accompanied by TCA, glycolysis, and FAO (Figure 4-3E and Figure 4-4E).

To further explore signalling and metabolic pathways during heart regeneration, we performed system-wide label-free quantitative (LFQ) proteomics to assess the proteome of adult, 3 dpi and 7 dpi hearts (Figure 4-5A). Principle component analysis of the proteomics data, revealed that regenerating hearts clustered separately from the uninjured heart on PC1 (Figure 4-5B). At 3 dpi, we found many GO Terms associated with metabolic processes were down-regulated while at 7 dpi many GO Terms associated with DNA packaging and assembly where up-regulated (Figure 4-5C,D). One significantly changed protein was succinate dehydrogenase complex assembly factor 3 (sdhaf3), related to complex II of the electron transport chain (ETC). We found that at 3 dpi and 7 dpi, this OXPHOS protein was less abundant than in the un-injured heart (Figure 4-5E). However, on a transcript level, sdhaf3 was significantly up-regulated at 7 dpi. This indicated that OXHPOS up-regulation may result in the replacement and expansion of the mitochondrial pool at this early stage of regeneration (Figure 4-5F). In total, system-wide RNA-sequencing and LFQ proteomics analysis suggest that dynamic metabolic regulation is a key component of endogenous cardiac regeneration in zebrafish.

Our data suggest that the regeneration of zebrafish myocardium is driven by metabolic remodeling. We hypothesized that by 7 dpi, newly generated cardiomyocytes would be undergoing metabolic maturation in order to drive the primitive cardiomyocyte towards a fully matured state. This hypothesis is supported by our finding that the upregulated Wnt target, Myc, is associated with metabolic re-organization and promotes expression of complexes of the ETC [218, 219]. We

have shown that ETC complex 1 is upregulated during heart regeneration by activation of Wnt/β-catenin following over expression of Wnt8a. Moreover, it is down-regulated by inhibition of Wnt/β-catenin signaling due to overexpression of DKK1b (Figure 4-1F).

It has been recently shown that mitophagy is required for cardiomyocyte maturation [155]. We tested if mitophagy was being engaged to remove damaged mitochondria and replaced with more mature ones. Importantly, we found that genes associated with mitophagy were up-regulated at both 3 dpi and 7 dpi as compared to uninjured hearts (Figure 4-6A). Furthermore, at 7 dpi, we found that mitochondrial-protective gene network was engaged (*park7*, *hax1*, *tomm7*; Figure 4-6A). To assess mitochondrial state, we used transmission electron microscopy (TEM) to examine mitochondrial morphology during early stages of heart regeneration. Adult uninjured zebrafish hearts have large mitochondria packed against long myofibrils (Figure 4-3F). However, at 3 dpi and 7 dpi, we observed a significantly increased number of small mitochondria (Figure 4-3G). By 12 dpi the mitochondria appeared larger in size, similar to uninjured cardiomyocyte (Figure 4-3H,I). The gene expression data and the TEM analysis support the hypothesis that metabolism, and specifically mitochondrial dynamics as shown previously in cardiomyocyte maturation [155], play a key role in Wnt-dependent regeneration of the Zebrafish heart.

Supporting the critical metabolism function during the first weeks of regeneration post-injury, the mitochondrial TCA cycle metabolic pathway was highly modulated during the first weeks of heart regeneration with many TCA cycle enzymes (Figure 4-6B). To directly identify amino acids and TCA cycle intermediates involved in heart regeneration, we performed metabolite analysis using gas chromatography mass spectrometry (GC-MS) for adult, 3 dpi and 7 dpi heart samples. We found that many amino acids and TCA cycle intermediates were enriched at 3 dpi or 7 dpi or both (Figure 4-3J). However, one amino acid, glutamine, was highly enriched at the

uninjured adult stage and was depleted over the first week of heart regeneration (Figure 4-3K). Glutamine has many roles in the cell including serving as a precursor to glutamate production and as a critical amino acid in driving mammalian Target of Rapamycin Complex 1 (mTORC1) activation [220]. Since the TCA cycle intermediate, αKG was enriched at 3 dpi we considered a potential role of glutamine as a component for anaplerotic flux. However, the enzymes controlling the metabolism of glutamine to glutamate were either unchanged, *gls*, or significantly down-regulated at 3 dpi, *gls2b*.

We therefore investigated whether the dynamic changes of glutamine during regeneration correlated with regulation of mTORC1. Amino acid activation of mTORC1 has been shown to be a result of glutamine import and then export, for the exchange of essential amino acids like leucine that can specifically inhibit Sestrin2 and thereby activate mTORC1 pathway [221, 222]. We found leucine abundance was increased during the first week of heart regeneration (Figure 4-3L). Furthermore, the transporters governing these amino acids import and export were dynamically and tightly regulated at 3 and 7 dpi suggesting that the increased abundance of leucine is a result of the export of glutamine (Figure 4-3M). These data suggest that the amino acid conditions to stimulate mTORC1 signalling are present during the first week of heart regeneration.

We next examined the regulation of mTORC1 and asked whether it is required during zebrafish early heart regeneration. We found that the phosphorylation at ser235/236 (pS6) of S6, a target and readout of mTORC1 activity, was more abundant over the course of early heart regeneration following the trend of PCNA abundance (Figure 4-7A). This supports activation of mTORC1 and corroborates the dynamic flux of glutamine and leucine as well as the up-regulation of amino acid transporters at 3 dpi. Since mTORC1 can be activated by both amino acids and by crosstalk between signalling pathways, including Wnt/β-catenin signalling [223], we tested the

effects of mTORC1 activation via Wnt/β-catenin signaling by overexpression of Wnt8a and reciprocally, we tested the effects of inhibiting Wnt/β-catenin signaling by overexpression of Dkk1b. While Wnt8a overexpression did not increase S6 phosphorylation beyond its already elevated levels in the regenerating heart, repression of Wnt signaling by Dkk1b led to reduced phosphorylation of S6 (Figure 4-7B). This places mTORC1 activation downstream of Wnt signaling in this context. To specifically test mTORC1 function during regeneration, we used rapamycin, a selective mTORC1 inhibitor [224], to assess whether mTORC1 activation was necessary for *in vivo* adult zebrafish cardiac cell proliferation after injury (Figure 4-7C). We found that rapamycin significantly inhibited pS6 and PCNA expression *in vivo* zebrafish heart after injury (Figure 4-7D). Furthermore, rapamycin did not inhibit the expression of Myc and Axin abundance suggesting that inhibition of mTORC1 does not affect Wnté β-catenin activity. This result shows that mTORC1 is necessary for cardiac cell proliferation during endogenous *in vivo* zebrafish heart regeneration.

Since injured adult zebrafish hearts use Wnt/β-catenin and amino acids to stimulate mTORC1 signalling during regeneration, we next monitored these components in young mouse hearts, which, like zebrafish, are able to regenerate damaged hearts. Strikingly, the zebrafish heart can regenerate into adulthood whereas the mouse heart can regenerate only during the first week of life. Indeed, through metabolic analysis we showed that, similar to the primed pro-regenerative adult zebrafish heart, pro-regenerative young P0 mouse hearts possessed higher amounts of glutamine, suggesting that they are also primed for regeneration. This correlation between glutamine and regeneration is also evident by examining adult mouse hearts which have lost their ability to regenerate, and which display lower amounts of glutamine (Figure 4-8A,B). We postulate that high levels of glutamine keep the heart in a primed state for regeneration so that activation of

mTORC1 via the export of glutamine for the import of leucine happens readily leading to heart regeneration.

Supportingly, RNA-sequencing of young P0 mouse heart showed higher Wnt/β-catenin activity than an adult mouse heart (Figure 4-8C) [225]. At the cusp of potential mouse heart regeneration, P7, we see a downward trend of Wnt ligand and Wnt target gene expression until it reaches the adult levels (Figure 4-8C). These data suggest that, just like in regeneration-competent adult zebrafish, a young mouse heart is primed for mTORC1 activity jointly through amino acid and Wnt/β-catenin signalling. This hypothesis is further supported by comparing RNA-sequencing data using a time course of *ex vivo* cardiomyocyte de-differentiation assay from O'Meara *et al.* (Figure 4-9) [225]. As adult murine cardiomyocytes de-differentiated, they showed greater proliferation and Wnt/β-catenin signalling activity, coupled with a depressed metabolic signature (Figure 4-9B,C), similar to 3 dpi zebrafish hearts. These data suggest that a mammalian cardiomyocyte requires Wnt/β-catenin signalling, priming of mTORC1, and remodeling of several metabolic pathways to de-differentiate and re-enter the cell cycle.

We next sought to understand how Wnt/β-catenin and mTORC1 signalling pathways interacted to regulate cell proliferation. For these studies we used human embryonic stem cell derived cardiomyocytes (hESC-CM) as a model system (Figure 4-8D). We first showed that stimulation of Wnt/β-catenin signalling by recombinant Wnt3A increased hESC-CM proliferation while inhibiting the pathway with XAV939 decreased hESC-CM proliferation. Moreover, mTORC1 inhibition through rapamycin treatment inhibited hESC-CM proliferation which was rescued by increased Wnt/β-catenin signalling (Figure 4-8E,F). Immunoblotting for key protein targets of Wnt/β-catenin and mTORC1 signalling identified that Wnt3A induced phosphorylation of the co-receptor LRP6 and stimulated pS6 and c-Myc. Moreover, inhibition of mTORC1 by

rapamycin inhibited pS6 and c-Myc which was also observed by inhibiting Wnt/β-catenin signalling by XAV939 (Figure 4-8G). Furthermore, we showed that this activation of mTORC1 in hPSC-CMs is in part due to amino acid signalling (Figure 4-8H). Utilizing a glutamine transport inhibitor (γ-L-Glutamyl-p-nitroanilide hydrochloride, GPNA) [221] we found that Wnt3A-induced p-S6 activation in hPSC-CMs was dictated by glutamine. Together, these data indicate that Wnt/β-catenin and mTORC1 signalling axes cooperate to promote cardiomyocyte cell cycle re-entry following terminal differentiation (Figure 4-9I).

4.5   DISCUSSION

Metabolic and functional analysis revealed that adult zebrafish cardiomyocyte regeneration of the heart is a result of Wnt/β-catenin signaling and amino acid primed mTORC1 activation (Figure 4I). Previous findings have shown that in order for heart regeneration to commence in the zebrafish, microRNAs-Let7a/c and -99/100 must be repressed [213]. Wnt/β-catenin signaling has been shown to stimulate Lin28 expression which is a known repressor of the family of microRNAs Let7 [214]. We have now shown that in the context of zebrafish heart regeneration, Wnt/β-catenin regulates Lin28 expression and thereby regulates previously identified microRNA repression during regeneration [213]. These data show that Wnt/β-catenin signaling is an early responder after zebrafish heart injury. One possibility is that Wnt/β-catenin signaling, in this context, is activated as a direct consequence to a loss of cell-cell junctions. After cell-cell junctions are lost in response to cardiomyocyte ablation, p-120 catenin may no longer be localized to intercalated disks [226] and be free to bind to ZTB33 (Kaiso) a known repressor of Wnt/β-catenin signaling and of β-catenin target genes such as Myc [227, 228]. This initiation of Wnt/β-catenin signaling to activate mTORC1 along with the primed amino acid profile may spark the cardiomyocyte proliferation signaling cascade leading to heart regeneration. Similar to zebrafish, we showed that regeneration competent neonatal mouse cardiomyocytes also display elevated glutamine levels, predisposing them to amino acid-driven activation of mTORC1. Since activating Wnt/β-catenin and mTORC1 signalling in human cardiomyocytes also leads to a proliferative state, these data reveal a common mTORC1 primed stage as the prerequisite for heart regeneration in zebrafish and mammals.

4.6 FIGURES
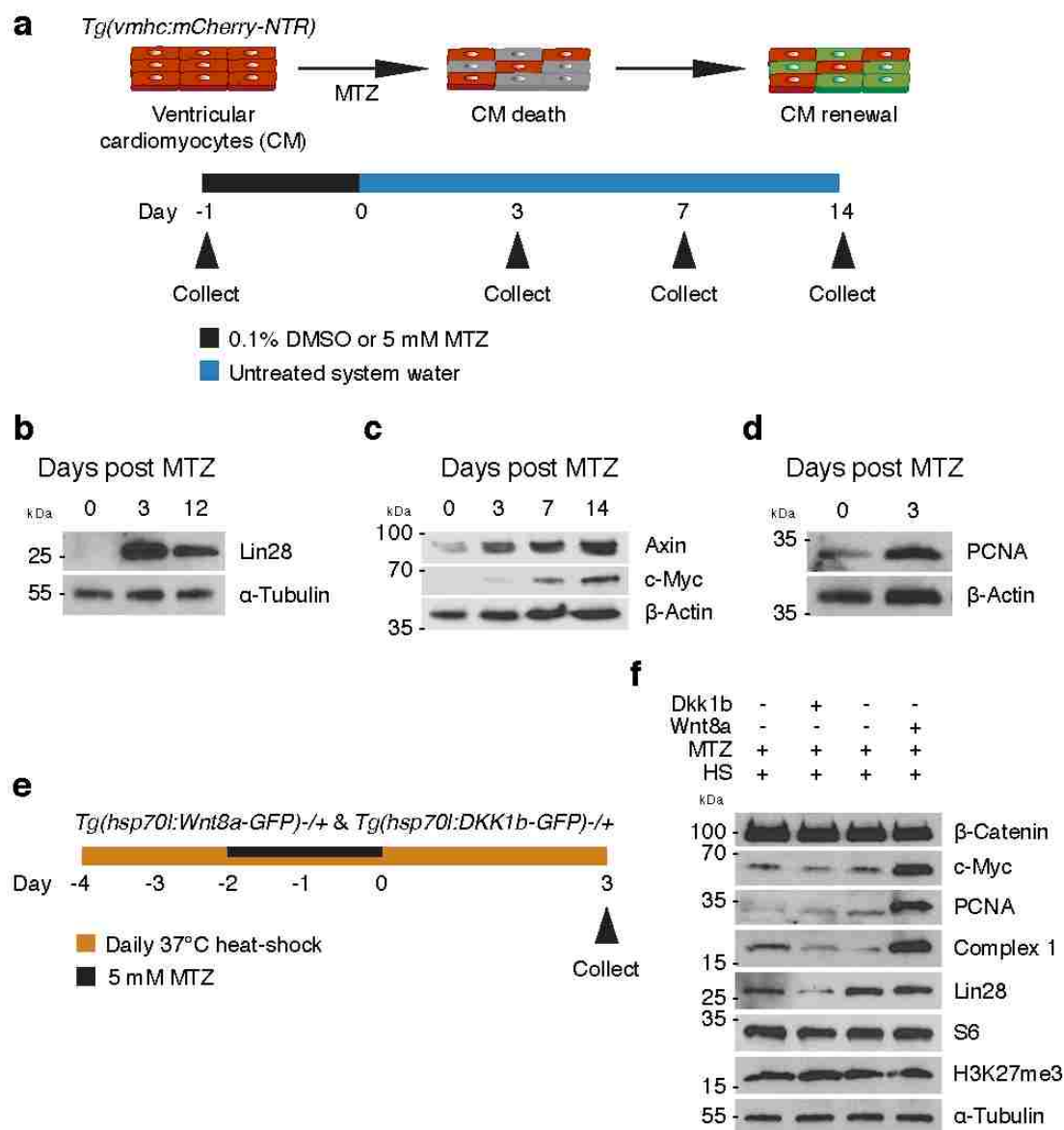
Figure 4-1: Wnt regulates the early stages of zebrafish heart regeneration.

A) Schematic of adult zebrafish heart ablation experiments. B) Protein analysis of uninjured (0 dpi) and 3 and 12 dpi hearts for Lin28. C) Protein analysis of 0 dpi, 3 dpi, 7 dpi and 14 dpi adult zebrafish hearts for Wnt targets. D) Protein analysis of 0 dpi and 3 dpi zebrafish hearts for proliferating cells after injury. E) Schematic of adult zebrafish heart ablation and heat shock

protocol for Wnt modulation fish. F) Protein analysis of Wnt modulation during adult zebrafish

heart regeneration.
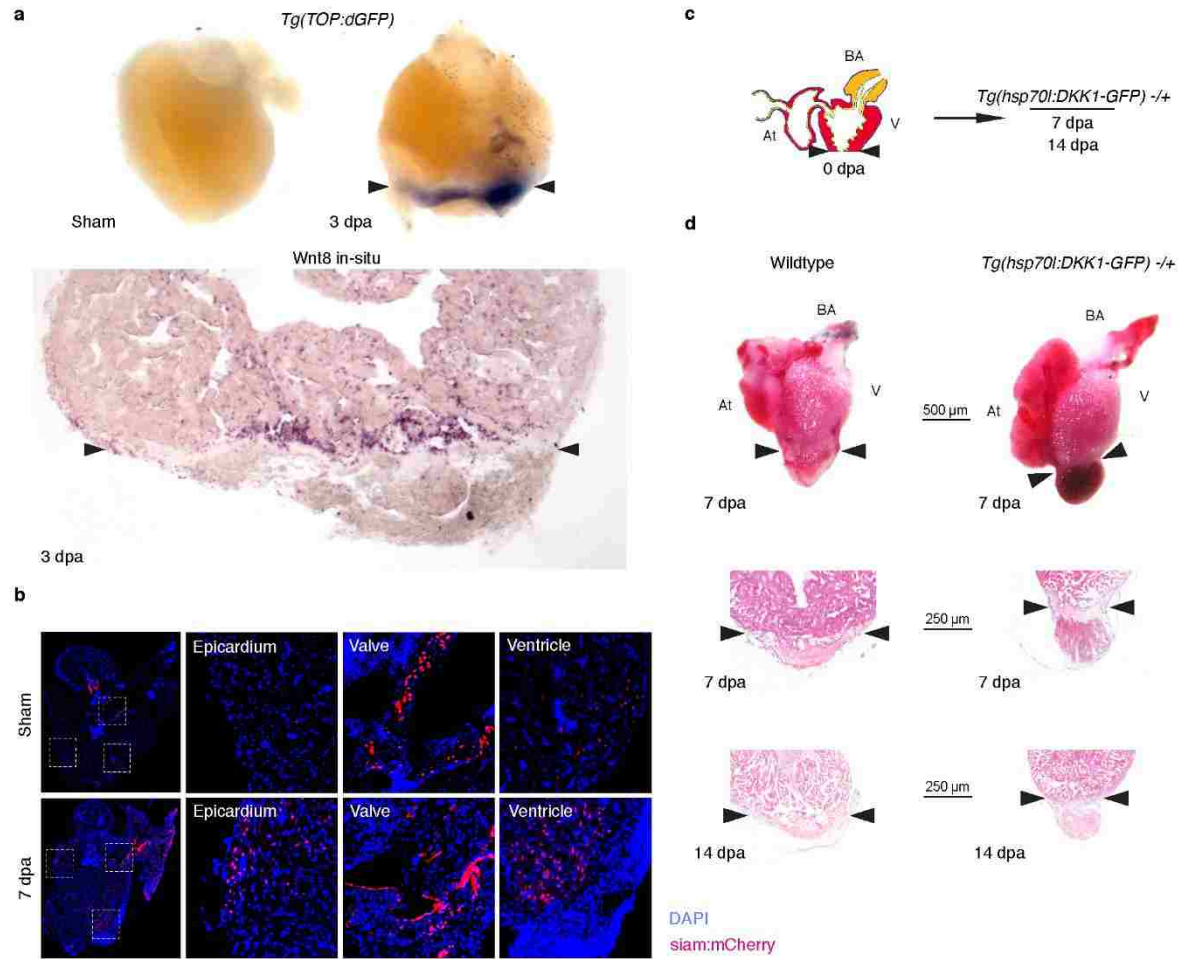
Figure 4-2: Wnt/β-catenin signalling activates after ventricular resection in adult zebrafish hearts.

A) In situ hybridization of the Wnt/β-catenin reporter TOP 3 dpa and Wnt8 ligand. B) Immuno-histochemistry of Wnt/β-catenin activity via the Siam:mCherry reporter in sham and 7 dpa hearts. Red: Siam and Blue: DAPI. C) Schematic of adult zebrafish amputation and Wnt/β-catenin inhibition. D) Gross morphology and histology of wild type and Wnt inhibited amputated adult zebrafish heart regeneration at 7 and 14 dpa.
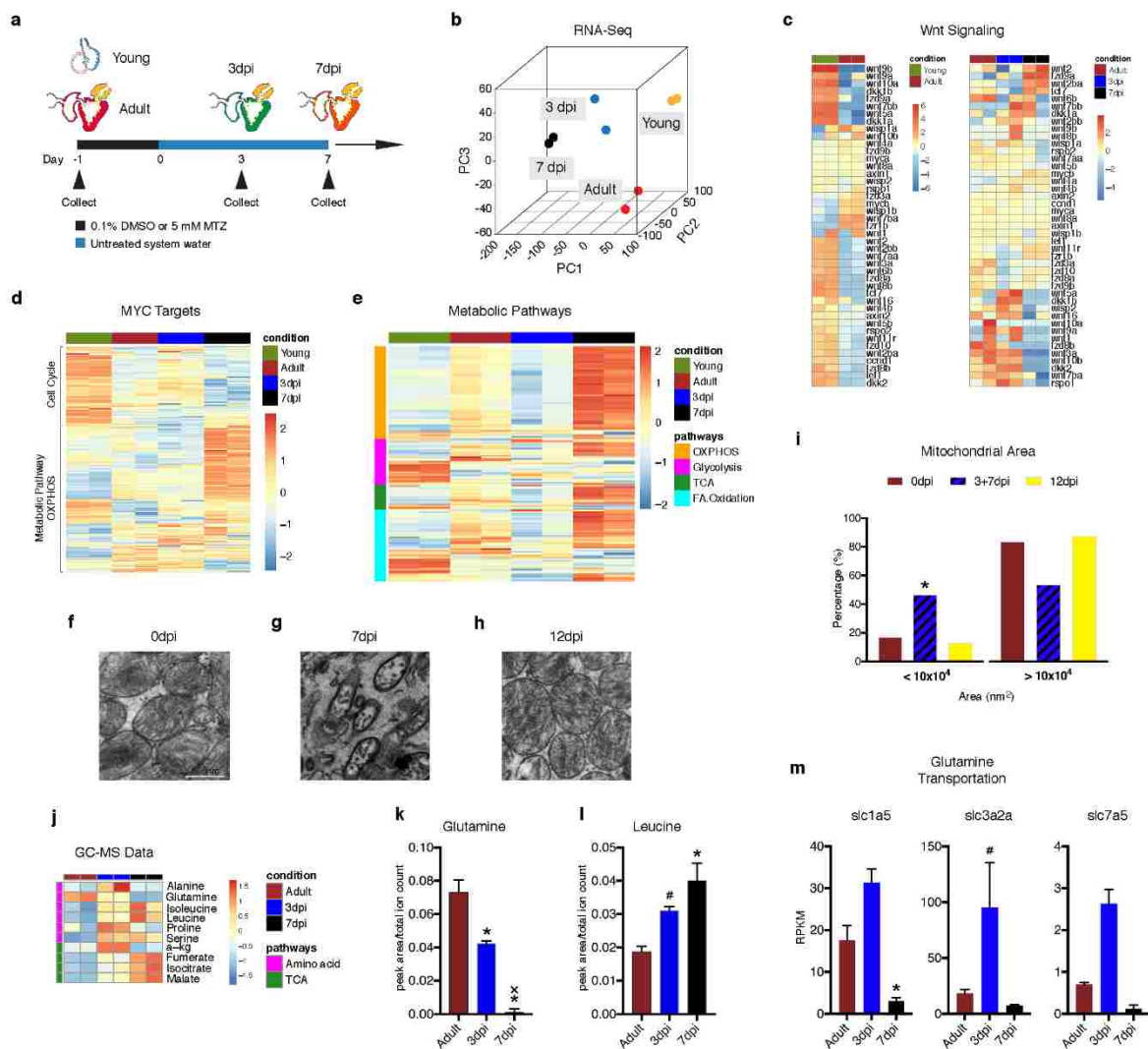
Figure 4-3: Metabolic pathways are dynamically regulated during the early stages of zebrafish heart regeneration.

A) Schematic of zebrafish heart samples prepared for RNA-Sequencing. B) Principle component analysis of young, 3-day old hearts, adult, uninjured hearts, and 3 dpi and 7 dpi adult zebrafish hearts. C) Heat map of Wnt ligands and targets in zebrafish hearts. D) Heat map of Myc targets in zebrafish hearts. E) Heat map of four metabolic pathways in zebrafish hearts. F-H) Transmission electron microscopy of zebrafish hearts. I) Mitochondria area quantification in 0, 3, 7 and 12 dpi ZF hearts. A Chi-squared test was used to assess the ratio between observed/expected.

3dpi and 7dpi showed enrichment in the area bin $<10\text{x}10^4$ nm^2, while 0 dpi and 12 dpi has depletion in area bin $<10\text{x}10^4$ nm^2. $P < 2.2\text{x}10^{-16}$. J) Heat map of significantly different amino acids and TCA cycle intermediates in zebrafish hearts. K) Abundance of glutamine in zebrafish hearts. * denotes significance to adult. (3 dpi vs adult P =0.012, 7 dpi vs adult P=0.001). X denotes significance to 3 dpi (7 dpi vs 3 dpi P=0.005). L) Abundance of leucine in zebrafish hearts. * denotes significance to adult. (7 dpi vs adult P =0.013). # denotes near significance to adult. (3 dpi vs adult P=0.058). M) RNA-Seq quantification of glutamine and essential amino acid transporters engaged during mTORC1 activation. (slc1a5: 7 dpi vs adult P=0.02) (slc3a2a: 3 dpi vs adult P=0.09).
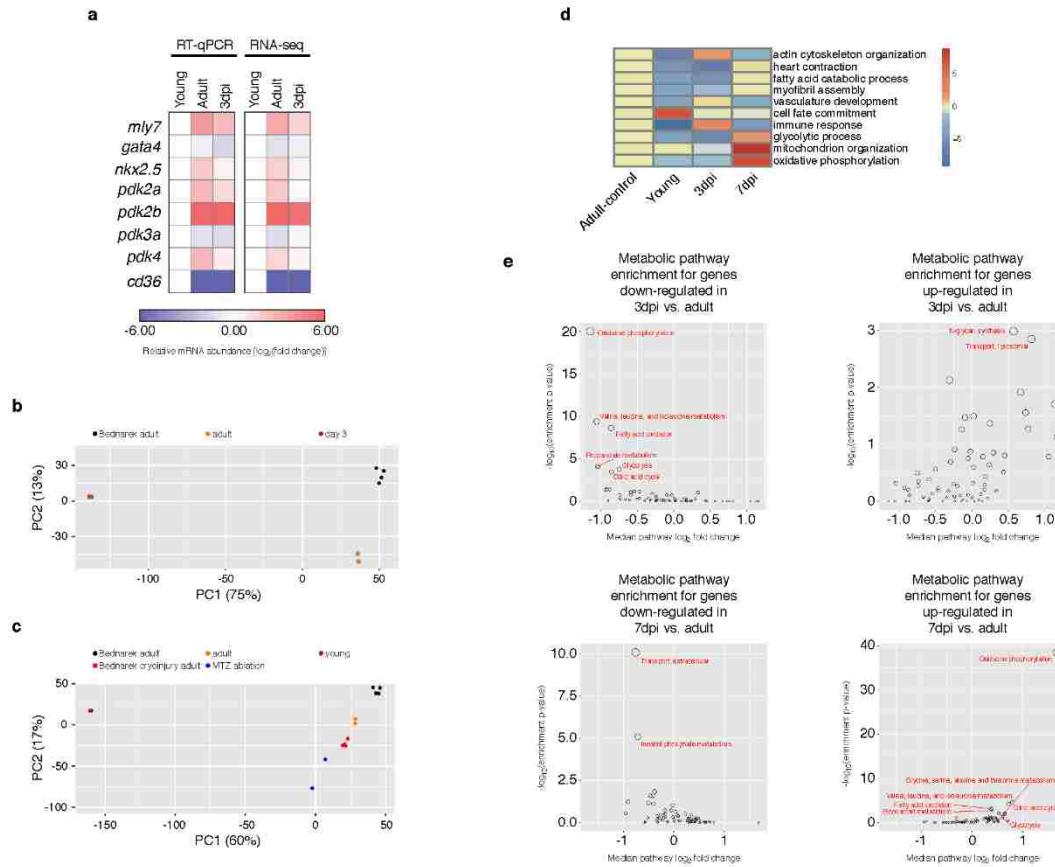
Figure 4-4: Metabolism is dynamically regulated during the first week of adult zebrafish heart regeneration.

A) RNA-Seq cardiac transcription factor, structural and metabolic gene expression during adult zebrafish heart regeneration and RT-qPCR validation of these genes. B) Principle component analysis of isolated young, 3-day old hearts, and adult zebrafish hearts as compared to Bednarek *et al*. adult zebrafish hearts. C) Principle component analysis of isolated young, 3-day old hearts, and uninjured and ablated adult zebrafish hearts as compared to Bednarek *et al*. uninjured and cryo-injured adult zebrafish hearts. D) Key cardiac pathways that are differentially expressed during adult zebrafish heart regeneration. E) Metabolic pathways enrichment for up- and down-regulated genes during the first week of adult zebrafish heart regeneration.
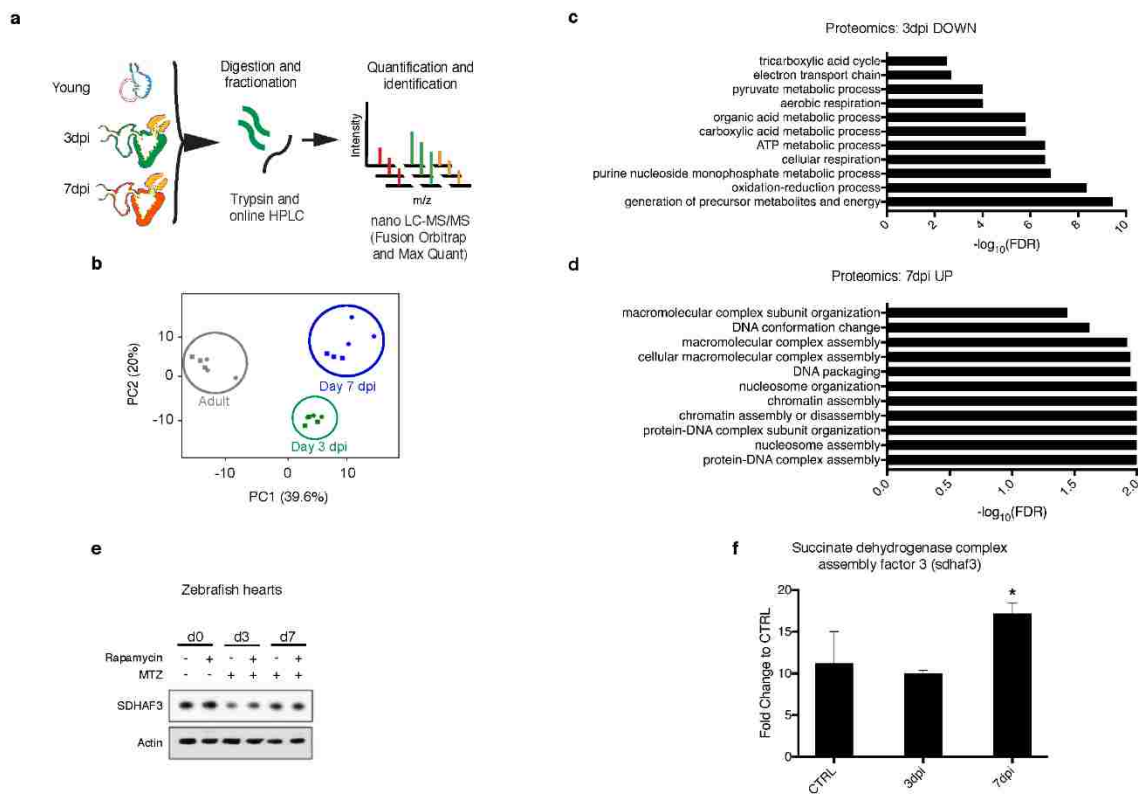
Figure 4-5: Proteomics analysis of adult zebrafish regeneration.

A) Schematic of adult zebrafish hearts used for proteomics analysis at 3 or 7 days post injury (dpi). B) Principle component analysis of full proteome analysis during the first week of heart regeneration. C) Gene ontology terms that were down-regulated at 3 dpi. D) Gene ontology terms that were up-regulated at 7 dpi. E) Protein validation of Succinate dehydrogenase complex assembly factor 3 expression during the first week of adult zebrafish heart regeneration. F) RNA-Seq expression of succinate dehydrogenase complex assembly factor 3.
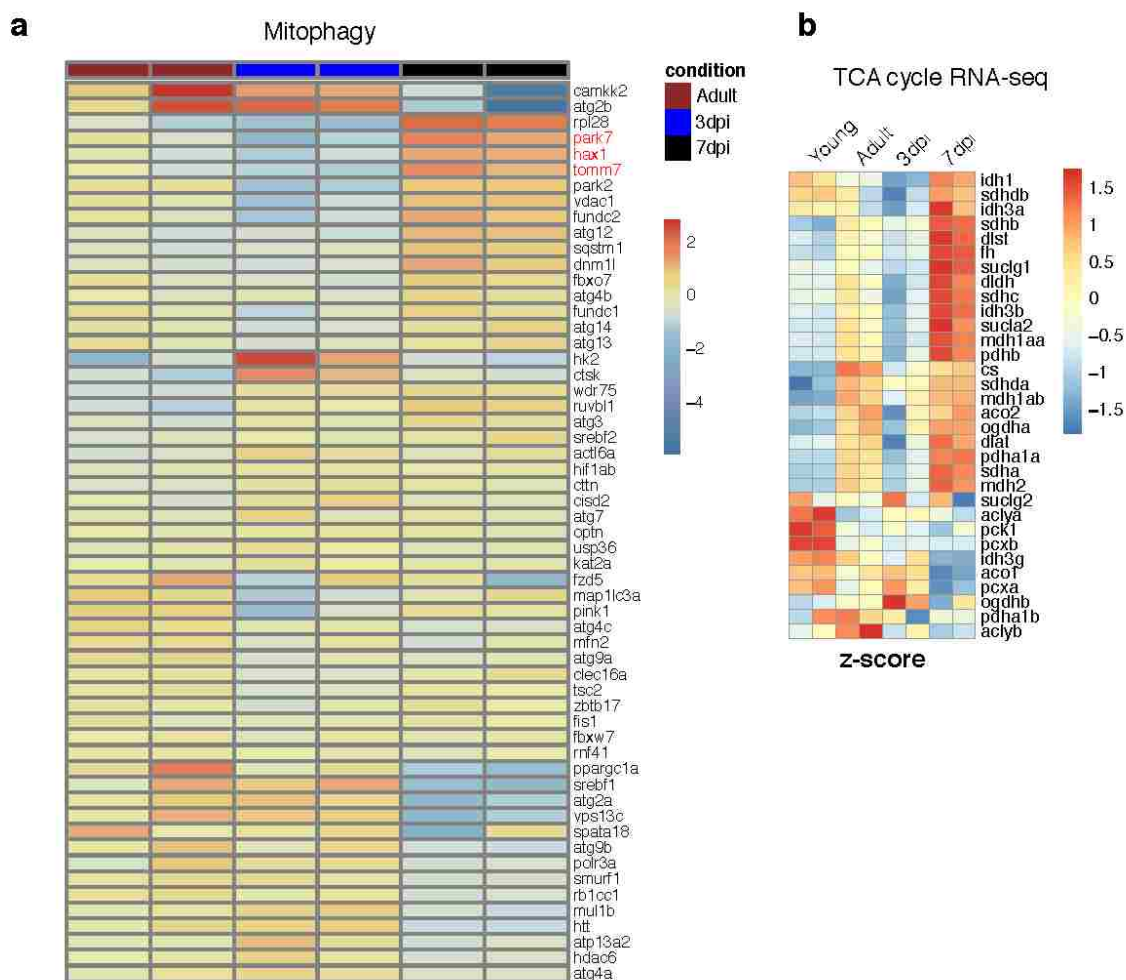
Figure 4-6: mTORC1 activates during the first week of adult zebrafish heart regeneration. A) Heat map of mitophagy and autophagy genes during adult zebrafish heart regeneration. B) Heat map of TCA cycle enzyme gene expression from RNA-Seq data.
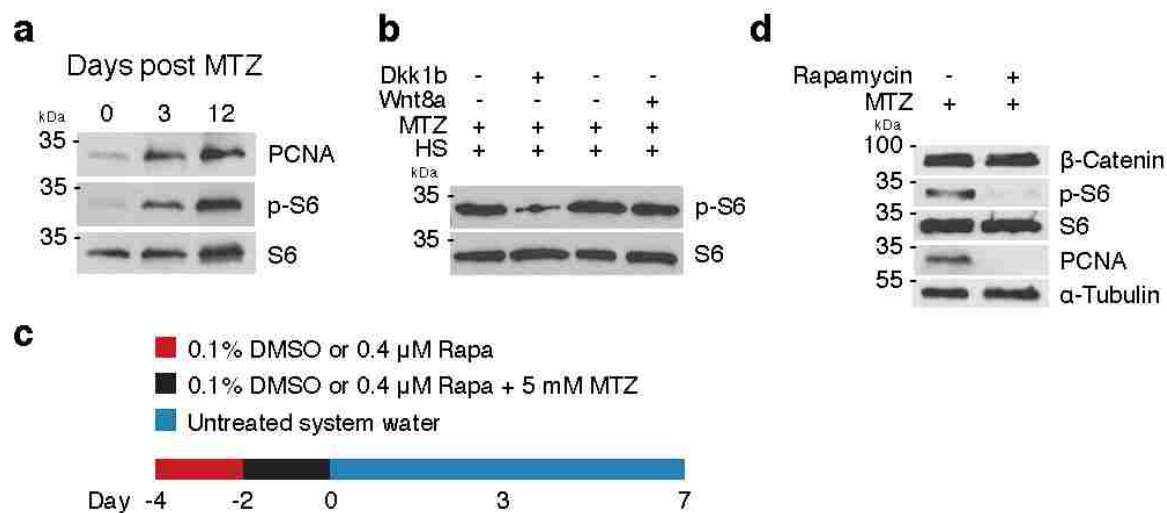
Figure 4-7: mTORC1 regulates the early stages of zebrafish heart regeneration.
A) Protein analysis of mTORC1 activity monitored via the phosphorylation of S6 and proliferation via PCNA in regenerating adult zebrafish hearts B) Protein analysis of mTORC1 activity monitored via the phosphorylation of S6 in regenerating adult zebrafish hearts that have either Wnt/β-catenin activity or inhibition through the expression of Wnt8a or DKK1b. C) Schematic of adult zebrafish heart ablation and mTORC1 inhibition via rapamycin. D) Protein analysis of mTORC1 inhibited regenerating adult zebrafish hearts.
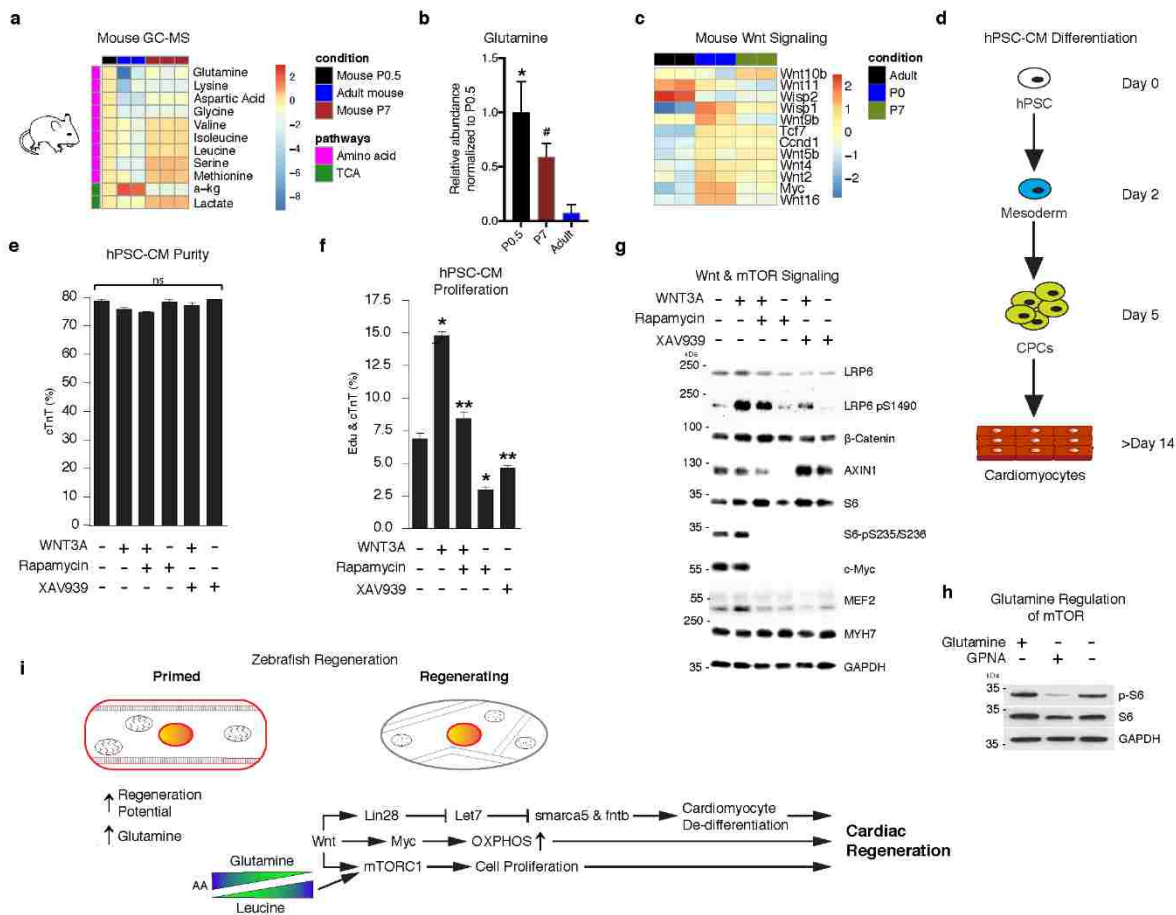
Figure 4-8: Wnt and mTORC1 are active in regenerating mouse and human cardiomyocytes. A) Heat map of significantly different amino acids and TCA cycle intermediates in mouse hearts. B) Abundance of glutamine in mouse hearts. * denotes significance to adult. (P0.5 vs adult *P* =0.004). # denotes near significance to adult. (P7 vs adult *P*=0.057). C) Heat map of Wnt ligands and targets in mouse hearts. D) Schematic of embryonic stem cell derived cardiomyocyte (hESC-CM) generation. E) Purity of cardiomyocytes after Wnt activation, inhibition and/or mTORC1 inhibition as determined by FACs. F) Percentage of proliferating hESC-CMs after Wnt activation, inhibition and/or mTORC1 inhibition as determined by FACs. G) Protein analysis of hESC-CMs after Wnt activation, inhibition and/or mTORC1 inhibition. H) Protein analysis of hESC-CMs mTORC1 activation after glutamine transporter inhibition via GPNA. I) Schematic of AA primed

pro-regenerative cardiomyocyte and the signalling cascade that Wnt/β-catenin drives to turn on

mTORC1, Lin28 and Myc to bring about zebrafish heart regeneration.
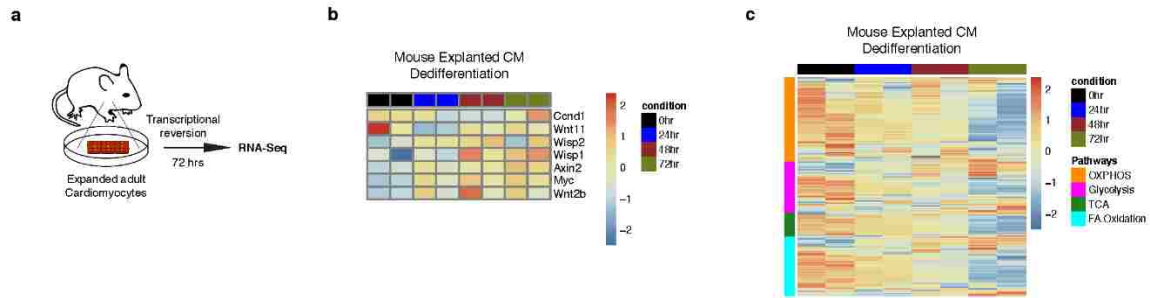
Figure 4-9: Adult mouse cardiomyocyte de-differentiation resembles a regenerative transcript profile.

A) Schematic of adult mouse cardiomyocyte isolation and *in vitro* culture. B) Heat map of cell proliferation and Wnt ligand and targets during cardiomyocyte de-differentiation. C) Heat map of metabolic pathways during cardiomyocyte de-differentiation

Chapter 5. SUMMARY AND FUTURE DIRECTIONS

The above work addressed several of the key challenges associated with stem cell derived cardiomyocyte maturation, disease modeling and cardiac regeneration. In chapter 2, we developed a microRNA maturation cocktail termed MiMaC. MiMaC was about to mature many aspects of stem cell derived cardiomyocytes including: cell size, force of contraction, metabolic function and also the ability to metabolize long chain fatty acids. In chapter 3, we created the first human cardiac model of mitochondrial tri-functional protein deficiency. In studying this disease we were able to generate a robust human *in vitro* model of the disease and elucidate a novel function of the protein HADHA. We discovered that the underlying pathology in MTP deficiency is a misregulation of cardiolipin remodeling and that mutations in HADHA result in these cardiolipin remodeling issues. Finally, in chapter 4 we identified that the "primed" state of a pro-regenerative cardiomyocyte is one that that high amounts of glutamine which, in turn along with Wnt/β-catenin signaling drives heart regeneration.

There are a few different avenues of new discoveries that can be made from the MTP deficient disease modeling and zebrafish heart regeneration projects. For the MTP deficient CM project, we have generated a compound heterozygous (mutant) HADHA iPSC line and a knockout HADHA iPSC line in the WTC-11 iPSC line background. Furthermore, we now have a patient iPSC line derived from HADHA deficient patient fibroblasts that have the hallmark point mutation in HADHA at 1528G>C [229]. Using these four lines (3 disease and 1 WT), it would be very exciting to perform three key experiments: 1. Full lipidomics 2. Targeted lipidomics for 20 different cardiolipin species 3. HADHA enzyme assay to assess the acyl-CoA transferase capability of HADHA.

It is still unclear if HADHA is acting as an acyl-CoA transferase and if it does, where in the protein this enzymatic function resides. The three disease lines could begin to unravel this question. Most interestingly will be the clinical point mutation line which can be used to determine if a mutation in exon 15, the dehydrogenase enzyme pocket, doubles as the region that acts as or facilitates an acyl-CoA transferase function. If it does, this would mean the main way in which the disease manifests in MTP deficient patients is currently misunderstood. However, if it do, this would suggest that a lipid toxic intermediate may be the key element precipitating the disease. Full lipidomics will assess what kind of lipid intermediates are generated in each line, targeted lipidomics will assess how cardiolipin is being remodeled in each line and finally the enzyme assay will definitively determine if HADHA can act as an acyl-transferase and begin to tease out where in HADHA this function resides.

For the zebrafish heart regeneration project, there are two main areas that would be very interesting to provide follow up studies upon. This would be 1. Determining if glutamine transporter inhibition *in vivo* in zebrafish halts or blunts heart regeneration and 2. How do the metabolic genes and glutamine transporters change during mammalian neonatal mouse heart regeneration.

It would be very exciting and also important to show that the glutamine inhibitor is able to inhibit or halt heart regeneration. This can be done in a similar workflow as the current rapamycin treated zebrafish experiments performed in chapter 4. If inhibiting glutamine transporters results in a halt of zebrafish heart regeneration bit would be very exciting to follow this up with a conditional knockout of these transporters in the adult zebrafish heart. Understanding and confirming this is cardiomyocyte specific response will be very interesting.

While we found an interested primed state of a cardiomyocyte which is pro-regenerative, we have not shown that glutamine is essential for an amino acid driven mammalian cardiomyocyte regeneration response. As a result, it would be exciting to use a neonatal mouse regeneration model to assess if the glutamine and leucine driven mTORC1 activation, Wnt/β-catenin signalling and metabolic shifts are occurring in the neonatal regenerating heart. One way in which this could be approached would be to perform single cell RNA-sequencing during the first week of mouse heart regeneration. Using a transcriptomics approach, the metabolic shifts, glutamine and leucine transporter regulation can be resolved on a single cell level. Ideally, if this glutamine priming is essential for neonatal mouse heart regeneration, potentially novel therapeutics could be designed around augmenting the levels of this amino acid in adult mammalian cardiomyocytes.

Vita

Jason Wayne Miklas grew up in Thornhill, Ontario, Canada, a suburb of Toronto. Jason completed his Bachelor's of Applied Science from the University of Toronto in Materials Science Engineering and a Master's of Applied Science from the University of Toronto in Biomedical Engineering. Jason pursued his master's in the laboratory of Professor Milica Radisic. During Jason's master's, he designed, fabricated and validated an electromechanical stimulation platform to mature cardiac engineered heart tissues. This work was published in Biofabrication with the successful generation of an electromechanical platform. Jason also worked on studies with Dr. Sara Nunes de Vasconcelos that looked more deeply at the role of electrical stimulation in human stem cell derived cardiomyocytes (Nunes *et al*. Nature Methods. 2013) and utilizing human stem cell derived cardiac organoids as a means to study human pathological hypertrophy *in vitro* (Nunes *et al*. ACS Biomaterials Science & Engineering. 2016). In the Fall of 2013, Jason moved to Seattle, Washington to pursue his PhD in Bioengineering at the University of Washington. When not working in the laboratory, Jason enjoys traveling the world, trying new restaurants and playing racket sports with his friends.

References

1.   Mathers, C.D. and D. Loncar, *Projections of global mortality and burden of disease from 2002 to 2030.* PLoS medicine, 2006. **3**(11): p. e442.

2.   Heidenreich, P.A., et al., *Forecasting the future of cardiovascular disease in the United States: a policy statement from the American Heart Association.* Circulation, 2011. **123**(8): p. 933-44.

3.   DiMasi, J.A., R.W. Hansen, and H.G. Grabowski, *The price of innovation: new estimates of drug development costs.* Journal of Health Economics, 2003. **22**(2): p. 151-185.

4.   Gobaa, S., et al., *Artificial niche microarrays for probing single stem cell fate in high throughput.* Nat Meth, 2011. **8**(11): p. 949-955.

5.   Yang, L., et al., *Human cardiovascular progenitor cells develop from a KDR+ embryonic-stem-cell-derived population.* Nature, 2008. **453**(7194): p. 524-8.

6.   Zhang, J., et al., *Functional cardiomyocytes derived from human induced pluripotent stem cells.* Circ Res, 2009. **104**(4): p. e30-41.

7.   Snir, M., et al., *Assessment of the ultrastructural and proliferative properties of human embryonic stem cell-derived cardiomyocytes.* Am J Physiol Heart Circ Physiol, 2003. **285**(6): p. H2355-63.

8.   McDevitt, T.C., M.A. Laflamme, and C.E. Murry, *Proliferation of cardiomyocytes derived from human embryonic stem cells is mediated via the IGF/PI 3-kinase/Akt signaling pathway.* J Mol Cell Cardiol, 2005. **39**(6): p. 865-73.

9.   Lee, P., et al., *Simultaneous Voltage and Calcium Mapping of Genetically Purified Human Induced Pluripotent Stem Cell-Derived Cardiac Myocyte Monolayers.* Circulation research, 2012.

10.   Dolnikov, K., et al., *Functional properties of human embryonic stem cell-derived cardiomyocytes: intracellular Ca2+ handling and the role of sarcoplasmic reticulum in the contraction.* Stem cells, 2006. **24**(2): p. 236-45.

11.   Gherghiceanu, M., et al., *Cardiomyocytes derived from human embryonic and induced pluripotent stem cells: comparative ultrastructure.* Journal of cellular and molecular medicine, 2011. **15**(11): p. 2539-51.

12.   Yang, X., et al., *Tri-iodo-l-thyronine promotes the maturation of human cardiomyocytes-derived from induced pluripotent stem cells.* J Mol Cell Cardiol, 2014. **72**: p. 296-304.

13.   Kuppusamy, K.T., et al., *Let-7 family of microRNA is required for maturation and adult-like metabolism in stem cell-derived cardiomyocytes.* Proc Natl Acad Sci U S A, 2015.

14.   Lundy, S.D., et al., *Structural and Functional Maturation of Cardiomyocytes Derived from Human Pluripotent Stem Cells.* Stem cells and development, 2013.

15.   Tulloch, N.L., et al., *Growth of engineered human myocardium with mechanical loading and vascular coculture.* Circulation research, 2011. **109**(1): p. 47-59.

16.   Schaaf, S., et al., *Human engineered heart tissue as a versatile tool in basic research and preclinical toxicology.* PloS one, 2011. **6**(10): p. e26397.

17.   Nunes, S.S., et al., *Biowire: a platform for maturation of human pluripotent stem cell-derived cardiomyocytes.* Nature methods, 2013. **10**(8): p. 781-7.

18.   Shachar, M., N. Benishti, and S. Cohen, *Effects of mechanical stimulation induced by compression and medium perfusion on cardiac tissue engineering.* Biotechnology progress, 2012. **28**(6): p. 1551-9.

19. Dvir, T., et al., *Activation of the ERK1/2 cascade via pulsatile interstitial fluid flow promotes cardiac tissue assembly.* Tissue engineering, 2007. **13**(9): p. 2185-93.

20. Thavandiran, N., et al., *Design and formulation of functional pluripotent stem cell-derived cardiac microtissues.* Proceedings of the National Academy of Sciences of the United States of America, 2013. **110**(49): p. E4698-707.

21. French, K.M., et al., *A naturally derived cardiac extracellular matrix enhances cardiac progenitor cell behavior in vitro.* Acta biomaterialia, 2012. **8**(12): p. 4357-64.

22. Singelyn, J.M., et al., *Naturally derived myocardial matrix as an injectable scaffold for cardiac tissue engineering.* Biomaterials, 2009. **30**(29): p. 5409-16.

23. Rinaldo, P., D. Matern, and M.J. Bennett, *Fatty acid oxidation disorders.* Annu Rev Physiol, 2002. **64**: p. 477-502.

24. Van Nieuwenhoven, F.A., G.J. Van der Vusse, and J.F. Glatz, *Membrane-associated and cytoplasmic fatty acid-binding proteins.* Lipids, 1996. **31 Suppl**: p. S223-7.

25. McGarry, J.D. and N.F. Brown, *The mitochondrial carnitine palmitoyltransferase system. From concept to molecular analysis.* Eur J Biochem, 1997. **244**(1): p. 1-14.

26. Ikeda, Y., K. Okamura-Ikeda, and K. Tanaka, *Purification and characterization of short-chain, medium-chain, and long-chain acyl-CoA dehydrogenases from rat liver mitochondria. Isolation of the holo- and apoenzymes and conversion of the apoenzyme to the holoenzyme.* J Biol Chem, 1985. **260**(2): p. 1311-25.

27. Izai, K., et al., *Novel fatty acid beta-oxidation enzymes in rat liver mitochondria. I. Purification and properties of very-long-chain acyl-coenzyme A dehydrogenase.* J Biol Chem, 1992. **267**(2): p. 1027-33.

28. Djouadi, F., et al., *Mitochondrial trifunctional protein deficiency in human cultured fibroblasts: effects of bezafibrate.* J Inherit Metab Dis, 2016. **39**(1): p. 47-58.

29. Uchida, Y., et al., *Novel fatty acid beta-oxidation enzymes in rat liver mitochondria. II. Purification and properties of enoyl-coenzyme A (CoA) hydratase/3-hydroxyacyl-CoA dehydrogenase/3-ketoacyl-CoA thiolase trifunctional protein.* J Biol Chem, 1992. **267**(2): p. 1034-41.

30. Carpenter, K., R.J. Pollitt, and B. Middleton, *A unique, membrane-bound, multifunctional enzyme from human liver mitochondria catalysing three steps of fatty acid beta-oxidation.* Biochem Soc Trans, 1993. **21**(1): p. 35S.

31. Ushikubo, S., et al., *Molecular characterization of mitochondrial trifunctional protein deficiency: formation of the enzyme complex is important for stabilization of both alpha- and beta-subunits.* Am J Hum Genet, 1996. **58**(5): p. 979-88.

32. Weinberger, M.J., et al., *Intact alpha-subunit is required for membrane-binding of human mitochondrial trifunctional beta-oxidation protein, but is not necessary for conferring 3-ketoacyl-CoA thiolase activity to the beta-subunit.* Biochem Biophys Res Commun, 1995. **209**(1): p. 47-52.

33. Kobayashi, A., L.L. Jiang, and T. Hashimoto, *Two mitochondrial 3-hydroxyacyl-CoA dehydrogenases in bovine liver.* J Biochem, 1996. **119**(4): p. 775-82.

34. Camtosun, E., et al., *A Deep Intronic HADH Splicing Mutation (c.636+471G>T) in a Congenital Hyperinsulinemic Hypoglycemia Case: Long Term Clinical Course.* J Clin Res Pediatr Endocrinol, 2015. **7**(2): p. 144-7.

35. Kamijo, T., et al., *Medium chain 3-ketoacyl-coenzyme A thiolase deficiency: a new disorder of mitochondrial fatty acid beta-oxidation.* Pediatr Res, 1997. **42**(5): p. 569-76.

36.   Martines, A.M.F., et al., *The promiscuous enzyme medium-chain 3-keto-acyl-CoA thiolase triggers a vicious cycle in fatty-acid beta-oxidation.* PLoS Comput Biol, 2017. **13**(4): p. e1005461.

37.   Shekhawat, P.S., D. Matern, and A.W. Strauss, *Fetal fatty acid oxidation disorders, their effect on maternal health and neonatal outcome: impact of expanded newborn screening on their diagnosis and management.* Pediatr Res, 2005. **57**(5 Pt 2): p. 78R-86R.

38.   Vishwanath, V.A., *Fatty Acid Beta-Oxidation Disorders: A Brief Review.* Ann Neurosci, 2016. **23**(1): p. 51-5.

39.   Zytkovicz, T.H., et al., *Tandem mass spectrometric analysis for amino, organic, and fatty acid disorders in newborn dried blood spots: a two-year summary from the New England Newborn Screening Program.* Clin Chem, 2001. **47**(11): p. 1945-55.

40.   Ibdah, J.A., et al., *A fetal fatty-acid oxidation disorder as a cause of liver disease in pregnant women.* N Engl J Med, 1999. **340**(22): p. 1723-31.

41.   Gregersen, N., et al., *Mutation analysis in mitochondrial fatty acid oxidation defects: Exemplified by acyl-CoA dehydrogenase deficiencies, with special focus on genotype-phenotype relationship.* Hum Mutat, 2001. **18**(3): p. 169-89.

42.   Brackett, J.C., et al., *Two alpha subunit donor splice site mutations cause human trifunctional protein deficiency.* J Clin Invest, 1995. **95**(5): p. 2076-82.

43.   den Boer, M.E., et al., *Mitochondrial trifunctional protein deficiency: a severe fatty acid oxidation disorder with cardiac and neurologic involvement.* J Pediatr, 2003. **142**(6): p. 684-9.

44.   Orii, K.E., et al., *Genomic and mutational analysis of the mitochondrial trifunctional protein beta-subunit (HADHB) gene in patients with trifunctional protein deficiency.* Hum Mol Genet, 1997. **6**(8): p. 1215-24.

45.   Wanders, R.J., et al., *Sudden infant death and long-chain 3-hydroxyacyl-CoA dehydrogenase.* Lancet, 1989. **2**(8653): p. 52-3.

46.   L, I.J., et al., *Molecular basis of long-chain 3-hydroxyacyl-CoA dehydrogenase deficiency: identification of the major disease-causing mutation in the alpha-subunit of the mitochondrial trifunctional protein.* Biochim Biophys Acta, 1994. **1215**(3): p. 347-50.

47.   Sims, H.F., et al., *The molecular basis of pediatric long chain 3-hydroxyacyl-CoA dehydrogenase deficiency associated with maternal acute fatty liver of pregnancy.* Proc Natl Acad Sci U S A, 1995. **92**(3): p. 841-5.

48.   L, I.J., et al., *Common missense mutation G1528C in long-chain 3-hydroxyacyl-CoA dehydrogenase deficiency. Characterization and expression of the mutant protein, mutation analysis on genomic DNA and chromosomal localization of the mitochondrial trifunctional protein alpha subunit gene.* J Clin Invest, 1996. **98**(4): p. 1028-33.

49.   Spierkerkoetter, U., et al., *The early-onset phenotype of mitochondrial trifunctional protein deficiency: a lethal disorder with multiple tissue involvement.* J Inherit Metab Dis, 2004. **27**(2): p. 294-6.

50.   Eskelin, P. and T. Tyni, *LCHAD and MTP Deficiencies - Two disorders of mitochondrial fatty Acid β-oxidation with unusual features.* Current Pediatric Reviews, 2007. **3**(1): p. 53-59.

51.   den Boer, M.E., et al., *Long-chain 3-hydroxyacyl-CoA dehydrogenase deficiency: clinical presentation and follow-up of 50 patients.* Pediatrics, 2002. **109**(1): p. 99-104.

52.   Olpin, S.E., et al., *Biochemical, clinical and molecular findings in LCHAD and general mitochondrial trifunctional protein deficiency.* J Inherit Metab Dis, 2005. **28**(4): p. 533-44.

53. Rector, R.S., R.M. Payne, and J.A. Ibdah, *Mitochondrial trifunctional protein defects: clinical implications and therapeutic approaches.* Adv Drug Deliv Rev, 2008. **60**(13-14): p. 1488-96.

54. Gillingham, M.B., et al., *Optimal dietary therapy of long-chain 3-hydroxyacyl-CoA dehydrogenase deficiency.* Mol Genet Metab, 2003. **79**(2): p. 114-23.

55. Sander, J., et al., *Neonatal screening for defects of the mitochondrial trifunctional protein.* Mol Genet Metab, 2005. **85**(2): p. 108-14.

56. Ibdah, J.A., et al., *Lack of mitochondrial trifunctional protein in mice causes neonatal hypoglycemia and sudden death.* J Clin Invest, 2001. **107**(11): p. 1403-9.

57. Wanders, R.J., et al., *Human trifunctional protein deficiency: a new disorder of mitochondrial fatty acid beta-oxidation.* Biochem Biophys Res Commun, 1992. **188**(3): p. 1139-45.

58. Jones, P.M., et al., *Accumulation of free 3-hydroxy fatty acids in the culture media of fibroblasts from patients deficient in long-chain l-3-hydroxyacyl-CoA dehydrogenase: a useful diagnostic aid.* Clin Chem, 2001. **47**(7): p. 1190-4.

59. Mak, I.T., J.H. Kramer, and W.B. Weglicki, *Potentiation of free radical-induced lipid peroxidative injury to sarcolemmal membranes by lipid amphiphiles.* J Biol Chem, 1986. **261**(3): p. 1153-7.

60. Bonnet, D., et al., *Arrhythmias and conduction defects as presenting symptoms of fatty acid oxidation disorders in children.* Circulation, 1999. **100**(22): p. 2248-53.

61. Taylor, W.A., et al., *Human trifunctional protein alpha links cardiolipin remodeling to beta-oxidation.* PLoS One, 2012. **7**(11): p. e48628.

62. Osman, C., D.R. Voelker, and T. Langer, *Making heads or tails of phospholipids in mitochondria.* J Cell Biol, 2011. **192**(1): p. 7-16.

63. Lewis, R.N. and R.N. McElhaney, *The physicochemical properties of cardiolipin bilayers and cardiolipin-containing lipid membranes.* Biochim Biophys Acta, 2009. **1788**(10): p. 2069-79.

64. Claypool, S.M. and C.M. Koehler, *The complexity of cardiolipin in health and disease.* Trends Biochem Sci, 2012. **37**(1): p. 32-41.

65. Arnarez, C., S.J. Marrink, and X. Periole, *Identification of cardiolipin binding sites on cytochrome c oxidase at the entrance of proton channels.* Sci Rep, 2013. **3**: p. 1263.

66. He, Q. and X. Han, *Cardiolipin remodeling in diabetic heart.* Chem Phys Lipids, 2014. **179**: p. 75-81.

67. Kiebish, M.A., et al., *Myocardial regulation of lipidomic flux by cardiolipin synthase: setting the beat for bioenergetic efficiency.* J Biol Chem, 2012. **287**(30): p. 25086-97.

68. Schlame, M., S. Brody, and K.Y. Hostetler, *Mitochondrial cardiolipin in diverse eukaryotes. Comparison of biosynthetic reactions and molecular acyl species.* Eur J Biochem, 1993. **212**(3): p. 727-35.

69. Zachman, D.K., et al., *The role of calcium-independent phospholipase A2 in cardiolipin remodeling in the spontaneously hypertensive heart failure rat heart.* J Lipid Res, 2010. **51**(3): p. 525-34.

70. Han, X., et al., *Shotgun lipidomics identifies cardiolipin depletion in diabetic myocardium linking altered substrate utilization with mitochondrial dysfunction.* Biochemistry, 2005. **44**(50): p. 16684-94.

71. Sparagna, G.C., et al., *Loss of cardiac tetralinoleoyl cardiolipin in human and experimental heart failure.* J Lipid Res, 2007. **48**(7): p. 1559-70.

72.   Sparagna, G.C. and E.J. Lesnefsky, *Cardiolipin remodeling in the heart.* J Cardiovasc Pharmacol, 2009. **53**(4): p. 290-301.

73.   Hostetler, K.Y., H. van den Bosch, and L.L. van Deenen, *The mechanism of cardiolipin biosynthesis in liver mitochondria.* Biochim Biophys Acta, 1972. **260**(3): p. 507-13.

74.   Tamura, Y., et al., *Tam41 is a CDP-diacylglycerol synthase required for cardiolipin biosynthesis in mitochondria.* Cell Metab, 2013. **17**(5): p. 709-18.

75.   Chang, S.C., et al., *The PEL1 gene (renamed PGS1) encodes the phosphatidylglycero-phosphate synthase of Saccharomyces cerevisiae.* J Biol Chem, 1998. **273**(16): p. 9829-36.

76.   Kelly, B.L. and M.L. Greenberg, *Characterization and regulation of phosphatidylglycerolphosphate phosphatase in Saccharomyces cerevisiae.* Biochim Biophys Acta, 1990. **1046**(2): p. 144-50.

77.   Chen, D., X.Y. Zhang, and Y. Shi, *Identification and functional characterization of hCLS1, a human cardiolipin synthase localized in mitochondria.* Biochem J, 2006. **398**(2): p. 169-76.

78.   Lands, W.E., *Metabolism of glycerolipids. 2. The enzymatic acylation of lysolecithin.* J Biol Chem, 1960. **235**: p. 2233-7.

79.   Bione, S., et al., *A novel X-linked gene, G4.5. is responsible for Barth syndrome.* Nat Genet, 1996. **12**(4): p. 385-9.

80.   Taylor, W.A. and G.M. Hatch, *Identification of the human mitochondrial linoleoyl-coenzyme A monolysocardiolipin acyltransferase (MLCL AT-1).* J Biol Chem, 2009. **284**(44): p. 30360-71.

81.   Taylor, W.A. and G.M. Hatch, *Purification and characterization of monolysocardiolipin acyltransferase from pig liver mitochondria.* J Biol Chem, 2003. **278**(15): p. 12716-21.

82.   Lu, Y.W. and S.M. Claypool, *Disorders of phospholipid metabolism: an emerging class of mitochondrial disease due to defects in nuclear genes.* Front Genet, 2015. **6**: p. 3.

83.   Lane, R.K., T. Hilsabeck, and S.L. Rea, *The role of mitochondrial dysfunction in age-related diseases.* Biochim Biophys Acta, 2015. **1847**(11): p. 1387-400.

84.   Li, J., et al., *Cardiolipin remodeling by ALCAT1 links oxidative stress and mitochondrial dysfunction to obesity.* Cell Metab, 2010. **12**(2): p. 154-65.

85.   Paradies, G., et al., *Functional role of cardiolipin in mitochondrial bioenergetics.* Biochim Biophys Acta, 2014. **1837**(4): p. 408-17.

86.   Paradies, G., et al., *Reactive oxygen species affect mitochondrial electron transport complex I activity through oxidative cardiolipin damage.* Gene, 2002. **286**(1): p. 135-41.

87.   Paradies, G., et al., *Reactive oxygen species generated by the mitochondrial respiratory chain affect the complex III activity via cardiolipin peroxidation in beef-heart submitochondrial particles.* Mitochondrion, 2001. **1**(2): p. 151-9.

88.   Genova, M.L., et al., *Is supercomplex organization of the respiratory chain required for optimal electron transfer activity?* Biochim Biophys Acta, 2008. **1777**(7-8): p. 740-6.

89.   McKenzie, M., et al., *Mitochondrial respiratory chain supercomplexes are destabilized in Barth Syndrome patients.* J Mol Biol, 2006. **361**(3): p. 462-9.

90.   Musatov, A., *Contribution of peroxidized cardiolipin to inactivation of bovine heart cytochrome c oxidase.* Free Radic Biol Med, 2006. **41**(2): p. 238-46.

91.   Guertl, B., C. Noehammer, and G. Hoefler, *Metabolic cardiomyopathies.* Int J Exp Pathol, 2000. **81**(6): p. 349-72.

92.   Houtkooper, R.H., et al., *The enigmatic role of tafazzin in cardiolipin metabolism.* Biochim Biophys Acta, 2009. **1788**(10): p. 2003-14.

93. Wang, G., et al., *Modeling the mitochondrial cardiomyopathy of Barth syndrome with induced pluripotent stem cell and heart-on-chip technologies.* Nat Med, 2014. **20**(6): p. 616-23.

94. Mandavia, C.H., et al., *Molecular and metabolic mechanisms of cardiac dysfunction in diabetes.* Life Sci, 2013. **92**(11): p. 601-8.

95. Drawnel, F.M., et al., *Disease modeling and phenotypic drug screening for diabetic cardiomyopathy using human induced pluripotent stem cells.* Cell Rep, 2014. **9**(3): p. 810-21.

96. Ron, D. and P. Walter, *Signal integration in the endoplasmic reticulum unfolded protein response.* Nat Rev Mol Cell Biol, 2007. **8**(7): p. 519-29.

97. Go, A.S., et al., *Heart disease and stroke statistics--2013 update: a report from the American Heart Association.* Circulation, 2013. **127**(1): p. e6-e245.

98. van Berlo, J.H. and J.D. Molkentin, *An emerging consensus on cardiac regeneration.* Nat Med, 2014. **20**(12): p. 1386-93.

99. van Berlo, J.H., et al., *c-kit+ cells minimally contribute cardiomyocytes to the heart.* Nature, 2014. **509**(7500): p. 337-41.

100. Laflamme, M.A. and C.E. Murry, *Heart regeneration.* Nature, 2011. **473**(7347): p. 326-35.

101. Chong, J.J., et al., *Human embryonic-stem-cell-derived cardiomyocytes regenerate non-human primate hearts.* Nature, 2014.

102. Chen, J.X., et al., *Inefficient reprogramming of fibroblasts into cardiomyocytes using Gata4, Mef2c, and Tbx5.* Circ Res, 2012. **111**(1): p. 50-5.

103. Song, K., et al., *Heart repair by reprogramming non-myocytes with cardiac transcription factors.* Nature, 2012. **485**(7400): p. 599-604.

104. Foglia, M.J. and K.D. Poss, *Building and re-building the heart by cardiomyocyte proliferation.* Development, 2016. **143**(5): p. 729-40.

105. van Meer, B.J., L.G. Tertoolen, and C.L. Mummery, *Concise Review: Measuring Physiological Responses of Human Pluripotent Stem Cell Derived Cardiomyocytes to Drugs and Disease.* Stem Cells, 2016. **34**(8): p. 2008-15.

106. Chen, I.Y., E. Matsa, and J.C. Wu, *Induced pluripotent stem cells: at the heart of cardiovascular precision medicine.* Nat Rev Cardiol, 2016. **13**(6): p. 333-49.

107. Anderson, P.A., et al., *Developmental changes in cardiac contractility in fetal and postnatal sheep: in vitro and in vivo.* The American journal of physiology, 1984. **247**(3 Pt 2): p. H371-9.

108. Chattergoon, N.N., et al., *Thyroid hormone drives fetal cardiomyocyte maturation.* FASEB journal : official publication of the Federation of American Societies for Experimental Biology, 2012. **26**(1): p. 397-408.

109. Reiser, P.J., et al., *Human cardiac myosin heavy chain isoforms in fetal and failing adult atria and ventricles.* American journal of physiology. Heart and circulatory physiology, 2001. **280**(4): p. H1814-20.

110. Uosaki, H. and Y.H. Taguchi, *Comparative Gene Expression Analysis of Mouse and Human Cardiac Maturation.* Genomics Proteomics Bioinformatics, 2016.

111. Yang, X., L. Pabon, and C.E. Murry, *Engineering adolescence: maturation of human pluripotent stem cell-derived cardiomyocytes.* Circulation research, 2014. **114**(3): p. 511-23.

112. Oey, N.A., et al., *Long-chain fatty acid oxidation during early human development.* Pediatr Res, 2005. **57**(6): p. 755-9.
113. Kolwicz, S.C., Jr., S. Purohit, and R. Tian, *Cardiac metabolism and its interactions with contraction, growth, and survival of cardiomyocytes.* Circ Res, 2013. **113**(5): p. 603-16.
114. Lopaschuk, G.D. and J.S. Jaswal, *Energy metabolic phenotype of the cardiomyocyte during development, differentiation, and postnatal maturation.* J Cardiovasc Pharmacol, 2010. **56**(2): p. 130-40.
115. Kim, H.D., et al., *Human fetal heart development after mid-term: morphometry and ultrastructural study.* Journal of molecular and cellular cardiology, 1992. **24**(9): p. 949-65.
116. Kim, D.H., et al., *Nanoscale cues regulate the structure and function of macroscopic cardiac tissue constructs.* Proceedings of the National Academy of Sciences of the United States of America, 2010. **107**(2): p. 565-70.
117. Wilson, K.D., et al., *Dynamic microRNA expression programs during cardiac differentiation of human embryonic stem cells: role for miR-499.* Circulation. Cardiovascular genetics, 2010. **3**(5): p. 426-35.
118. Lee, D.S., et al., *Defined MicroRNAs Induce Aspects of Maturation in Mouse and Human Embryonic-Stem-Cell-Derived Cardiomyocytes.* Cell Rep, 2015. **12**(12): p. 1960-7.
119. Bruneau, B.G., *Signaling and transcriptional networks in heart development and regeneration.* Cold Spring Harb Perspect Biol, 2013. **5**(3): p. a008292.
120. Chang, C.P. and B.G. Bruneau, *Epigenetics and cardiovascular development.* Annu Rev Physiol, 2012. **74**: p. 41-68.
121. Bruneau, B.G., *Transcriptional regulation of vertebrate cardiac morphogenesis.* Circ Res, 2002. **90**(5): p. 509-19.
122. Bruneau, B.G., *The developmental genetics of congenital heart disease.* Nature, 2008. **451**(7181): p. 943-8.
123. Alaynick, W.A., et al., *ERRgamma directs and maintains the transition to oxidative metabolism in the postnatal heart.* Cell Metab, 2007. **6**(1): p. 13-24.
124. Lehman, J.J., et al., *Peroxisome proliferator-activated receptor gamma coactivator-1 promotes cardiac mitochondrial biogenesis.* J Clin Invest, 2000. **106**(7): p. 847-56.
125. Huss, J.M. and D.P. Kelly, *Nuclear receptor signaling and cardiac energetics.* Circ Res, 2004. **95**(6): p. 568-78.
126. Jain, R., et al., *HEART DEVELOPMENT. Integration of Bmp and Wnt signaling by Hopx specifies commitment of cardiomyoblasts.* Science, 2015. **348**(6242): p. aaa6071.
127. Kreitzer, F.R., et al., *A robust method to derive functional neural crest cells from human pluripotent stem cells.* Am J Stem Cells, 2013. **2**(2): p. 119-31.
128. Palpant, N.J., et al., *Generating high-purity cardiac and endothelial derivatives from patterned mesoderm using human pluripotent stem cells.* Nat Protoc, 2017. **12**(1): p. 15-31.
129. Burridge, P.W., et al., *Chemically defined generation of human cardiomyocytes.* Nat Methods, 2014. **11**(8): p. 855-60.
130. Tohyama, S., et al., *Distinct metabolic flow enables large-scale purification of mouse and human pluripotent stem cell-derived cardiomyocytes.* Cell Stem Cell, 2013. **12**(1): p. 127-37.
131. Moffat, J., et al., *A lentiviral RNAi library for human and mouse genes applied to an arrayed viral high-content screen.* Cell, 2006. **124**(6): p. 1283-98.

132.   Li, Q., et al., *A syntaxin 1, Galpha(o), and N-type calcium channel complex at a presynaptic nerve terminal: analysis by quantitative immunocolocalization.* J Neurosci, 2004. **24**(16): p. 4070-81.

133.   Beussman, K.M., et al., *Micropost arrays for measuring stem cell-derived cardiomyocyte contractility.* Methods, 2016. **94**: p. 43-50.

134.   Trapnell, C., L. Pachter, and S.L. Salzberg, *TopHat: discovering splice junctions with RNA-Seq.* Bioinformatics, 2009. **25**(9): p. 1105-11.

135.   Anders, S., P.T. Pyl, and W. Huber, *HTSeq--a Python framework to work with high-throughput sequencing data.* Bioinformatics, 2015. **31**(2): p. 166-9.

136.   Anders, S. and W. Huber, *Differential expression analysis for sequence count data.* Genome Biol, 2010. **11**(10): p. R106.

137.   Alexa, A., J. Rahnenfuhrer, and T. Lengauer, *Improved scoring of functional groups from gene expression data by decorrelating GO graph structure.* Bioinformatics, 2006. **22**(13): p. 1600-7.

138.   Satija, R., et al., *Spatial reconstruction of single-cell gene expression data.* Nat Biotechnol, 2015. **33**(5): p. 495-502.

139.   Roadmap Epigenomics, C., et al., *Integrative analysis of 111 reference human epigenomes.* Nature, 2015. **518**(7539): p. 317-30.

140.   DeLaughter, D.M., et al., *Single-Cell Resolution of Temporal Gene Expression during Heart Development.* Dev Cell, 2016. **39**(4): p. 480-490.

141.   Akat, K.M., et al., *Comparative RNA-sequencing analysis of myocardial and circulating small RNAs in human heart failure and their utility as biomarkers.* Proc Natl Acad Sci U S A, 2014. **111**(30): p. 11151-6.

142.   Yang, K.C., et al., *Deep RNA sequencing reveals dynamic regulation of myocardial noncoding RNAs in failing human heart and remodeling with mechanical circulatory support.* Circulation, 2014. **129**(9): p. 1009-21.

143.   Lewis, B.P., C.B. Burge, and D.P. Bartel, *Conserved seed pairing, often flanked by adenosines, indicates that thousands of human genes are microRNA targets.* Cell, 2005. **120**(1): p. 15-20.

144.   Nagalingam, R.S., et al., *A cardiac-enriched microRNA, miR-378, blocks cardiac hypertrophy by targeting Ras signaling.* The Journal of biological chemistry, 2013. **288**(16): p. 11216-32.

145.   Callis, T.E., et al., *MicroRNA-208a is a regulator of cardiac hypertrophy and conduction in mice.* J Clin Invest, 2009. **119**(9): p. 2772-86.

146.   van Rooij, E., et al., *A family of microRNAs encoded by myosin genes governs myosin expression and muscle performance.* Dev Cell, 2009. **17**(5): p. 662-73.

147.   Rodriguez, M.L., et al., *Measuring the contractile forces of human induced pluripotent stem cell-derived cardiomyocytes with arrays of microposts.* J Biomech Eng, 2014. **136**(5): p. 051005.

148.   Liberzon, A., et al., *The Molecular Signatures Database (MSigDB) hallmark gene set collection.* Cell Syst, 2015. **1**(6): p. 417-425.

149.   Listenberger, L.L., et al., *Triglyceride accumulation protects against fatty acid-induced lipotoxicity.* Proc Natl Acad Sci U S A, 2003. **100**(6): p. 3077-82.

150.   Iwai, N., H. Shimoike, and M. Kinoshita, *Cardiac renin-angiotensin system in the hypertrophied heart.* Circulation, 1995. **92**(9): p. 2690-6.

151.	Miklas, J.W., et al., *Bioreactor for modulation of cardiac microtissue phenotype by combined static stretch and electrical stimulation.* Biofabrication, 2014. **6**(2): p. 024113.

152.	Macadangdang, J., et al., *Nanopatterned Human iPSC-based Model of a Dystrophin-Null Cardiomyopathic Phenotype.* Cell Mol Bioeng, 2015. **8**(3): p. 320-332.

153.	Zhang, D., et al., *Tissue-engineered cardiac patch for advanced functional maturation of human ESC-derived cardiomyocytes.* Biomaterials, 2013. **34**(23): p. 5813-20.

154.	Ellen Kreipke, R., et al., *Metabolic remodeling in early development and cardiomyocyte maturation.* Semin Cell Dev Biol, 2016. **52**: p. 84-92.

155.	Gong, G., et al., *Parkin-mediated mitophagy directs perinatal cardiac metabolic maturation in mice.* Science, 2015. **350**(6265): p. aad2459.

156.	Kook, H., et al., *Cardiac hypertrophy and histone deacetylase-dependent transcriptional repression mediated by the atypical homeodomain protein Hop.* J Clin Invest, 2003. **112**(6): p. 863-71.

157.	Shin, C.H., et al., *Modulation of cardiac growth and development by HOP, an unusual homeodomain protein.* Cell, 2002. **110**(6): p. 725-35.

158.	Tonin, A.M., et al., *Long-chain 3-hydroxy fatty acids accumulating in long-chain 3-hydroxyacyl-CoA dehydrogenase and mitochondrial trifunctional protein deficiencies uncouple oxidative phosphorylation in heart mitochondria.* J Bioenerg Biomembr, 2013. **45**(1-2): p. 47-57.

159.	Tyni, T. and H. Pihko, *Long-chain 3-hydroxyacyl-CoA dehydrogenase deficiency.* Acta Paediatr, 1999. **88**(3): p. 237-45.

160.	Wajner, M. and A.U. Amaral, *Mitochondrial dysfunction in fatty acid oxidation disorders: insights from human and animal studies.* Biosci Rep, 2015. **36**(1): p. e00281.

161.	Sanjana, N.E., O. Shalem, and F. Zhang, *Improved vectors and genome-wide libraries for CRISPR screening.* Nat Methods, 2014. **11**(8): p. 783-4.

162.	Moreno-Mateos, M.A., et al., *CRISPRscan: designing highly efficient sgRNAs for CRISPR-Cas9 targeting in vivo.* Nat Methods, 2015. **12**(10): p. 982-8.

163.	Bae, S., J. Park, and J.S. Kim, *Cas-OFFinder: a fast and versatile algorithm that searches for potential off-target sites of Cas9 RNA-guided endonucleases.* Bioinformatics, 2014. **30**(10): p. 1473-5.

164.	Moody, J.D., et al., *First critical repressive H3K27me3 marks in embryonic stem cells identified using designed protein inhibitor.* Proc Natl Acad Sci U S A, 2017.

165.	Onay-Besikci, A., *Regulation of cardiac energy metabolism in newborn.* Mol Cell Biochem, 2006. **287**(1-2): p. 1-11.

166.	Gibson, R.A. and G.M. Kneebone, *Fatty acid composition of human colostrum and mature breast milk.* Am J Clin Nutr, 1981. **34**(2): p. 252-7.

167.	Bougneres, P.F., et al., *Lipid transport in the human newborn. Palmitate and glycerol turnover and the contribution of glycerol to neonatal hepatic glucose output.* J Clin Invest, 1982. **70**(2): p. 262-70.

168.	Miller, T.A., et al., *Oleate prevents palmitate-induced cytotoxic stress in cardiac myocytes.* Biochem Biophys Res Commun, 2005. **336**(1): p. 309-15.

169.	Tumova, J., et al., *Protective Effect of Unsaturated Fatty Acids on Palmitic Acid-Induced Toxicity in Skeletal Muscle Cells is not Mediated by PPARdelta Activation.* Lipids, 2015. **50**(10): p. 955-64.

170. Mills, R.J., et al., *Functional screening in human cardiac organoids reveals a metabolic mechanism for cardiomyocyte cell cycle arrest.* Proc Natl Acad Sci U S A, 2017. **114**(40): p. E8372-E8381.

171. Gilchrist, K.H., et al., *High-throughput cardiac safety evaluation and multi-parameter arrhythmia profiling of cardiomyocytes using microelectrode arrays.* Toxicol Appl Pharmacol, 2015. **288**(2): p. 249-57.

172. Li, F., et al., *Rapid transition of cardiac myocytes from hyperplasia to hypertrophy during postnatal development.* J Mol Cell Cardiol, 1996. **28**(8): p. 1737-46.

173. Herget, G.W., et al., *DNA content, ploidy level and number of nuclei in the human heart after myocardial infarction.* Cardiovasc Res, 1997. **36**(1): p. 45-51.

174. Fox, D.T. and R.J. Duronio, *Endoreplication and polyploidy: insights into development and disease.* Development, 2013. **140**(1): p. 3-12.

175. Nunes, S.S., et al., *Human Stem Cell-Derived Cardiac Model of Chronic Drug Exposure.* ACS Biomaterials Science & Engineering, 2016.

176. Cogliati, S., et al., *Mitochondrial cristae shape determines respiratory chain supercomplexes assembly and respiratory efficiency.* Cell, 2013. **155**(1): p. 160-71.

177. Valianpour, F., et al., *Quantitative and compositional study of cardiolipin in platelets by electrospray ionization mass spectrometry: application for the identification of Barth syndrome patients.* Clin Chem, 2002. **48**(9): p. 1390-7.

178. Valianpour, F., et al., *Linoleic acid supplementation of Barth syndrome fibroblasts restores cardiolipin levels: implications for treatment.* J Lipid Res, 2003. **44**(3): p. 560-6.

179. Murray, A.J., et al., *Plasma free fatty acids and peroxisome proliferator-activated receptor alpha in the control of myocardial uncoupling protein levels.* Diabetes, 2005. **54**(12): p. 3496-502.

180. Garlid, K.D., et al., *On the mechanism of fatty acid-induced proton transport by mitochondrial uncoupling protein.* J Biol Chem, 1996. **271**(5): p. 2615-20.

181. Thomas, D.A., et al., *Mitochondrial targeting with antioxidant peptide SS-31 prevents mitochondrial depolarization, reduces islet cell apoptosis, increases islet cell yield, and improves posttransplantation function.* J Am Soc Nephrol, 2007. **18**(1): p. 213-22.

182. Birk, A.V., et al., *The mitochondrial-targeted compound SS-31 re-energizes ischemic mitochondria by interacting with cardiolipin.* J Am Soc Nephrol, 2013. **24**(8): p. 1250-61.

183. Zhao, K., et al., *Cell-permeable peptide antioxidants targeted to inner mitochondrial membrane inhibit mitochondrial swelling, oxidative cell death, and reperfusion injury.* J Biol Chem, 2004. **279**(33): p. 34682-90.

184. Spencer, C.T., et al., *Ventricular arrhythmia in the X-linked cardiomyopathy Barth syndrome.* Pediatr Cardiol, 2005. **26**(5): p. 632-7.

185. Schlame, M. and M. Ren, *Barth syndrome, a human disorder of cardiolipin metabolism.* FEBS Lett, 2006. **580**(23): p. 5450-5.

186. Xu, Y., et al., *The enzymatic function of tafazzin.* J Biol Chem, 2006. **281**(51): p. 39217-24.

187. Bergmann, O., et al., *Dynamics of Cell Generation and Turnover in the Human Heart.* Cell, 2015. **161**(7): p. 1566-75.

188. Senyo, S.E., et al., *Mammalian heart renewal by pre-existing cardiomyocytes.* Nature, 2012.

189. Porrello, E.R., et al., *Transient regenerative potential of the neonatal mouse heart.* Science, 2011. **331**(6020): p. 1078-80.

190. Oyama, K., D. El-Nachef, and W.R. MacLellan, *Regeneration potential of adult cardiac myocytes.* Cell research, 2013. **23**(8): p. 978-9.

191. Jopling, C., et al., *Zebrafish heart regeneration occurs by cardiomyocyte dedifferentiation and proliferation.* Nature, 2010. **464**(7288): p. 606-9.

192. Kikuchi, K., et al., *Primary contribution to zebrafish heart regeneration by gata4(+) cardiomyocytes.* Nature, 2010. **464**(7288): p. 601-5.

193. Wang, J., et al., *The regenerative capacity of zebrafish reverses cardiac failure caused by genetic cardiomyocyte depletion.* Development, 2011. **138**(16): p. 3421-30.

194. Mahmoud, A.I., et al., *Nerves Regulate Cardiomyocyte Proliferation and Heart Regeneration.* Dev Cell, 2015. **34**(4): p. 387-99.

195. Zhang, R., et al., *In vivo cardiac reprogramming contributes to zebrafish heart regeneration.* Nature, 2013. **498**(7455): p. 497-501.

196. Gemberling, M., et al., *Nrg1 is an injury-induced cardiomyocyte mitogen for the endogenous heart regeneration program in zebrafish.* Elife, 2015. **4**.

197. Poss, K.D., L.G. Wilson, and M.T. Keating, *Heart regeneration in zebrafish.* Science, 2002. **298**(5601): p. 2188-90.

198. Hirose, K., et al., *Mechanistic target of rapamycin complex 1 signaling regulates cell proliferation, cell survival, and differentiation in regenerating zebrafish fins.* BMC Dev Biol, 2014. **14**: p. 42.

199. Gemberling, M., et al., *The zebrafish as a model for complex tissue regeneration.* Trends Genet, 2013. **29**(11): p. 611-20.

200. Laplante, M. and D.M. Sabatini, *mTOR signaling at a glance.* J Cell Sci, 2009. **122**(Pt 20): p. 3589-94.

201. Stoick-Cooper, C.L., et al., *Distinct Wnt signaling pathways have opposing roles in appendage regeneration.* Development, 2007. **134**(3): p. 479-89.

202. Mably, J.D., et al., *heart of glass regulates the concentric growth of the heart in zebrafish.* Curr Biol, 2003. **13**(24): p. 2138-47.

203. Moro, E., et al., *In vivo Wnt signaling tracing through a transgenic biosensor fish reveals novel activity domains.* Dev Biol, 2012. **366**(2): p. 327-40.

204. Dorsky, R.I., L.C. Sheldahl, and R.T. Moon, *A transgenic Lef1/beta-catenin-dependent reporter is expressed in spatially restricted domains throughout zebrafish development.* Dev Biol, 2002. **241**(2): p. 229-37.

205. Westerfield, M., *The Zebrafish book. A guide for the laboratory use of zebrafish (Danio rerio).* 4th ed ed. 2000, Eugene, OR: Univ. of Oregon Press.

206. Plavicki, J.S., et al., *Multiple modes of proepicardial cell migration require heartbeat.* BMC Dev Biol, 2014. **14**: p. 18.

207. Burns, C.G. and C.A. MacRae, *Purification of hearts from zebrafish embryos.* BioTechniques, 2006. **40**(3): p. 274, 276, 278 passim.

208. Marney, L.C., et al., *Sample preparation methodology for mouse heart metabolomics using comprehensive two-dimensional gas chromatography coupled with time-of-flight mass spectrometry.* Talanta, 2013. **108**: p. 123-30.

209. Bednarek, D., et al., *Telomerase Is Essential for Zebrafish Heart Regeneration.* Cell Rep, 2015. **12**(10): p. 1691-703.

210. Hofsteen, P., et al., *Quantitative proteomics identify DAB2 as a cardiac developmental regulator that inhibits WNT/β-catenin signaling.* Proc Natl Acad Sci U S A, 2016.

211. Palpant, N.J., et al., *Cardiac Development in Zebrafish and Human Embryonic Stem Cells Is Inhibited by Exposure to Tobacco Cigarettes and E-Cigarettes.* PLoS One, 2015. **10**(5): p. e0126259.

212. Weidinger, G., et al., *The Sp1-related transcription factors sp5 and sp5-like act downstream of Wnt/beta-catenin signaling in mesoderm and neuroectoderm patterning.* Curr Biol, 2005. **15**(6): p. 489-500.

213. Aguirre, A., et al., *In Vivo Activation of a Conserved MicroRNA Program Induces Mammalian Heart Regeneration.* Cell Stem Cell, 2014. **15**(5): p. 589-604.

214. Yao, K., et al., *Wnt Regulates Proliferation and Neurogenic Potential of Muller Glial Cells via a Lin28/let-7 miRNA-Dependent Pathway in Adult Mammalian Retinas.* Cell Rep, 2016. **17**(1): p. 165-178.

215. Niehrs, C. and S.P. Acebron, *Mitotic and mitogenic Wnt signalling.* EMBO J, 2012. **31**(12): p. 2705-13.

216. Bednarek, D., et al., *Telomerase Is Essential for Zebrafish Heart Regeneration.* Cell Rep, 2015. **12**(10): p. 1691-703.

217. Kim, J., J.H. Lee, and V.R. Iyer, *Global identification of Myc target genes reveals its direct role in mitochondrial biogenesis and its E-box usage in vivo.* PLoS One, 2008. **3**(3): p. e1798.

218. Brown, K., et al., *WNT/beta-catenin signaling regulates mitochondrial activity to alter the oncogenic potential of melanoma in a PTEN-dependent manner.* Oncogene, 2017. **36**(22): p. 3119-3136.

219. Li, F., et al., *Myc stimulates nuclearly encoded mitochondrial genes and mitochondrial biogenesis.* Mol Cell Biol, 2005. **25**(14): p. 6225-34.

220. Saxton, R.A. and D.M. Sabatini, *mTOR Signaling in Growth, Metabolism, and Disease.* Cell, 2017. **168**(6): p. 960-976.

221. Nicklin, P., et al., *Bidirectional transport of amino acids regulates mTOR and autophagy.* Cell, 2009. **136**(3): p. 521-34.

222. Wolfson, R.L., et al., *Sestrin2 is a leucine sensor for the mTORC1 pathway.* Science, 2016. **351**(6268): p. 43-8.

223. Shimobayashi, M. and M.N. Hall, *Making new contacts: the mTOR network in metabolism and signalling crosstalk.* Nat Rev Mol Cell Biol, 2014. **15**(3): p. 155-62.

224. Li, J., S.G. Kim, and J. Blenis, *Rapamycin: one drug, many effects.* Cell Metab, 2014. **19**(3): p. 373-9.

225. O'Meara, C.C., et al., *Transcriptional reversion of cardiac myocyte fate during mammalian cardiac regeneration.* Circ Res, 2015. **116**(5): p. 804-15.

226. Gutstein, D.E., et al., *The organization of adherens junctions and desmosomes at the cardiac intercalated disc is independent of gap junctions.* Journal of cell science, 2003. **116**(5): p. 875-885.

227. Park, J.I., et al., *Kaiso/p120-catenin and TCF/beta-catenin complexes coordinately regulate canonical Wnt gene targets.* Dev Cell, 2005. **8**(6): p. 843-54.

228. Del Valle-Perez, B., et al., *Wnt controls the transcriptional activity of Kaiso through CK1epsilon-dependent phosphorylation of p120-catenin.* J Cell Sci, 2011. **124**(Pt 13): p. 2298-309.

229. Piekutowska-Abramczuk, D., et al., *A comprehensive HADHA c.1528G>C frequency study reveals high prevalence of long-chain 3-hydroxyacyl-CoA dehydrogenase deficiency in Poland.* J Inherit Metab Dis, 2010. **33 Suppl 3**: p. S373-7.